Plasma Activated Solutions and their Synergy with Radiation for Cancer Therapy

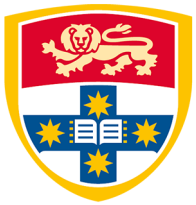

THE UNIVERSITY OF SYDNEY

Juliette Cornelia Harley

This thesis is submitted in fulfilment of the requirements for the degree of *Doctor of Philosophy*

School of Physics
The University of Sydney
November 2023

Declaration

I hereby declare that except where specific reference is made to the work of others, the contents of this thesis are original and have not been submitted in whole or in part for consideration for any other degree or qualification in this, or any other university. This thesis is my own work and contains nothing which is the outcome of work done in collaboration with others, except where specified in the Acknowledgements. This dissertation contains fewer than 80,000 words including appendices, bibliography, footnotes, tables and equations and has fewer than 150 figures.

Dedication

I would like to dedicate this thesis to my parents Kerry and Malcolm, my partner Lachlan, my grandparents and friends. I couldn't have done this without you.

Acknowledgements

I would like to acknowledge my supervisors for their support and guidance during my candidature. Thank you to Professor David McKenzie for his encouragement and eternal optimism and to Associate Professor Natalka Suchowerska for encouraging me to get in the driver's seat. I would also like to acknowledge Dr Ana Esteves for introducing us all.

I would like to deeply thank Mrs Linda Rogers and Ms Hedi Kruse for all of their help and training with cell culture and experiment design and for teaching me German style science.

I would like to thank my fellow PhD student in VectorLAB Dr Georgio Katsifis for his help building the plasma pen and navigating PhD life. I would like to thank fellow Honours students in VectorLAB Linda Losurdo and Caitlin Cummins, especially Caitlin for her work developing the Fractional Difference Synergy Method. I would also like to acknowledge Dalyell student Ryan Russell for his contribution to the methylene blue bleaching experiment in Figure 3.5.

I would like to acknowledge the Arto Hardy Family Biomedical Innovation hub at the Chris O'Brien Lifehouse where the experimental work for this thesis was conducted. I would like to acknowledge and thank Natalka Suchowerska and Elizabeth Claridge Mackonis for performing the irradiation work for this thesis.

I would like to acknowledge the University of Sydney for awarding me the Research Training Program scholarship for financial support during my candidature. I would like to acknowledge the Department of Applied and Plasma Physics for their equipment, technical support and staff. I would like to acknowledge and thank Dr Richard Bowden-Reid for the custom made current transformer, and to Dr Georgio Katsifis for assistance analysing the electrical traces detailed in Chapter 4.

Authorship

Throughout my PhD candidature 2 manuscripts have been published using the work distributed in this thesis. This thesis contains material published in the following manuscripts:

1. Harley, J. C., Suchowerska, N., & McKenzie, D. R. (2020). Cancer treatment with gas plasma and with gas plasma–activated liquid: Positives, potentials and problems of clinical translation. Biophysical Reviews, 12(4), 989-1006.

2. Harley, J. C., Suchowerska, N., Rogers, L. J., Lo, H., Choong, E. S., & McKenzie, D. R. (2022). Plasma activated liquid synergistically enhances response to radiation for improved cancer therapy. Plasma Processes and Polymers, 19(9), 2200026.

   I have also contributed to a third published manuscript:

3. Rogers, L. J., Harley, J. C., McKenzie, D. R., & Suchowerska, N. (2022). Radiation responses of cancer and normal cells to split dose fractions with uniform and grid fields: increasing the therapeutic ratio. International Journal of Radiation Biology, 98(9), 1424-1431.

Paper 1 was adapted to form the introduction Chapter 1. Paper 2 was adapted from Chapter 5 sections 5.1-5.6 and Chapter 6 section 6.3. Supplementary information in Paper 3 was adapted from Chapter 6 section 6.5.

In addition to the statements above, in cases where I am not the corresponding author of a published item, permission to include the published material has been granted by the corresponding author.

Juliette C. Harley

As supervisor for the candidature upon which this thesis is based, I can confirm that the authorship attribution statements above are correct.

David R. McKenzie

Abstract

Radiation therapy benefits nearly 50% of cancer patients, however there are patients for whom treatment fails. The application of radiosensitising agents to boost local effects to radioresistant cancers offers the potential to improve outcomes for these patients. An emerging radiosensitising agent is a Plasma Activated Liquid (PAL). PALs are generated when a liquid is exposed to a plasma (ionised gas), imparting to the liquid the Reactive Oxygen and Nitrogen species (RONS) created during plasma activation. The ability of PAL to sensitise three different cell lines (hormone resistant prostate cancer DU 145, non-malignant prostate cells PNT1A and melanoma MM576) to ionising radiation was investigated in this thesis.

First a custom underwater plasma treatment device was designed, built and optimised. Then the RONS output was characterised and calorimetry was developed as a method of dosimetry. To determine the radiosensitising potential of the PAL, the dose response relationships of both PAL and radiation was required for each cell line. Following dose response experiments, one concentration of PAL and one dose of ionising radiation was chosen for each cell line for combination therapy experiments. A synergy metric based upon the multiplicative survival principle was employed to assess the combination therapy experiments and found synergistic enhancement of radiation cytotoxicity for the DU 145 and the MM576 and found antagonistic reduction in radiation cytotoxicity for the non-malignant PNT1A.

Experiments were conducted with the MM576 cells to assess the effect on cytotoxicity of reversing the order of PAL and radiation administration using a new method of evaluating the synergy metric. While PAL and radiation were found to synergistically reduce cell survival using both methods of evaluating synergy regardless of the order of administration, application of PAL prior to irradiation is significantly more cytotoxic. Experiments were conducted on MM576 and DU 145 cells to determine the relationship between PAL and its major constituents: H_2O_2 and NO_2^-. No statistical difference was found between the cytotoxicity from PAL, H_2O_2 alone and H_2O_2 with NO_2^- for either cell line. These results provide compelling evidence for future studies in the use of H_2O_2 focused therapeutics to improve the response of radioresistant cancers to radiation therapy.

Contents

Chapter 1

Introduction

Cancer accounted for nearly one in six fatalities globally in 2020 [118], showing that it remains one of the leading causes of death worldwide. Some cancers remain hard to treat successfully with currently available therapies. For example, the overall five-year survival for ovarian cancer is 36-49% worldwide [117], pancreatic cancer 7% [57], and patients with glioblastoma continue to experience extremely poor outcomes [114]. Fifty percent of people who are diagnosed with cancer will receive ionising radiation as part of their treatment [23]. Radiation is effective against many cancers, however there are patients for whom radiation therapy still fails. Resistance to radiotherapy and subsequent treatment failure may be due to a number of factors including but not limited to insensitivity towards RONS or hormones, increased cancer stemness or over expression of pro survival related genes [2]. It is known that the tumour microenvironment plays an important role in the tumour response to a therapeutic agent; environmental factors such as hypoxic conditions and interactions with inflammatory or immune responses may negatively impact the efficacy of radiation therapy [69]. A promising method to overcome treatment ineffectiveness is to combine ionising radiation with another treatment, for example chemotherapy or immunotherapy. An emerging candidate therapy for use in combination with radiation is hydrogen peroxide (H_2O_2) which has been shown to be an effective radiosensitising agent *in vitro* ([26], [71], [44]), *in vivo* ([103]) and in clinical trials ([76], [71]). H_2O_2 has been shown to engage in a Fenton's reaction to induce single strand DNA damage [20] and the release of lysosomal enzymes due to peroxidation of the lysosomal membrane [44]. It has also been shown to inactivate cellular antioxidants such as glutathione and catalase which prevents the repair of lipid membrane oxidation and resulting in apoptotic signaling [7]. One way H_2O_2 can be produced is via atmospheric pressure plasma activation of liquids [25].

Plasma is the fourth state of matter; it is ionised gas that is generated when an electric discharge is carried in a gas or vapour between two electrodes, liberating electrons from the gas molecules, resulting in an electron avalanche. The plasma of interest in this work is a cold plasma, operating at a pressure of one atmosphere. For this work, the apparatus used to generate the plasma is a 'plasma pen': a type of dielectric barrier discharge where the dielectric barrier is in the form of a quartz tube. The tube has one external electrode and one coaxial electrode running down the center of the tube in the direction of gas flow. A high voltage electric current is applied to the tube, ionising the gas which forms a plasma plume at the exit of the device. By using this setup, the ejected plume can be used to interact directly with the target, such as a lesion or a liquid for injection into the treatment site.

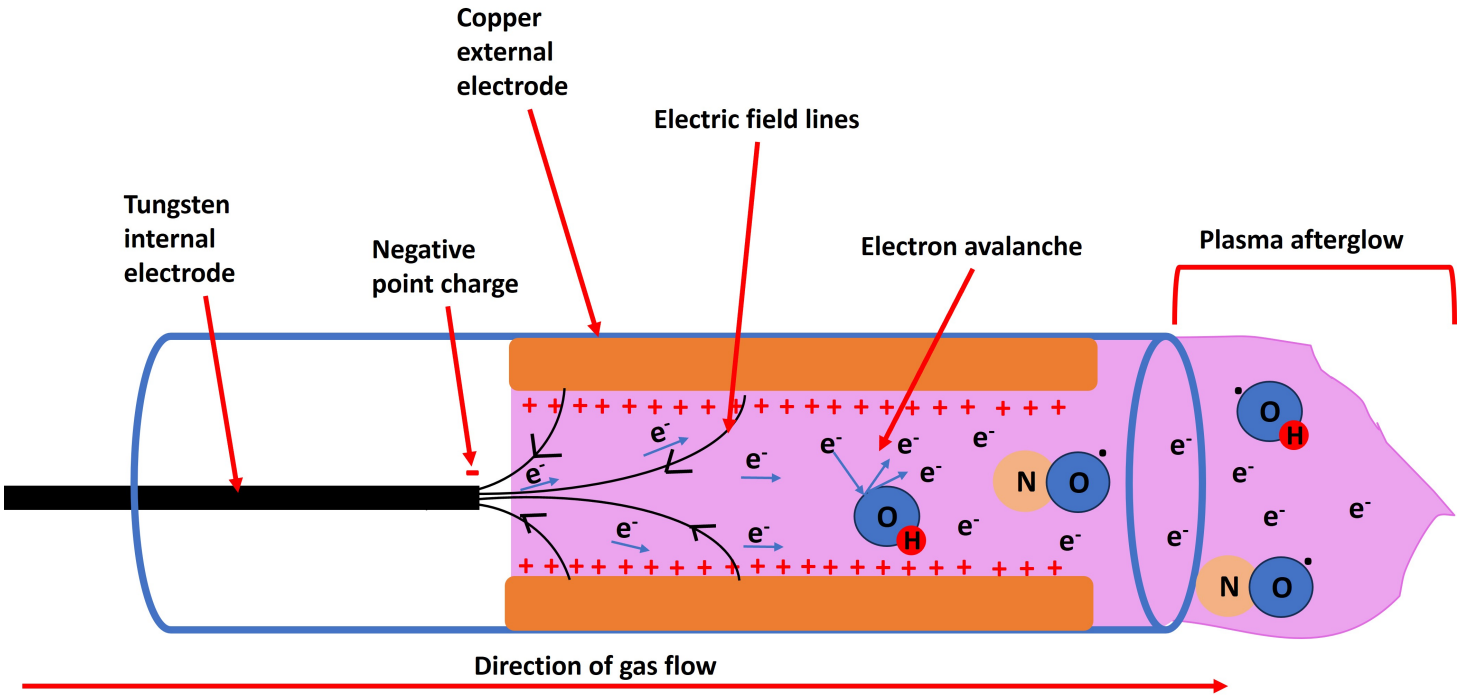

Figure 1.1: Schematic representation of a plasma breakdown inside a plasma pen. The electrons are supplied by the internal tungsten electrode and are attracted to the positive charge on the copper external electrode. As the electrons proceed down the length of the quartz tube, they collide with other molecules, knocking electrons out of their orbitals and creating radical species such as ·OH and NO·. The section of the plasma which extends beyond the end of the copper electrode is known as the 'afterglow'.

When oxygen and nitrogen are present in a plasma, Reactive Oxygen and Nitrogen Species (RONS) are formed. It is these RONS which interact with the target, often referred to as direct treatment, or are imparted into a liquid to create a Plasma Activated Liquid or PAL, often referred to as indirect treatment. Direct plasma and PAL based treatments may utilize different types of RONS. Many RONS present in plasma plumes are radicals with very short half lives such as superoxide and hydroxyl radicals [42], however PALs tend to contain more of the longer lived species such as hydrogen peroxide and nitrite/nitrate ions [24], [99]. For a comprehensive review of the chemistry of PALs see [37], [55], [128] and [33]. Some early studies have shown that PAL may have greater cytotoxic effect than solutions of equivalent H_2O_2 and NO_2^- [48], [58], however an increasing number of studies are indicating that these PAL analogues have equivalent cytotoxicity to PAL ([35], [99]).

Evidence continues to accumulate to support the efficacy of plasma and PAL treatment in cancer therapy ([66], [89], [84]). The current literature reports that plasma and PAL have selective cytotoxic effects, killing malignant cells while sparing healthy tissue. For example evidence is provided by Kurake *et al* [48] who found increased survival of normal human breast epithelial cells compared to human glioblastoma cells for the same treatment times. This effect is further supported by Mohades *et al* [67] who reported less toxicity for healthy canine kidney cells compared to squamous cell carcinoma cells, even though the non-malignant cells received longer treatment times. Biscop *et al* [8] argue that selective induction of apoptosis in malignant cells versus normal cells can only truly be assessed by comparing cells of the same tissue type (eg. prostate cancer and non-malignant prostate cells) and that more complex culture media, which is required for some non-malignant cell types, may contain more ROS scavengers than regular media, which may influence this apparent 'selectivity' in response.

Although the *in vitro* data demonstrating this selective cytotoxic effect may be debated, the *in vivo* mouse data shows selective tissue sparing and good tolerance ([72], [129], [121], [89]), particularly [22] showed no negative effects on healthy organs after acute and longer term administration of plasma activated saline. Schuster *et al* and Metelmann *et al* ([93], [92], [63]) have also shown tissue sparing, good tolerance and few side effects of direct plasma treatment in the few clinical trials which have been performed to date.

A key drawback of direct plasma treatment is depth of penetration as the radicals generated during direct plasma treatment have been shown to penetrate less than 1.25 mm [24], limiting access to the desired target. The potential advantage of using PAL is in the ease and speed of focused application via injection ([22], [72]). PAL may be an alternative or adjunct treatment in cases where a liquid therapy is already utilized, such as in the case of the commercialised KORTUC radiosensitisation method developed in Japan [77]. The KORTUC method revolves around two central ideas: that H_2O_2 produces oxygen microbubbles upon contact with tissue [77] and that it is a requirement for oxygen to be present in a tumour in order for oxygen based radicals to be produced during irradiation [36]. By combining the H_2O_2 with hyaluronic acid for an intratumoural injection, the KORTUC method is able to maintain elevated intratumoural oxygen levels for 24 hours after injection, sensitising these tumours to doses of ionising radiation [5], [4]. It is known that the general population exhibits a range in radiation sensitivity [43], therefore there will be a sub-population who would benefit from a selective radiosensitisation method to spare healthy tissue, making this an interesting avenue of research.

There is a gap in knowledge in the literature here: if PALs contain hydrogen peroxide as well as other radical species, does the therapeutic effect of PAL treatment influence the therapeutic effects of ionising radiation and if so how are these interactions quantified? Henceforth, for the sake of simplicity, the phrase 'interactions between PAL and ionising radiation' will be used to indicate 'interactions between the therapeutic effects of PAL and the therapeutic effects of ionising radiation'. A handful of studies have examined the interaction between direct plasma and radiation treatment [51], [70], [80], [70], [49], [47], [100], however to the best of the author's knowledge at the time of writing there is no study quantifying the interaction between PAL and radiation.

The aim of this project was to determine the ability of PAL therapy to enhance the cytotoxic effects of radiation therapy on two radioresistant cancerous human cell lines. The DU 145 hormone resistant prostate cancer cell line was chosen as the first radioresistant cell line in this study. In clinical practice, prostate cancer is one of the most common cancers in men and those that fail first line therapies are often hormone resistant and more difficult to treat successfully [120]. Melanoma, represented by the MM576 cell line, is another cancer which has been difficult to treat and is well-known for its radioresistance [38]. The immortalised normal prostate cell line PNT1A was chosen to assess the cytotoxic enhancement of PAL and radiation on normal cells.

As ionising radiation is a commonly used therapeutic strategy in cancer treatment, it is important to investigate any potential synergistic or antagonistic interactions between PAL and radiation *in vitro* prior to progression into more complex systems. In the assessment of therapeutic interactions, it is vital for clinical translation to have a well defined and rigorous framework to indicate the presence or absence of any interactions, as well as the extent of these interactions. This study used a metric for assessing the presence and the magnitude of synergistic interactions between two therapies based upon the Multiplicative Survival Principle (MSP) originally proposed by Bliss [9]. Two methods for evaluating this synergy metric (both based upon the MSP) were employed to assess interactions between PAL and radiation in three human cell lines. In order to assess the potential for further clinical translation, the effect of changes to administration and dose on the presence of synergy were also examined. Both methods of assessing the synergy metric were employed to determine the presence and extent of interaction when the order of administration of PAL and radiation were reversed.

To conduct this project, a device for the plasma activation of liquid was designed, built and characterised. Key criteria of our system were to design an instrument which: is clinically compatible, operates at atmospheric pressure to avoid the need for a vacuum system, uses argon gas which is much less expensive than helium, while still facilitating plasma breakdown at atmospheric pressure, and uses a commercially available neon light power supply to enhance portability of the system and improve affordability.

A range of experiments were conducted to optimise the configuration of the pen and liquid treatment which are summarised in Chapter 3. Most plasma medicine papers in the literature generated PAL in an open topped vessel with the plasma pen directed onto the surface of the liquid. Some agricultural and antimicrobial studies have used underwater discharges, using bespoke devices and equipment [88]. Many reports using above surface treatment demonstrated that an increased distance between the liquid surface and the plasma plume reduced the concentration of reactive species and/or cytotoxic effect of the liquid [104], [48]. This was further supported by El Shaer *et al.* [25] who showed greater H_2O_2 production from

a subsurface treatment compared to above surface treatment. Thus it was decided to create a device for the subsurface plasma treatment of liquids. Chapter 4 describes the measurement of the energy deposited in the plasma using calorimetry.

Experiments were conducted to assess the effect of PAL exposure time and concentration on each cell line which are detailed in Chapter 5. Once these were established, a dose of radiation and a concentration of PAL were selected for combination therapy experiments which were assessed for synergy using the methods described above. In addition, in Chapter 6 the synergy metric was applied to assess the differences between PAL and H_2O_2 as radiosensitising agents and the importance of the order of therapy administration. This thesis concludes with a discussion of possible mechanisms of PAL induced cytotoxicity.

Chapter 2

General experimental Methods

2.1 General methods

Techniques and protocols that are common to multiple sections of this project are described here to avoid repetition. Any specific modifications will be highlighted at the beginning of the relevant chapter.

2.1.1 PAL generation

A solution of compound sodium lactate, or Hartmann's solution (Fresenius Kabi, Germany), was chosen as the target solution for PAL generation. This solution is commonly used in the clinic and is standard hospital stock. For each experiment, 15 mL Hartmann's solution was treated in our purpose-built plasma syringe system which is depicted and described in greater detail in Chapter 3, at a flow rate of 2.3 L/min of argon for 37.5 minutes in the presence (Plasma treated) or absence (Sham treated) of a plasma plume. The Hartmann's solution was drawn up into a 60 mL polypropylene syringe modified with a side-port to allow attachment of the plasma pen for direct contact between the plasma plume and the treatment liquid through sub-surface injection. In order to compensate for any evaporated Hartmann's solution, the volume was adjusted back to 15 mL with deionized water after plasma treatment.

2.1.2 Cell culture

DU 145 (hormone resistant prostate cancer) and MM576 (melanoma) cells were purchased from American Type Culture Collection (ATCC), and the immortalized normal prostate cell line, PNT1A was purchased from CellBank Australia (95012614, Westmead, Australia). The MM576 and PNT1A cell lines were maintained in culture medium: RPMI-1640 medium (Gibco Life Technologies, Australia) and the DU 145 cells were maintained in EMEM medium with L-glutamine (ATCC); all three were supplemented with 10%v/v foetal bovine serum (FBS) (Gibco Life Technologies, Australia) as recommended by the suppliers. All cell cultures were grown in a humidified incubator with 5% CO_2 at 37 °C and were allowed to reach 50-80% confluence. The culture medium was discarded and adherent cells washed twice with phosphate buffered saline (Gibco Life Technologies, Australia). Cells were then detached using 0.05% trypsin-EDTA solution for 2-4 minutes at 37 °C [27]. The detached cells were centrifuged at 252 x g for 5 minutes at room temperature. No antibiotics or antifungal agents were used in order to avoid introducing confounding factors [83]. As these three cell lines are used repeatedly, the colours used to represent each cell line are consistent throughout the work to enable comparison between chapters. DU 145 is represented in dark pink, PNT1A in purple and MM576 in green.

2.1.3 Resazurin reduction assay

The Resazurin reduction assay measures the metabolic activity of cells as an indirect measure of their viability. Resazurin is a blue, non-fluorescent molecule which is metabolised by cells to a pink coloured, fluorescent molecule resorufin. The change in fluorescence over a set period of time is directly proportional to the number of metabolically active (viable) cells [73]. Cells were seeded in culture medium in a 96 well plate at densities described in Table 2.1 and allowed to adhere overnight. The culture medium was removed and cells incubated with 100 μL sham treated Hartmann's or PAL as described later. The cellular metabolic activity was analysed using a solution of 10% v/v Resazurin solution in culture medium

(Resazurin solution 0.15 mg/mL in PBS, Resazurin powder from Sigma-Aldrich, product number 199303) using a Clariostar microplate reader (BMG LabTech, Victoria, Australia).

Cell line	Culture medium	Seeding density (cells per well)
DU 145	EMEM	4000
PNT1A	RPMI1640	3000
MM575	RPMI1640	3000

Table 2.1: The cells, the culture medium and seeding density used for Resazurin reduction assays.

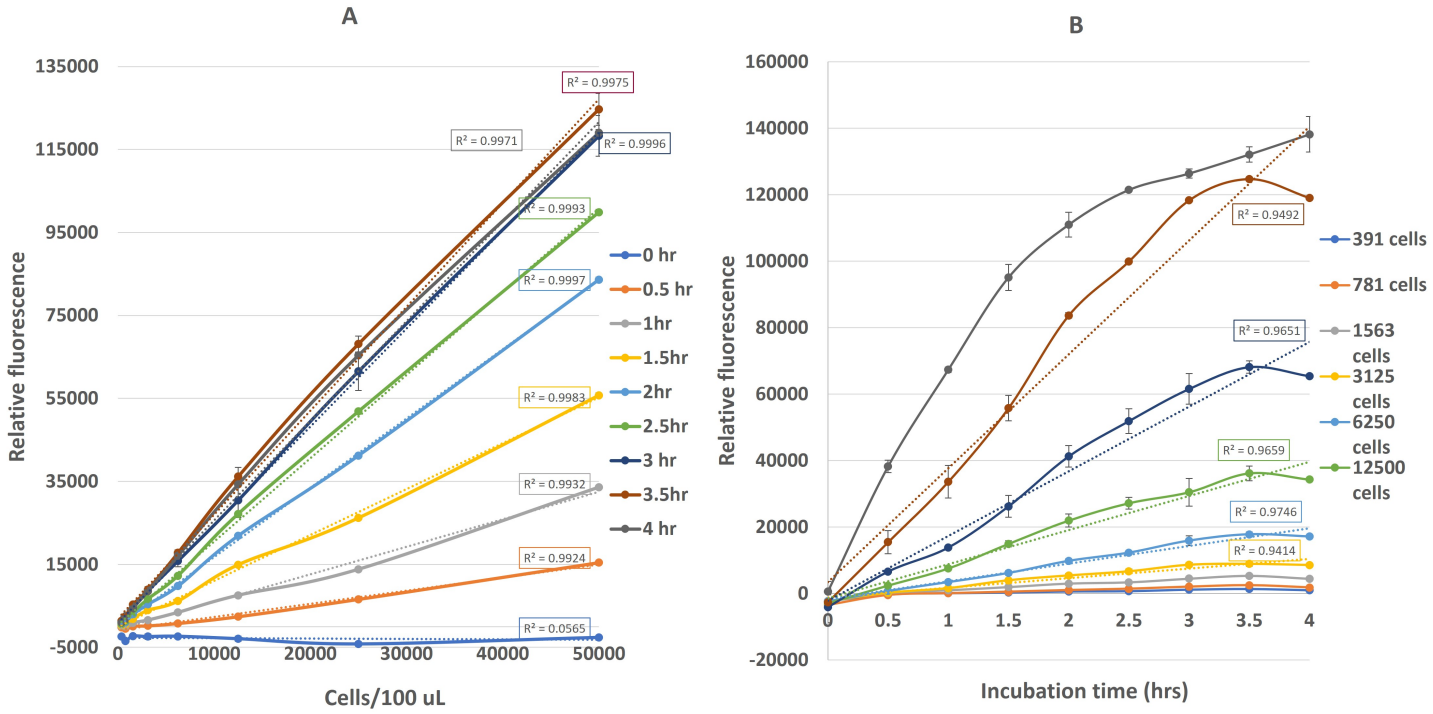

Figure 2.1: Change in resorufin fluorescence with time and cell density as a result of the metabolic activity of DU145 cells. Panel A shows the increase in fluorescence over time is linerly associated with increase in cell density. Panel B shows how the fluorescence changes over time for different levels of cell density.

2.1.4 Clonogenic assay

To quantify interactions between radiation and PAL, a clonogenic assay was used as it is considered the 'gold standard' to measure radiation therapy treatment effects in vitro [27], [10], [60]. After radiation treatment a damaged cell may continue to divide several times, however may ultimately fail to form a colony due to damage caused by radiation treatment. Such cells are considered unable to form a new tumour and are therefore harmless. A cell on a lethal trajectory following radiation treatment may well survive for some time, which explains differences between the outcomes assessed by the clonogenic assay and other assays. The clonogenic assay measures colony forming potential and provides a survival fraction, the number of colonies formed after treatment divided by the number of colonies formed without treatment.

To establish the dose response to individual treatments cells were seeded in culture medium at the densities given in Table 2.2, and allowed to adhere overnight prior to treatment. After treatment, the

cells were then allowed to grow until the staining day as shown in Table 2.2 when the cells were fixed and stained using 3% methylene blue in 70% ethanol or methanol. The seeding density and staining days had been previously experimentally optimised in line with the protocol outlined in Franken *et. al* (2006)[27] to allow the control flasks of each cell line to obtain colony sizes of at least 50 cells without the colonies merging. The number of colonies were counted using a Gelcount^{TM} automated colony counter (Oxford Optronix, United Kingdom). The survival fraction was calculated as the number of colonies after an intervention as a fraction of the number of colonies in the untreated or sham treated group, resulting in a decrease in survival fraction following an increase in dose. Each experiment was repeated at least three times for a total n in the range 9 to 44.

Cell line	**Culture medium**	**Seeding density, cells per well (cells per flask)**	**Staining day post seeding**
DU 145	EMEM	600	8
PNT1A	RPMI1640	750 (1500)	14
MM575	RPMI1640	1500 (3000)	7

Table 2.2: The culture medium type, seeding density and number of days after seeding cells were stained for each of the clonogenic experiments. Values were chosen according to Franken *et. al* (2006) [27] to allow the control flasks of each cell line to obtain colony sizes of at least 50 cells without the colonies merging.

2.1.5 Cell irradiation

Radiation experiments were performed according to the protocols described by Claridge *et al.* in [17] and [16]. The cells were exposed to a 6MV photon beam, produced by either a Varian Clinac 6X$^{(TM)}$ linear accelerator or a Varian TrueBeam$^{(TM)}$ linear accelerator as specified. The dose rate was 6 Gy per minute at a Focus to Axis Distance (FAD) calibrated using a 10cm X 10 cm field size. Cells were seeded in a 6 well plate or T25 cm^2 flask as described in Section 2.1.4. The well plate/flasks were placed on the patient bed of the linear accelerator in the appropriate phantom (shown in Figures 2.3 and 2.4) between two blocks of Solid Water$^{(TM)}$ (5 cm beneath the cell culture flasks and 2 cm above). The gantry angle was set at 180^o to irradiate from the bottom of the well/plate flask at a distance of 100 cm between the radiation source and the cell layer. The size of the irradiated field was 20cm x 20 cm. This setup is shown schematically in Figure 2.2.

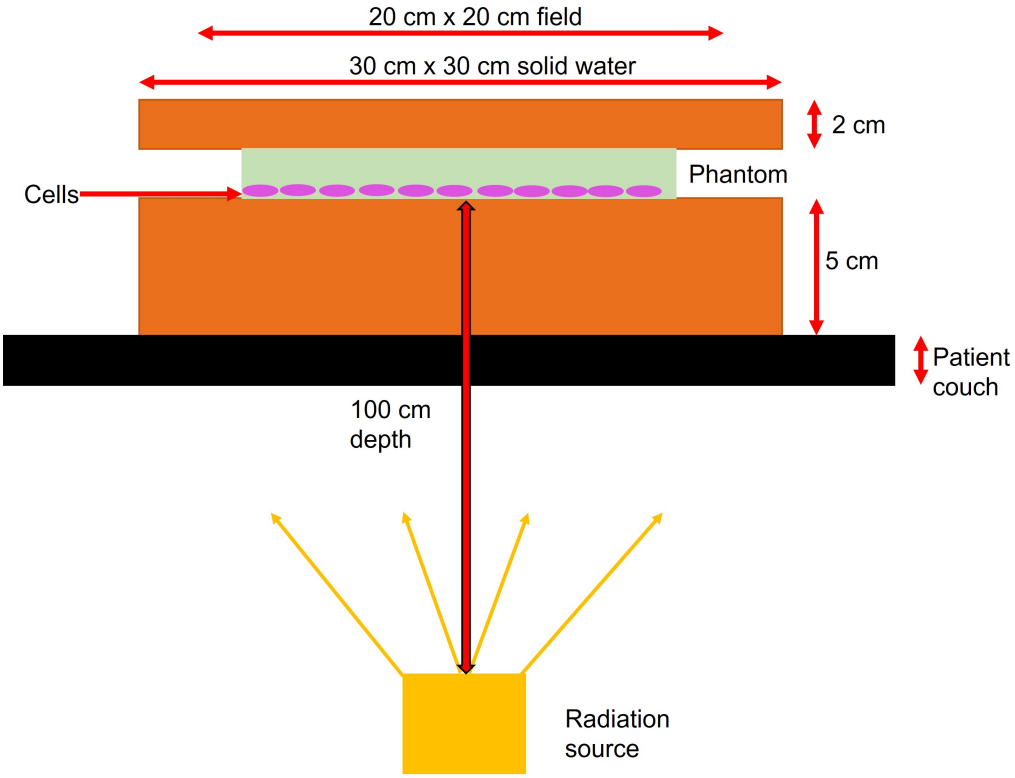

Figure 2.2: Schematic of irradiation setup used to irradiate cells. The phantoms shown in Figures 2.3 and 2.4 were placed between two blocks of Solid Water$^{(TM)}$ (5 cm on the bottom and 2 cm on the top) on top of the patient bench. The cells were irradiated from the bottom (gantry angle 180°) at a depth of 100 cm from the source in a 20cm x 20cm field. This setup was first described by Claridge *et al* [16]

When a photon beam enters a material, the photon interacts with the material to produce secondary electrons (generally referred to as scatter). The degree of scattering changes with the density, thickness and the atomic number of the material and this affects the dose absorbed by the material. A *phantom* is a piece of material which mimics the radiation absorption and scattering properties of the biological tissue of interest and is often used in radiation dosimetry [62]. Phantoms are also used to describe the environment in which the radiation detector is placed for dosimetric measurements, or in our case, the environment in which the well plates/flasks are placed for irradiation.

Water is often used as a phantom by physicists as it is cheap, readily available and its density and effective atomic number are similar to muscle tissue [62], effectively mimicking the behaviour of muscle tissue under a photon beam. Solid Water$^{(TM)}$, used here, is a patented material which possesses very similar properties to water under a radiation beam and is thus used as a water substitute. Claridge *et al.* used radiochromic film to measure the dose uniformity of this setup. They show that surrounding/covering the well plate/flasks with Solid Water$^{(TM)}$ results in a more uniform and accurate absorbed dose to cells across the whole plate/flask compared to when the well plate/flask is surrounded by air [17], [16]. As a clinical radiation beam, its uniformity is regularly tested with a comprehensive quality assurance program.

The well plate/flasks are placed inside custom made phantoms shown in Figures 2.3 and 2.4 and irradiated from below as shown in Figure 2.2. These phantoms act as masks to ensure that the well plates/flasks are reliably positioned inside the radiation field for reproducible results. The phantom for the 6 well plate shown in Figure 2.3 was made from PLA (Raise3D Premium 3D printing filament, 1.75 mm diameter).

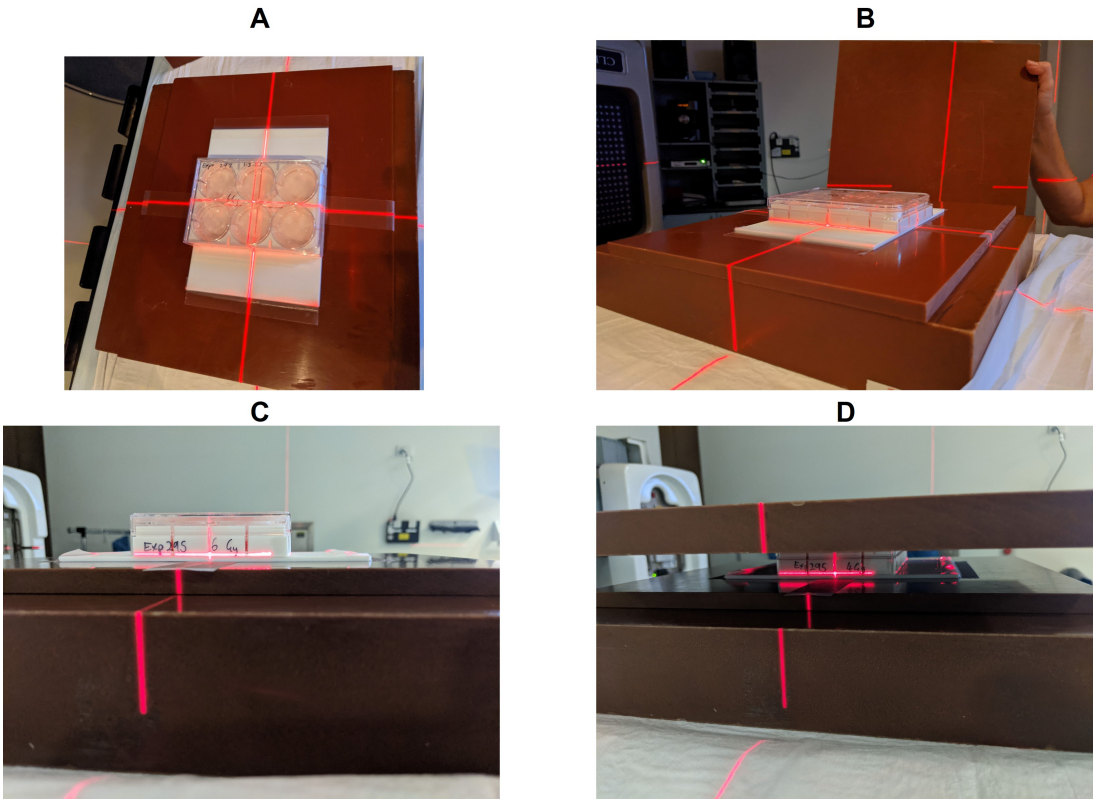

Figure 2.3: Top (A) and side views (B-D) of the 6 well plate phantom (white) 3D printed in PLA (Raise3D Premium 3D printing filament, 1.75 mm diameter). Panels A shows the top-down view of the phantom lined up in the irradiation field. Panels B-D show various side views of the phantom, with Panel D showing the arrangement between the Solid Water$^{(TM)}$ blocks used for irradiation as described in [16] and Figure 2.2.

The phantom for the T25 cm^2 flasks shown in Figure 2.4 was made from perspex and was not 3D printed.

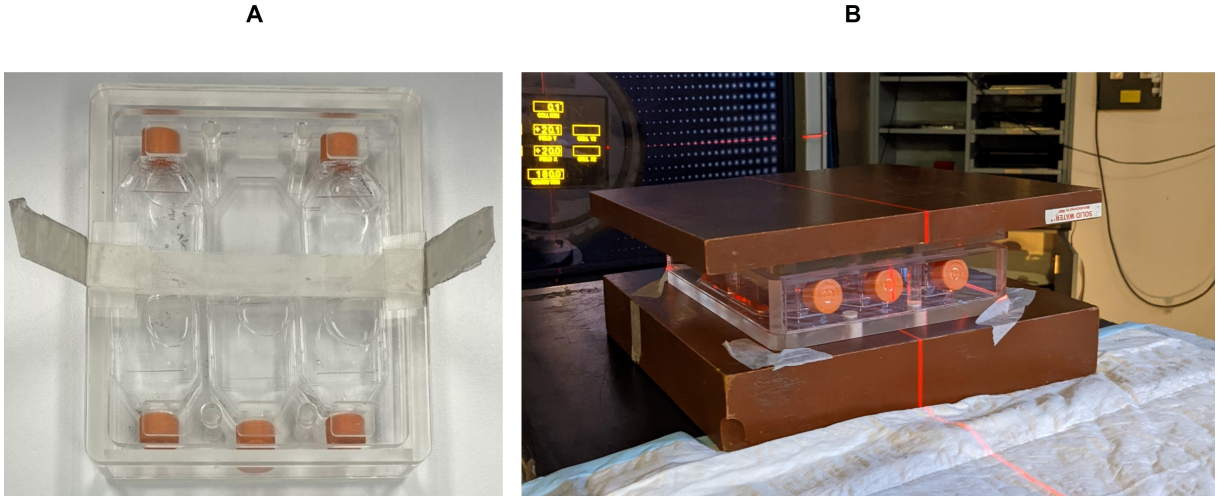

Figure 2.4: Top (A) and side view (B) of the perspex phantom used to irradiate T25 cm^2 flasks as described in [17]. Panel A shows the phantom only, where as Panel B shows the arrangement of the phantom between blocks of Solid Water$^{(TM)}$ on a linear accelerator aligned in the irradiation field as shown in Figure 2.2.

Irradiation from above allows the photon beam to pass through Solid Water$^{(TM)}$, then a pocket of air between the top of the well plate/flask and the liquid surface before reaching the cells, which may result in a less uniform dose delivered to the cells than irradiation from the bottom which we do in this study [17].

2.1.6 Radiation, PAL and Combination experiments

The culture medium was topped up with fresh medium before irradiation to the volume shown in Table 2.3 to provide sufficient scattering material above the cells. All cells were irradiated at the topped up volume and maintained in this medium without refreshment until staining day. This volume ensures the cells are allowed adequate gas exchange for optimal cell growing conditions and are located within a stable radiation scattering volume.

Seeding vessel	**Seeding volume (mL)**	**Top-up volume (mL)**	**PAL Treatment volume (mL)**
6 well plate	1	5	1
T25 cm^2 flask	5	10	2

Table 2.3: Summary of liquid volumes used in Clonogenic assays in both 6 well plates and T25 cm^2 flasks.

When radiation was the first intervention, the culture medium was topped up just prior to the irradiation. Where PAL or H_2O_2 was the first intervention, the culture medium was removed and replaced with the designated volume of treatment solution (either PAL, sham treated Hartmann's solution or H_2O_2 in Hartmann's solution as specified) in accordance with Table 2.3. Cells were incubated in the treatment solution for 30 minutes before it was removed and replaced with culture medium up to the top up volume and incubated until staining day.

When PAL or H_2O_2 treatment was followed by irradiation, the culture medium was removed and replaced with the designated volume of treatment solution (either PAL, sham treated Hartmann's solution or H_2O_2 in Hartmann's solution as specified) in accordance with Table 2.3. Cells were incubated in the treatment solution for 30 minutes before it was removed and replaced with culture medium up to the top up volume. Cells were then incubated for one hour before immediate irradiation. The cells were incubated until staining day without medium refreshment.

When irradiation was followed by PAL or H_2O_2, the culture medium was removed one hour after irradiation, replaced with the designated volume of treatment solution (either PAL, sham treated Hartmann's solution or H_2O_2 in Hartmann's solution as specified) in accordance with Table 2.3 and incubated for 30 minutes. The treatment solution was then removed, replaced with culture medium to the top up volume and cells were incubated until staining day.

2.1.7 Hydrogen peroxide assay

A hydrogen peroxide assay kit (Amplex Red assay kit, Thermo Fisher A22188, Waltham, MA) was used to detect the concentration of H_2O_2 in the PAL after treatment. The Amplex red reagent (10-acetyl-3,7-dihydroxyphenoxazine) is oxidised by H_2O_2 to the red fluorescent molecule resorufin, in the presence of horseradish peroxidase. The fluorescence is proportional to the amount of H_2O_2 reacted, but at high concentrations the H_2O_2 can oxidise resorufin to produce resazurin which is not fluorescent, resulting in a loss of signal. Samples were diluted 1:100 prior to preparation for analysis. Fluorescence measurements were read using a microplate reader (Clariostar microplate reader, BMG LabTech, Victoria, Australia).

2.1.8 Nitrite assay

A nitrite detection kit (Griess reagent kit, Sigma-Aldrich, product code MAK367) was used to quantify the nitrite content in PAL post treatment. Nitrite is reduced to nitrogen oxide using Griess Reagent I. Then, nitrogen oxide reacts with Griess Reagent II, to form a stable product that can be detected by its absorbance at 540 nm. PAL was diluted 1:2 prior to analysis. Absorbance measurements were read using a microplate reader (Clariostar microplate reader, BMG LabTech, Victoria, Australia).

2.1.9 Methylene blue

Methylene blue is a cationic, highly pigmented blue dye commonly used for dyeing cloth and also as a biological stain. When a hydroxyl radical ($OH^{\cdot}$) reacts with the methylene blue cation, this produces a hydroxide ion and a methylene blue radical cation, which is colourless [90]. Contact between a solution of methylene blue and hydroxyl radicals results in the bleaching of the dye in a concentration dependent manner, thus it has been used to assess the hydroxyl radical forming capacity of plasmas ([1], [41]). This has applications in water management for the treatment of dye contamination of waterways, as well as in agriculture for the decontamination of produce [88]. In this project, a 50 mg/L solution of methylene blue was used to assess the efficacy of several plasma treatment devices as a function of treatment time, treatment distance, electrode configuration and gas flow.

Chapter 3

Devices for the generation of a plasma activated liquid

3.1 Introduction

Plasma pens, also known as Atmospheric Pressure Plasma Jets (APPJs), are a form of dielectric barrier discharge, where the dielectric barrier is formed by a tube of some dielectric material, usually quartz or glass, through which gas flows. The specific design of plasma pens reported in the literature varies considerably [125]. The two most commonly used electrode geometries consist of either two external electrodes, or one external electrode and one internal electrode. Each arrangement has its own specific characteristics and features, which can be modified to suit each user's needs. There has been considerable focus on understanding how the characteristics of a plasma are affected by gas flow, gas composition, electrode geometry, voltage and frequency on the characteristics of a plasma [125], [126], [1].

Since Plasma Activated Liquid (PAL) is the focus of this project, the first step is to design and create an instrument for the generation of PAL. Many researchers generate plasma activated solutions in open topped vessels such as well plates, where the plasma pen itself is discharged several centimeters above the liquid surface ([48], [108], [116], [74]). Takeda *et al.* [104] note that increasing the distance between the plume and the liquid surface reduced cytotoxicity, which was further supported by El Shaer *et al.* [25], who found that subsurface treatment by a plasma produced vastly larger concentrations of H_2O_2 than above surface treatment. Thus the aim for this part of the study became the creation of an underwater plasma treatment device suitable for PAL generation in a clinical setting.

3.2 Device design

The first step was to design, build and optimise a plasma pen and then to build and optimise the treatment vessel for PAL. Here 'treatment vessel' refers to the syringe part of the device which contains the liquid; the 'treatment device' as a whole consists of the plasma pen and the treatment vessel. Methylene blue was used as a relative measure of RONS production to assess differences between plasma pen and treatment vessel designs. Once a design for the plasma pen and PAL treatment vessel were optimised, pilot cytotoxicity studies were performed.

3.2.1 Creating a plasma pen

To create a device for underwater plasma treatment, we first needed a plasma pen. Our first approach (the first generation) was a design using two external electrodes for the plasma pen, several variations of which are depicted in Figure 3.1 A-D. These were constructed using a 10 mL polypropylene syringe (though no liquid was involved at this stage), a tube of soda-lime glass with dimensions 8 mm outer diameter (O.D) and 6 mm inner diameter (I.D), copper tape, a RUP6 low frequency pulsed power supply (GBS Elektronik GmbH) and argon gas. Trials of these configurations did not yield the plasma that was desired for our intended application. The plasma was very small, the plume did not extend far beyond the copper tape electrodes (or beyond the end of the soda-lime tube) and it was prone to external arcing.

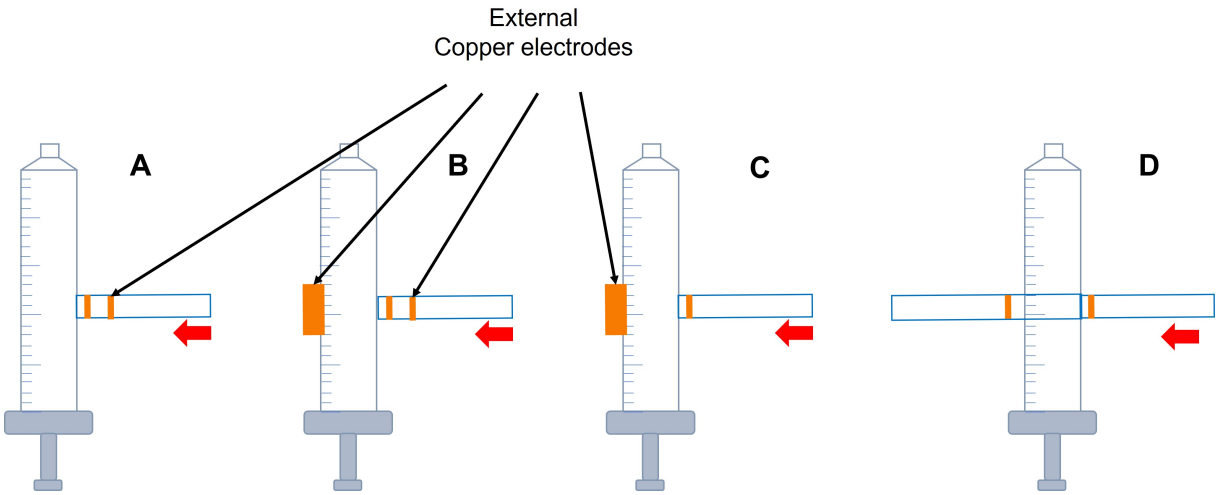

Figure 3.1: Summary of first generation plasma pen and treatment vessel designs utilising external copper electrodes. These designs were created using a 10 mL polypropylene syringe, a first generation plasma pen of soda-lime glass of dimensions 8 mm O.D and 6 mm I.D. Electrodes were made of adhesive copper tape, and a RUP6 power supply was used. Argon gas was passed through the pen in the direction of the red arrow. Liquid was not used in these trials.

In the second generation of plasma pens, the addition of an internal, high voltage electrode improved the plume so that it extended beyond the external electrode and into the body of the syringe. The internal high voltage electrode used in these designs was a copper wire. Schematics of the soda-lime plasma pen using an internal electrode are depicted in Figure 3.2. The T-shaped arrangement in panels B-D were inspired by Lu *et. al* [56], who used a similar plasma pen configuration to propagate a second plasma. This secondary propagation was unsuccessful with our setup, as the voltage required to achieve an initial plasma caused the glass tubes to overheat and break, or create an external arc between the electrodes. The most reliable plasma plume was generated using the design depicted in Figure 3.2E which was then used for all future plasma pens.

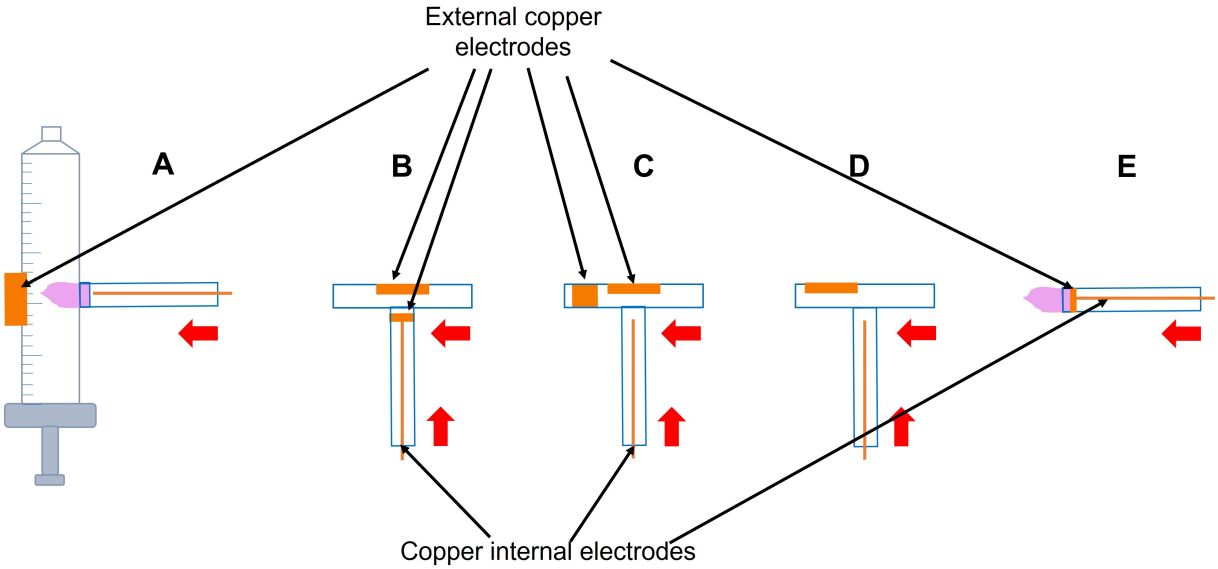

Figure 3.2: Summary of second generation plasma pens and treatment vessel designs utilising internal and external electrodes. These designs were created using a 20 mL polypropylene syringe, a second generation plasma pen of soda-lime glass of dimensions 8 mm O.D and 6 mm I.D. External electrodes were made of adhesive copper tape and the internal electrode was a copper wire. A RUP6 power supply was used and argon gas was passed through the pen in the direction of the red arrow.

Third generation improvements to the design of the device included replacing the soda-lime plasma pen with one of quartz, and replacing the copper high voltage internal electrode with one of tungsten. Both tungsten and quartz are higher durability and more refractory materials with higher melting points than soda lime and copper. The higher refractory nature of the tungsten electrode results in fewer tungsten ions contaminating the plasma, which was a concern using the copper internal electrode due to the lower melting point of copper.

Turbulent gas flow was found not to be conducive to the formation of the plasma plume. Due to the diameter of the soda-lime tube, it was found that the gas flow was already turbulent when the flow rate was sufficient to ignite the plasma as shown in Table 3.1. Changing from soda-lime to quartz glass facilitated plasma ignition and the reduction in diameter allowed for stable plasma generation in the laminar flow region, assisting the stabilisation of the plasma plume.

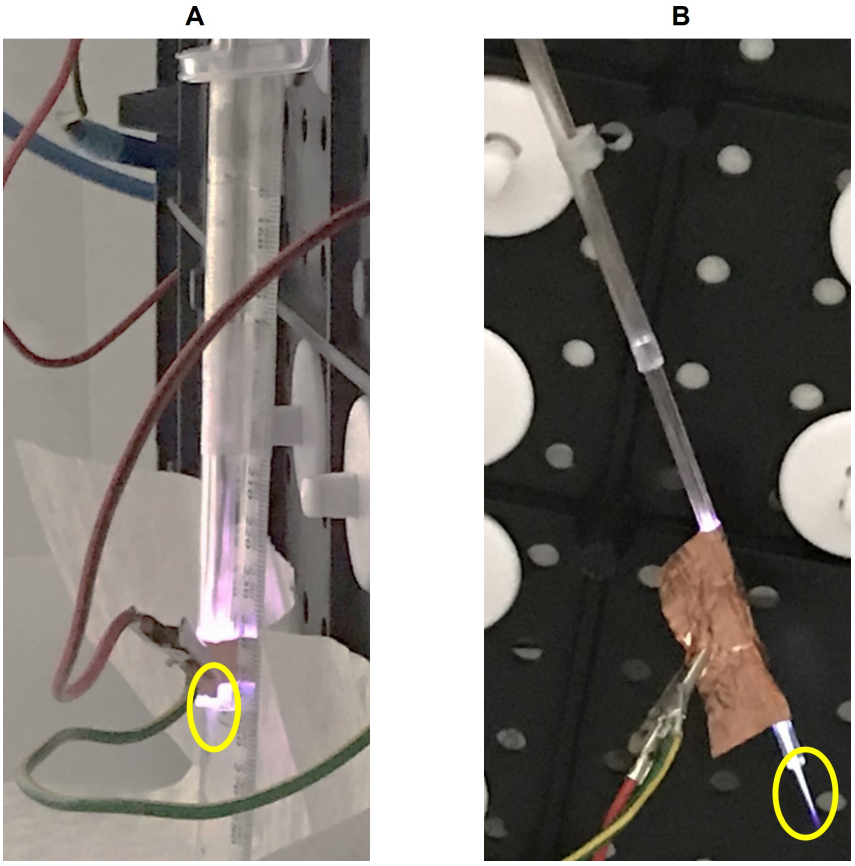

Figure 3.3: Plasma plumes (circled) generated by the second generation soda-lime pen with copper internal electrode (Panel A) and the third generation quartz pen with tungsten internal electrode (Panel B). The plume generated by the quartz pen is vastly superior to the soda lime pen. Both were activated using the NeonPro neon light power supply.

The RUP6 was also replaced with a NeonPro, a commercially available neon light power supply (details in Chapter 3, Section 3.2.3). The NeonPro greatly assisted our efforts in making this device portable, affordable and compatible with the clinincal environment.

Characteristic	**Soda-lime pen**	**Quartz Pen**
Inner Diameter (mm)	6	2
Ar flow rate (L/min)	20	1.5
Ar flow speed (m/s)	31.8	7.9
Ar gas density (kg/m^3)	1.784	
Dynamic viscosity of Ar	2.23x10^{-5}	
Reynold's Number	15278.4	1273.6

Table 3.1: Comparisons of pen characteristics and Reynolds numbers for two different plasma pens. A Reynolds number <2000 indicates gas flow in the laminar region and >2000 in the turbulent region [1].

3.2.2 Plasma liquid interactions

To test whether the design of the second generation plasma pen depicted in Figure 3.2E generated a plasma of optimal performance for further experiments, the RONS production by the pen was established. RONS production is a key measure of the device performance as it is the RONS which are responsible for the cytotoxic effects of plasmas and PALs. A 50 mg/L stock solution of Methylene blue in water described in Chapter 2, Section 2.1.9, was used as a relative measure of radical production under various conditions. The methylene blue molecule is destroyed by hydroxyl radicals produced in a plasma. This results in the bleaching of the blue colour of the solution, which can be quantified using the absorbance of light at 660 nm. Methylene blue is not bleached by H_2O_2 at concentrations under 3% [90].

Figure 3.4 shows how the second generation soda lime plasma pen reduced the absorbance of the methylene blue solution at 660 nm. 100 μL of a 50 mg/L methylene blue solution was placed on the treatment stage directly below the plasma pen at a distance of 1 cm from the end of the soda-lime tube (Figure 3.4A). Argon flow was approximately 20 L/minute, for a total treatment time of 120 seconds. The treatment stage in Panel A was a flat piece of polystyrene. Due to high gas flow during both plasma and sham treatment of the methylene blue solution, a significant proportion of the solvent evaporated. The evaporation increased with increased treatment time, resulting in a higher absorbance for the sham treated methylene blue than the stock solution.

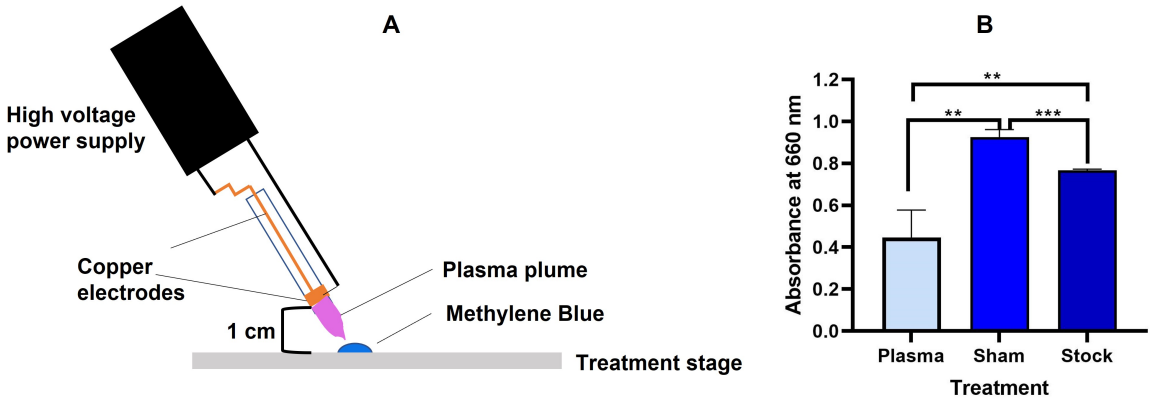

Figure 3.4: Panel A depicts the plasma pen set up for treatment of methylene blue for ultra low liquid volumes as droplets. Panel B shows the change in absorbance at 660 nm after plasma and sham treatment. Plasma treatment resulted in a statistically significant reduction in absorbance compared to sham treatment. Here 'Stock' refers to the 50 mg/L solution of methylene blue used as the starting concentration. These experiments were conducted using the second generation of plasma pen (soda-lime plasma pen with copper internal electrode); the power supply was the NeonPro neon light power supply. Stars indicate significance (** = $p < 0.01$, *** = $p < 0.001$).

To minimise evaporation of the solution, the above test was repeated using 100 μL methylene blue solution in a polystyrene 96 well plate. A range of treatment times were used to determine the extent of methylene blue bleaching over time.

Figure 3.5 shows the changes in absorbance at 660 nm when the time of treatment was altered. The experiment was performed as above using a 96 well plate as the treatment stage. As expected, the absorbance decreased with increasing plasma treatment time. Evaporation still occurred, though to a lesser extent than on the flat treatment stage. These results confirmed findings from the literature and supported further use of methylene blue could be used as a measure of the $^{\cdot}$OH radical production under various conditions.

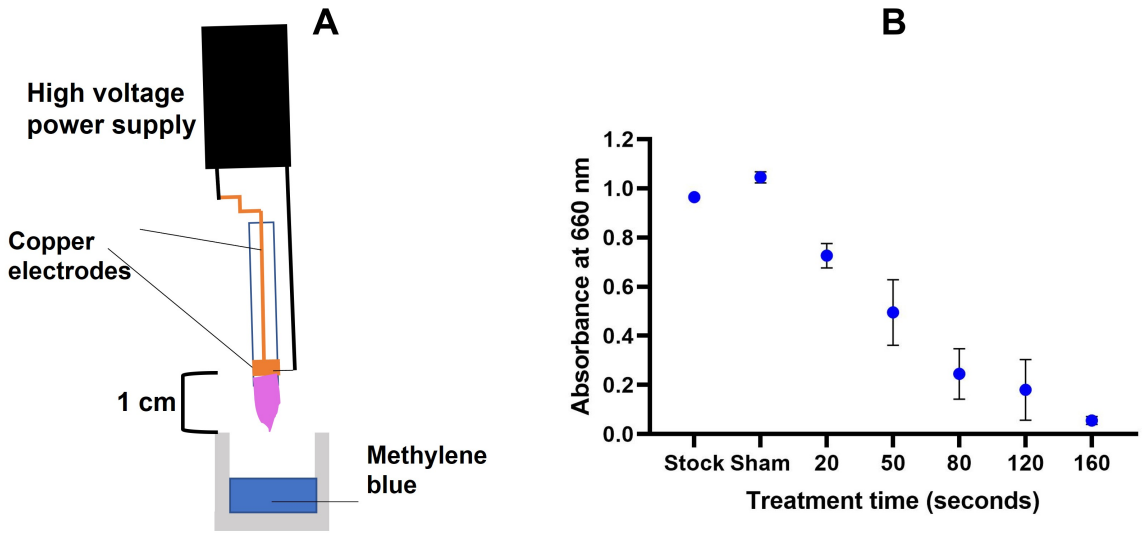

Figure 3.5: Panel A depicts the set up for plasma pen treatment of methylene blue for small volumes in a 96 well plate. Panel B shows the change in absorbance at 660 nm after plasma and sham treatment, showing that increased treatment time decreased methylene blue absorbance. These experiments were conducted using the second generation of plasma pen (soda-lime plasma pen with copper internal electrode); the power supply was the NeonPro neon light power supply. Error bars represent the standard deviation for $n = 3$ experiments.

The experiments in Figures 3.4 and 3.5 show proof of concept: the RONS from our plasma pen are sufficient to bleach methylene blue in small volumes. However to use PAL in clonogenic assays, a much larger volume of PAL was required. When treating larger volumes in vessels such as a 6 well plate, the gas flow displaced the liquid so that the plume treated the bottom of the plate rather than the liquid. Disrupting the surface via stirring or rocking improved the contact between the liquid and the plasma (data not shown), though there was no single superior method. Plasma-to-liquid distance in these cases was still an important factor affecting methylene blue bleaching efficiency. A distinct issue when performing treatments in open vessels over a surface was the treatment angle. As the electrodes are not covered, directing the plasma pen onto a surface at a 90^o angle resulted in argon gas being reflected back along the axis of the pen and resulting in arcing between the plasma and the copper tape electrode. This arcing was prevented when treating at an angle, or by using a barrier to direct the gas flow away from the electrode as shown in Figure 3.6. These factors combined re-confirmed the advantage of using subsurface treatment in an enclosed system rather than above surface treatment.

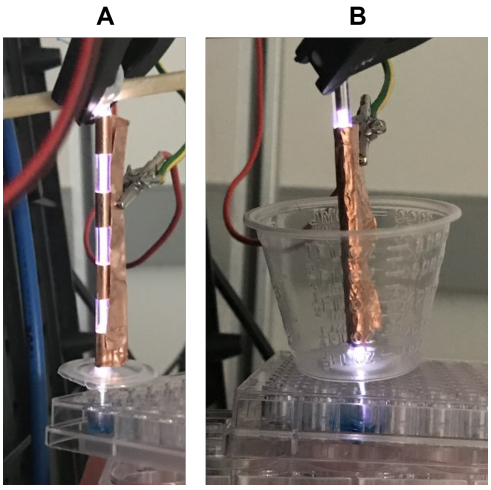

Figure 3.6: Examples of methylene blue bleaching experiments conducted with gas shielding to protect from arcing. Panel A shows a flat shield and panel B shows an extended shield extending further along the pen. The plasma pen shown in this image is a third generation quartz pen with tungsten internal electrode.

Several designs (Figure 3.7) were considered for the attachment of the third generation plasma pen to the treatment vessel with the following characteristics: allow for the greatest contact between plasma and liquid, agitate the liquid to improve reactive species distribution, protect the plasma pen from gas reflected along the axis of the pen during treatment, minimise evaporation and retain functionality and robustness. For the sake of functionality and to minimise the risk of arcing, designs A-C in Figure 3.7 were discarded in favour of design D, which is depicted in greater detail in Figure 3.11.

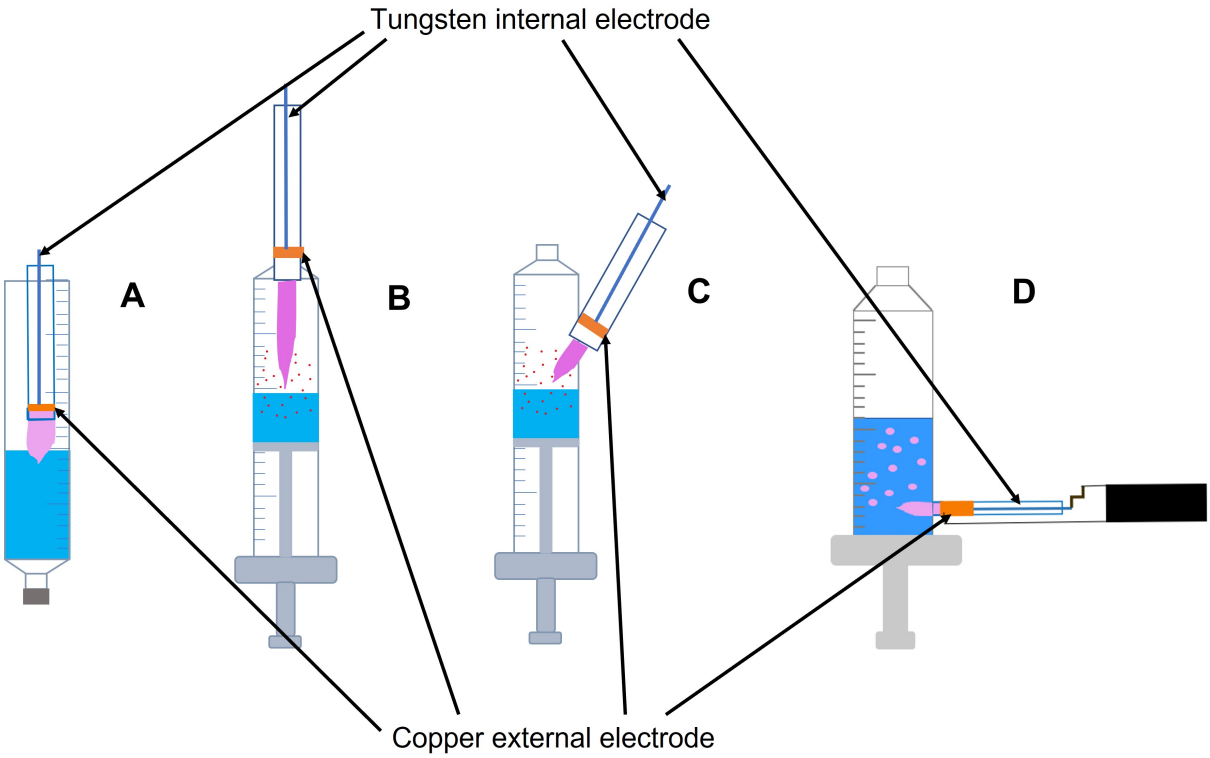

Figure 3.7: Summary of alternate third generation treatment vessel designs for incorporation into the plasma treatment device. Design D was the final design used for experiments. This design was created using a 60 mL polypropylene syringe, a third generation plasma pen of quartz glass of dimensions 4 mm O.D and 2 mm I.D. External electrodes depicted were made of adhesive copper tape and the internal electrode was a tungsten wire. The power supply was the NeonPro neon light power supply.

Figure 3.9A depicts the first methylene blue bleaching trial performed using the third generation plasma pen and the treatment vessel design from Figure 3.7D in a 20 mL syringe. This trial assessed the methylene blue bleaching efficacy of each electrode setup shown in Figure 3.8. 3 mL of a 50 mg/L methylene blue solution was loaded into the syringe and treated for 5 minutes at an argon flow rate of 1.4 L/min, n=3.

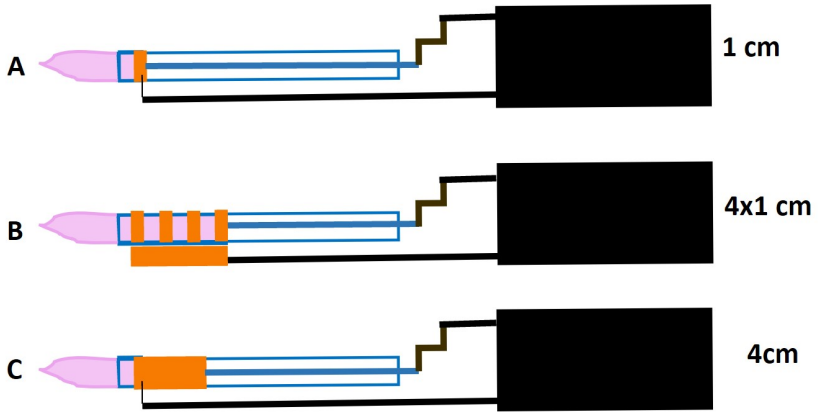

Figure 3.8: Alternative electrode configurations for the third generation plasma pen tested for the most efficient ·OH generation. Design A consisted of one 1 cm copper tape external electrode and a tungsten coaxial internal electrode. The external electrodes in Design B were modified to consist of 4x1 cm copper tape external electrodes inspired by [125], and was found to have similar efficacy as design C, though the electrodes were less robust. The external electrode in Design C was a 4 cm piece of copper tape and was ultimately the configuration which was decided upon. For all designs the tungsten electrode ended 1 cm before the copper tape began, depicted in Figure 3.11 and for these experiments the power supply was the commercially available NeonPro neon light power supply.

Figure 3.9B shows the same experiment repeated for the 60 mL syringe, using 10 mL methylene blue treated for 5 minutes at an argon flow rate of 0.78 and 2.3 L/min respectively. Although the results from 3.9B are not statistically different, the higher gas flow rate appeared to increase the bleaching of the methylene blue. The 4x1 cm electrode appeared to be the most effective at bleaching the methylene blue (non significant), however the 4 cm electrode was more robust during treatment (the small pieces of copper tape used for the multi electrode pen fell apart easily). The largest and most stable plume was achieved with 2.3 L/min gas flow (Reynolds number = 1952) for both the 4x1cm and 4 cm electrode designs. Images of the plasma plumes in the syringe showing changes in gas flow rate and electrode design are summarised in Figure 3.10. These results, taken together with the effect of the electrodes on the plume length and stability described above resulted in the large, single electrode becoming the optimal plasma pen design for all future experiments in this study.

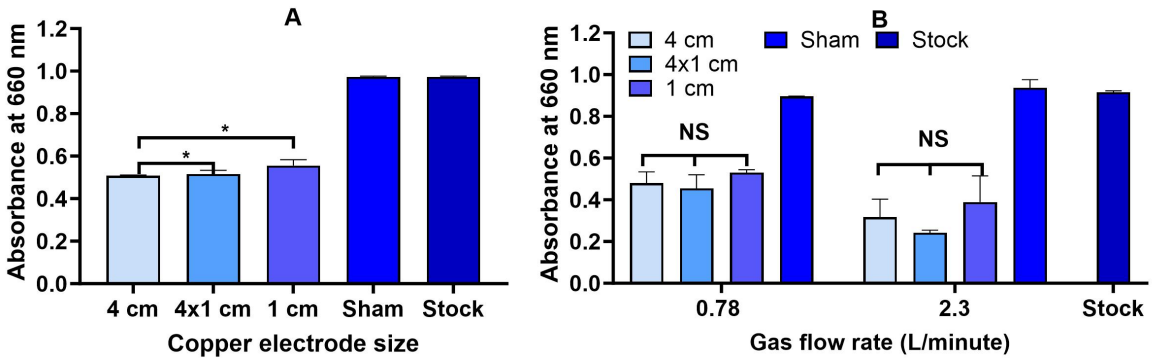

Figure 3.9: Panel A shows the reduction in absorbance at 660 nm after changing the electrode configuration to bleach 3 mL 50 mg/mL methylene blue (Stock) in a 20 mL syringe. Panel B shows the results of the same experiment repeated in a 60 mL syringe with 10 mL methylene blue solution and the addition of variable gas flow rates. Increased gas flow increased methylene blue bleaching. For these experiments the third generation quartz plasma pen with tungsten internal electrode was used.

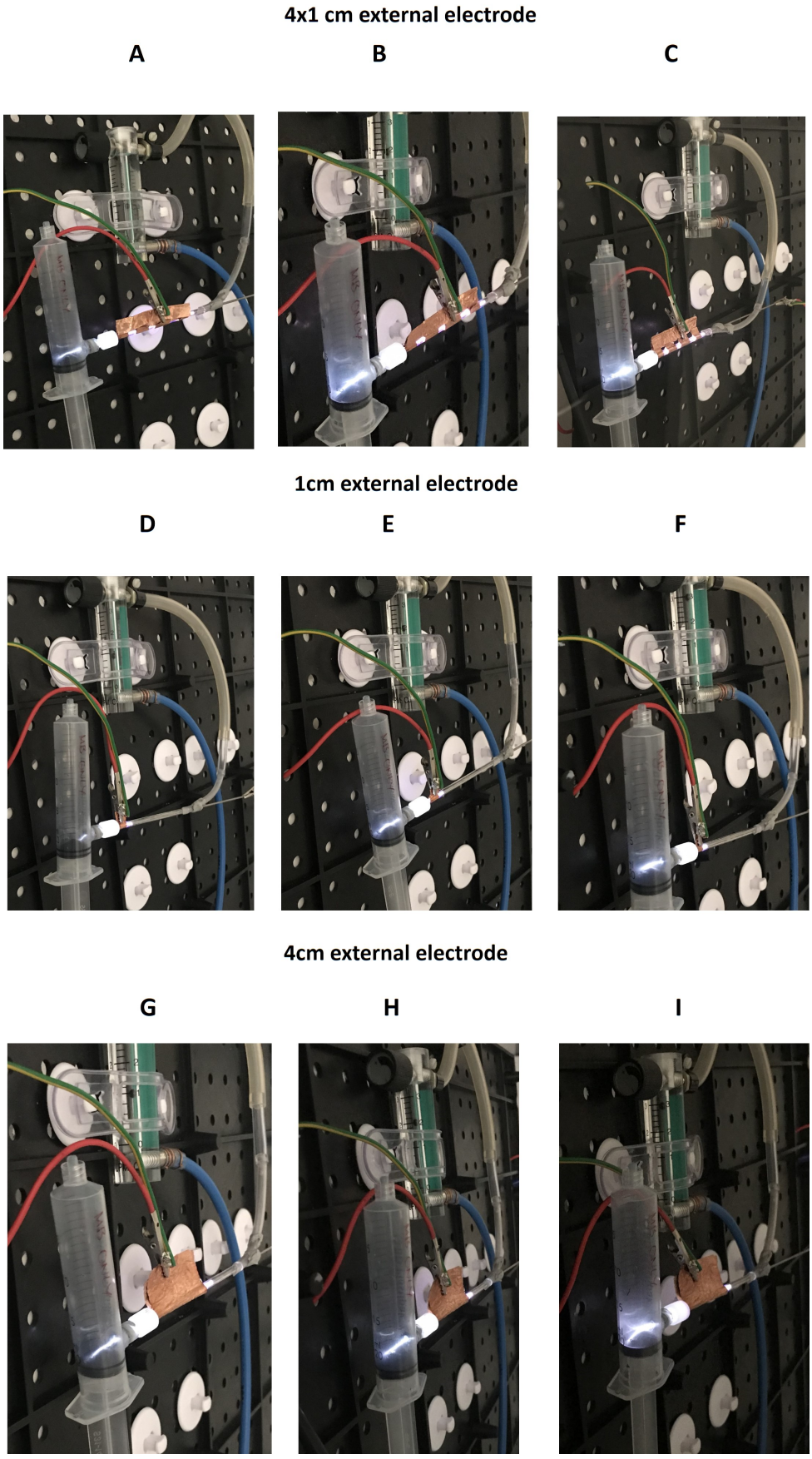

Figure 3.10: Effects of variations in the gas flow and electrode configuration on the length of the plasma plume. Electrode configurations are depicted in Figure 3.8. The plasma pen used here is a third generation plasma pen of quartz and an internal tungsten electrode. The same syringe was used for all three plasma pens; the syringe is a 20mL polypropylene syringe with a 21.3mm outer diameter [94].

3.2.3 Final device design

The PAL treatment device, depicted in Figure 3.11, consists of two main parts: the plasma pen and the treatment vessel (the syringe body). The plasma pen consists of a 10 cm quartz glass tube with outer and inner diameters of 4 mm and 2 mm. A tungsten electrode was passed coaxially through the tube, and a 40 mm copper tape electrode was placed around the outside of the tube. The tungsten electrode ends 1 cm before the copper tape begins. The electrodes are attached to a Neolite NeonPro power supply (NP-7500-30). The NeonPro power supply has an input of 240 VAC, 50/60 Hz, 300 mA and a nominal AC output of 30 mA, 7.5 kV (peak to peak) at 20 kHz. A load resistor (200 kω) was connected in parallel to the plasma pen to act as a dummy load to enable power supply activation. A custom current transformer (see Chapter 4 for details) was placed in series between the load resistor and the copper tape electrode to measure the current. When argon gas was passed through the quartz tube ($\sim$2.3 L/min) a capacitively coupled plasma discharge was observed in the tube. The syringe was a standard luer lock, 60 mL disposable syringe which was modified to include a side port near the base of the syringe. The plasma pen was fitted with a modified cap to allow the pen to be attached and removed from the side port.

There are several advantages to this design. It allows the plasma plume to make direct contact with the treatment solution through sub-surface injection. The end of the quartz tube does not protrude into the barrel of the syringe, so as to allow standard operation of the plunger during filling and transfer of solution. Having the plasma pen attach near the base rather than at the top allows the user greater flexibility with treatment volume and the bubbles mix the solution as they rise. Using the syringe as the treatment vessel reduces the evaporation during long treatments, and reduces volume loss due to splashing while still allowing the gas to exit the device. Designing the device to separate into two pieces allows for individual parts to be replaced in the event of breakage and allows the pieces to be cleaned and stored more safely.

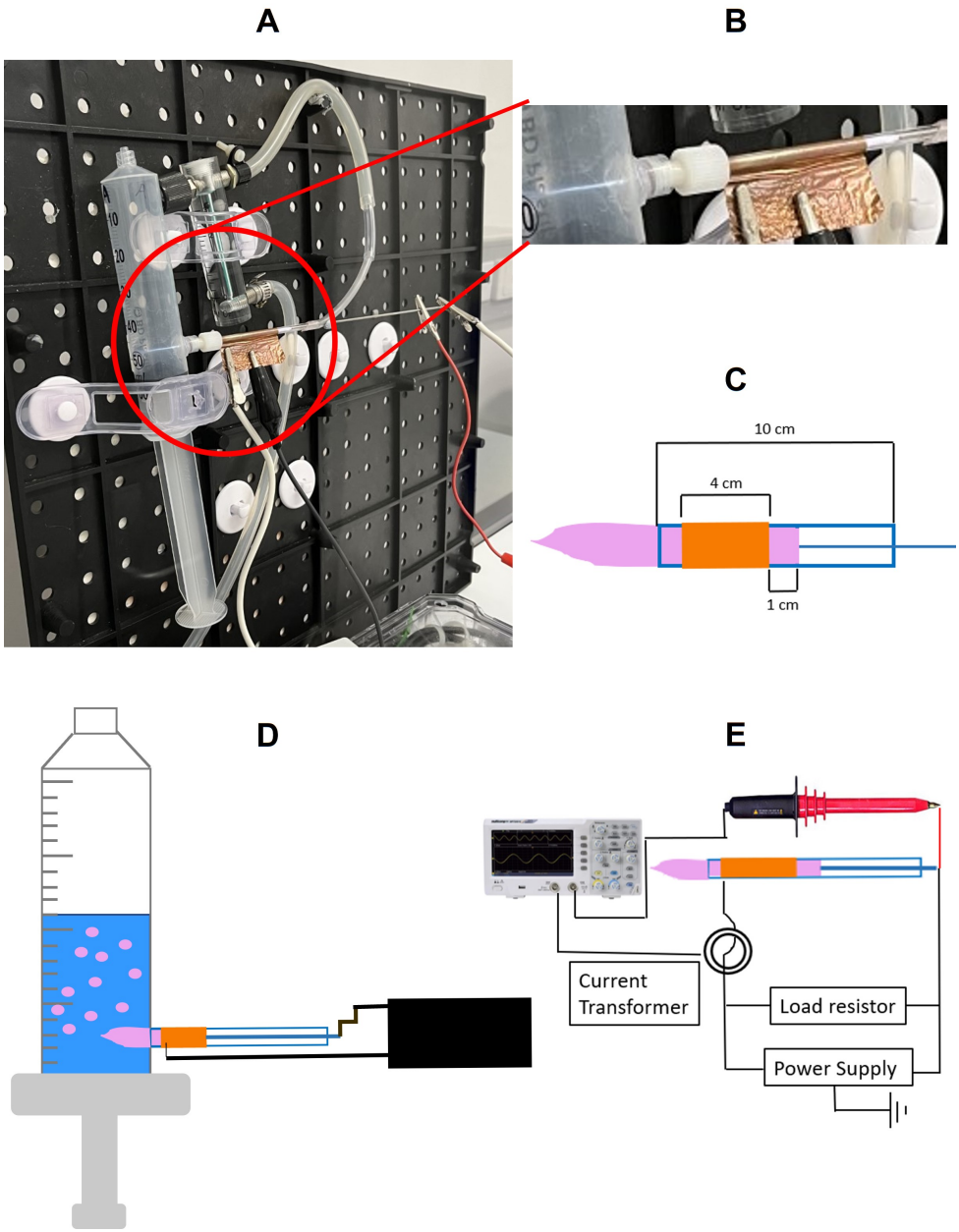

Figure 3.11: The plasma syringe device showing A) a photograph of the complete plasma syringe system attached to a mounting board B), an enlargement of the plasma plume inside the syringe in air C) a schematic diagram of the plasma pen, D) a schematic of the whole plasma treatment device from Figure 3.7D and E) the electrical circuit diagram.

Figure 3.12 depicts an unused plasma treatment vessel. During the making of the syringe, the side port slipped as the glue was drying so that the opening into the syringe body was semi-obstructed and thus disrupted the plasma flow into the syringe. This obstructed opening led to this filamentary discharge, reminiscent of a plasma ball seen in science museums. It is unknown what exactly led to this kind of discharge, though obstructed and possibly turbulent gas flow in the treatment vessel is thought to play a role as all other conditions were kept the same as the other syringes.

Figure 3.12: Photograph of a unused version of the plasma treatment vessel design from Figure 3.7D with the quartz plasma pen (O.D. 4 mm I.D. 2 mm) and the power supply was the commercially available NeonPro neon light power supply. The side port slipped so that the opening into the syringe body was semi-obstructed, resulting in this filamentary discharge.

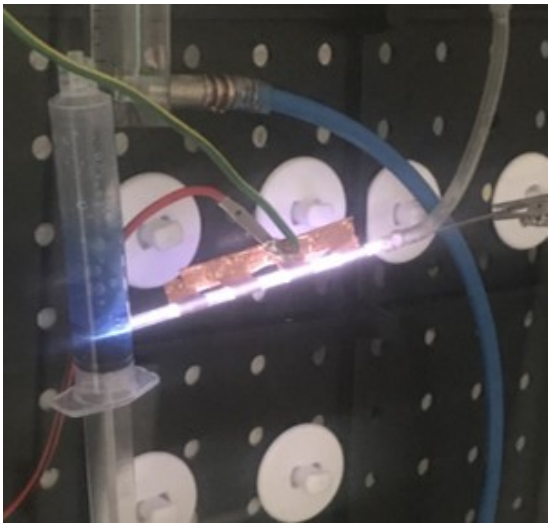

Figure 3.13: Subsurface plasma treatment of methylene blue in the syringe device.

3.3 Pilot cytotoxicity studies

Using the optimised third generation quartz plasma pen (Figure 3.11 to generate PAL using methods described in Section 2.1.1 it was possible to perform initial pilot cytotoxicity studies. It is known from Section 3.2.2 that the RONS generated by the plasma pen are able to bleach methylene blue. It was hypothesised that these RONS imparted to the PAL for sufficient time would be cytotoxic to cells.

The pilot cytotoxicity study of our PAL consisted of a time course of exposure and a dilution series to both sham treated and plasma treated phosphate buffered saline (PBS). Previous to this, only solutions of methylene blue had been plasma treated in our device, so the plasma treatment and cell exposure times necessary to elicit a response were unknown. The maximum plasma treatment time for the methylene blue was 5 minutes for 3 mL of solution, however this first cell experiment required a greater volume (6mL) and to ensure the plasma treatment time elicited a response it was treated for 15 minutes. For the sham treated PBS, 6mL of PBS was treated with Argon gas only for 15 minutes.

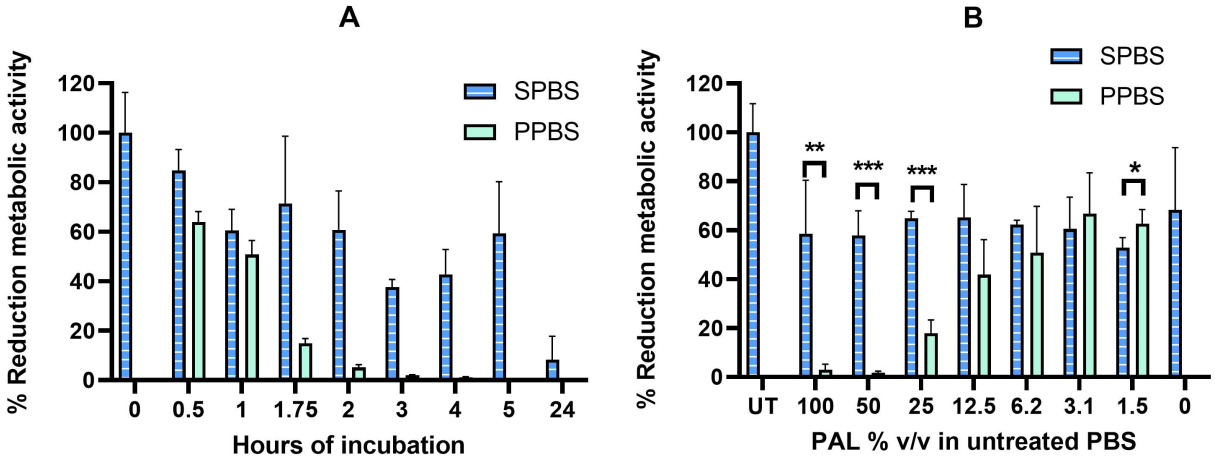

Figure 3.14: The reduction in metabolic activity of MM576 cells after exposure to Plasma treated PBS (PPBS) and sham treated PBS (SPBS) analysed with a Resazurin assay. MM576 cells A) time course of exposure and B) exposure to various concentrations of PPBS or SPBS 26 hours post treatment. All time points were significantly different compared to the matched sham Hartmann's treatment unless otherwise stated. Error bars are +/- Std deviation, n=3.

MM576 cells were seeded as described in Chapter 2, Section 2.1.3. For the first pilot study the culture medium was removed and cells were incubated with 100 μL plasma treated PBS (PPBS) or sham treated PBS (SPBS) for a range of time intervals specified in Figure 3.14 A. After each time point, the PPBS or SPBS was removed and replaced with culture medium. The time points were analysed in order to choose an incubation time for the clonogenic assay which would show good effect by the PPBS but not be obscured by the effect of the sham treated solution.

In the second pilot study PPBS and SPBS were serially diluted to the concentrations shown in Figure 3.14B in untreated PBS and incubated with MM576 cells for 120 minutes. This was done to establish the effect of concentration of the PPBS on the cytotoxicity and ensure that the sham treatment of PBS had no effect on the cells. Both experiments were analysed using a Resazurin assay (Chapter 2, Section 2.1.3) at 26 hours post treatment.

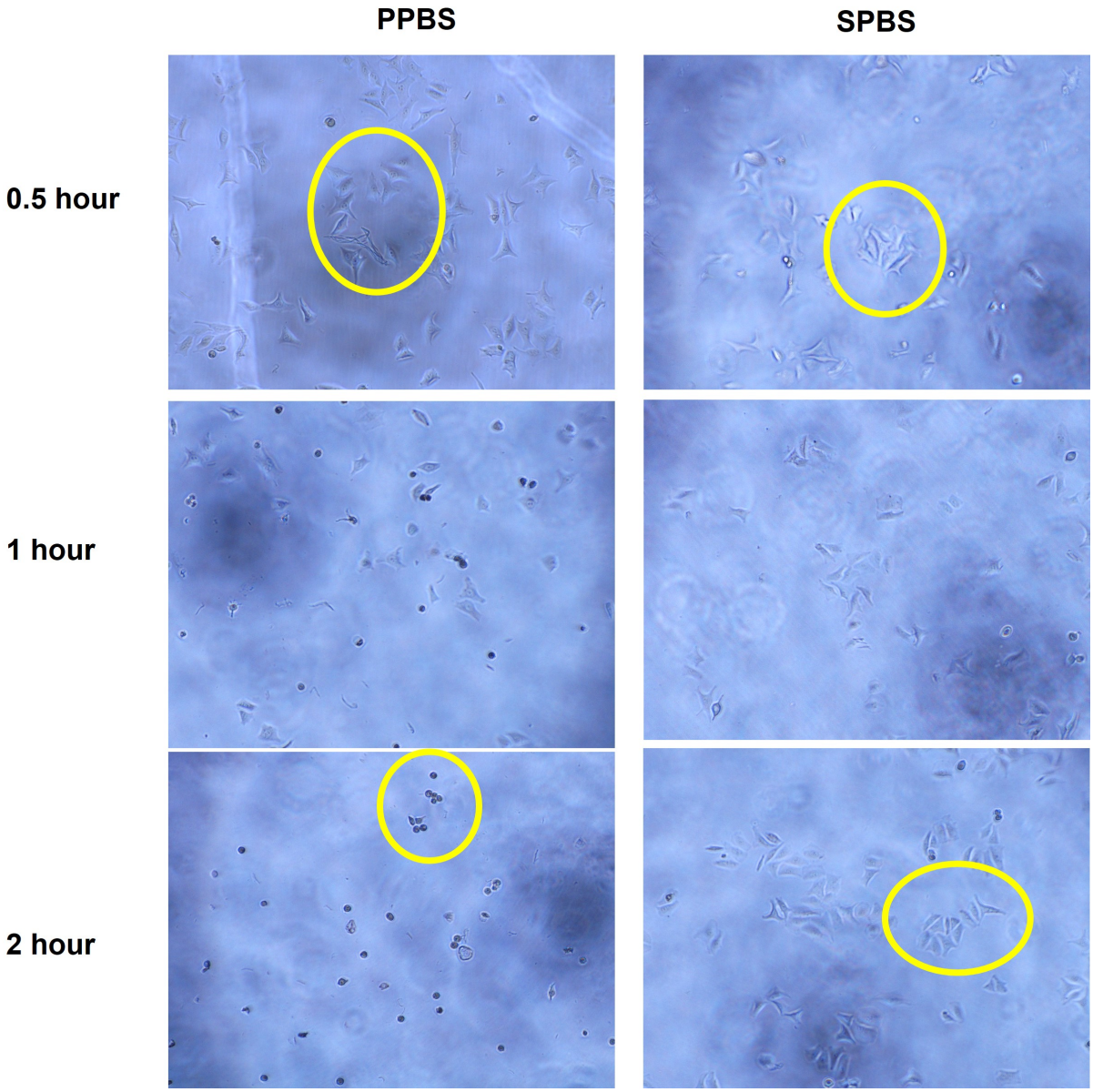

Figure 3.15: Shrunken morphology of MM576 cells after extended exposure to plasma activated PBS (PPBS) compared to epithelial morphology after exposure to sham activated PBS (SPBS) from the experiment presented in Figure 3.14. Cells were incubated with the designated solution for 0.5, 1 or 2 hours after which the culture medium was replaced. Shrunken morphology after PPBS incubation indicates lack of recovery, whereas the star-like morphology indicates cell recovery. Images were taken 24 hours after medium replacement.

Figure 3.15 shows how exposure to PPBS and SPBS affects cell morphology over a 2 hour period. These images were taken 24 hours after the replacement of culture medium and shows how extended exposure to PPBS results in very dark and condensed morphology, which is distinct from the typical star-like epithelial morphology typical of untreated cells, indicating lack of recovery from PPBS treatment.

The results from this pilot cytotoxicity study, displayed in Figure 3.14 were very encouraging, with the PPBS resulting in both concentration and time of exposure related reduction in metabolic activity of MM576 cells as expected. Metabolic reduction at the 100%, 50% and 25% concentrations of PAL in the dilution series and at all time points in the time course (using 100% PAL) was statistically different from the metabolic reduction from the sham treated PBS.

3.4 Conclusion

In this chapter we designed, built and optimised a device for the plasma treatment of liquids suitable for PAL generation in a clinical setting. The final optimised design consists of a quartz plasma pen attached to a syringe via a side port to allow subsurface plasma treatment. We used methylene blue as a measure of the $^{\cdot}OH$ radical production to validate the relative efficiency of the plasma device under various conditions to assist in the optimisation of the design. Finally we performed a pilot cytotoxicity study, confirming that our device and chosen treatment times were producing RONS in adequately cytotoxic concentrations.

Chapter 4

Characterisation of a custom underwater plasma activation device

In order for a device or method of treatment to be suitable for clinical translation, a quick, reproducible and reliable method of quantifying the dose is needed. The aim of this chapter was to characterise the custom built device we introduced in the previous chapter, assess the RONS production and introduce calorimetry as a method to measure the dose to a plasma activated liquid.

In radiotherapy clinical practice, the output of radiation beam is calibrated under standard conditions, where the industry standard calibration is performed using calorimetry [85]. This output, known as the *absorbed dose*, is defined as the energy deposition per unit mass, units of which are the gray (Gy).

The dose administered by a direct plasma treatment has been reported in terms of time of treatment [6], time at a specified power density (watts/cm^3) [28] or power flow at a specified distance [82]. The 'activity' of a PAL has been variously referred to as 'time of treatment' [3], [106], 'H_2O_2 and/or NO_2^- concentration' [66] and 'cytotoxicity'. Many papers have demonstrated the effect of varying voltage [47], gas flow rate and composition [116], time of treatment [105], [13], treatment distance [104], medium composition [75] and electrode geometry, among other parameters [122], on the generation of ROS and/or cytotoxicity. At the time of writing, the most common method of measuring dose to activate a PAL is 'time of treatment' under prescribed conditions, which vary between research groups. As a result of using the concentration of H_2O_2 and/or NO_2^- as a measure of PAL activity, reports such as [99] and [35] show that solutions containing only H_2O_2 are responsible for a large majority of the cytotoxic effect of plasma activated liquids *in vitro*. Kurake et. al [48] effectively shows that H_2O_2 concentration is a convenient way of comparing the output of different devices with a summary of a number of treatment devices, liquid types and treatment regimens resulting in large variations in H_2O_2 concentration.

It may be useful in the field of plasma activated liquids to take inspiration from radiotherapy dosimetry practices and apply a similar approach to the dosimetry of a PAL: have one method to assess plasma dose to liquid and have other methods to assess the biological effect. PAL contains reactive species of quantifiable concentrations with predictable biological effects, therefore in this study PAL was treated as a RONS containing drug with H_2O_2 being the predominant ingredient, rather than using a modifier to convert *absorbed dose* to *effective dose* as in radiation therapy.

Here we take the concept of 'absorbed dose' from radiation therapy - the energy deposited per unit mass - and use it in the assessment of a dose absorbed from a plasma to activate a PAL. We used a range of techniques in addition to calorimetry to characterise our plasma treatment device. The Amplex red assay (Chapter 2, Section 2.1.7) was used to quantify H_2O_2 production as a function of treatment time. The voltage and current were examined in order to determine the power drawn by the plasma under standard operating conditions. Calorimetry was used to determine the quantity of heat energy delivered to the liquid by the plasma. It was not the aim of this work to fully elucidate the relationship between the characteristics of the plasma treatment and RONS production as this has been sufficiently covered elsewhere [75], [112], [24], [25].

4.1 Calorimetric assessment of absorbed dose to PAL

A calorimetric method was used to calculate the energy delivered to the medium under treatment. In order to calculate the dose delivered to Hartmann's solution by the plasma alone, it was necessary to understand the effects of heat loss and heat gain from the device. This was done (1) without gas flow, (2) with gas flow and (3) with gas flow and plasma over time. For the first experiment, a 15 mL aliquot of hot water was loaded into the syringe device and the temperature was recorded every minute for 40 minutes by a thermocouple attached to the exterior of the syringe in order to measure the heat loss characteristics of the device in its normal operating environment.

The second experiment was a gas 'sham' identical to the first experiment except that argon gas was passed through the liquid at a rate of 2.3 L/minute without the plasma activated. The gas sham determined the additional heat loss caused by the evaporative cooling effect of the gas flow. For the third experiment, 15 mL water at room temperature was loaded into the syringe and the temperature recorded every minute for 40 minutes while plasma was ignited at a gas flow rate of 2.3 L/minute. In this test, energy from the plasma heats the water while all of the heat loss mechanisms are also active. Using the principles of calorimetry and Newton's law of cooling and heating, a formula was derived (Equations (2)-(8)) to calculate the heat lost from the device without gas flow and with gas flow which increases evaporative cooling. Measurements were an average of three separate experiments for each condition.

The temperature $T(t)$ of a cooling body as a function of time is described by Newton's law of cooling:

$$\frac{dQ(t)}{dt} = mc_p\frac{dT(t)}{dt} = -K_1(T - T_a) \tag{4.1}$$

Where $Q(t)$ is the heat energy as a function of time, m is the mass of the object, c_p is the specific heat capacity, T_a is the ambient temperature and K_1 is a constant. In the case of the cooling syringe, $m = 0.015\,\text{kg}$, $c_p = 4180\text{J/K·kg}$ and $T_a = 23.5°C$. Equation 4.1 may be solved to give

$$T = T_0e^{-\alpha t} + T_a \tag{4.2}$$

where

$$\alpha = \frac{K_1}{mc_p}. \tag{4.3}$$

and T_0 is the starting temperature. The temperature, as a function of time, of the cooling syringe is presented in Figure 4.1. The results were fitted according to Equation 4.1 using least-squares regression. The fitted coefficients yielded values of $K_1 = 0.05\,\text{J/(s·K)}$ and $\alpha = 0.0479$.

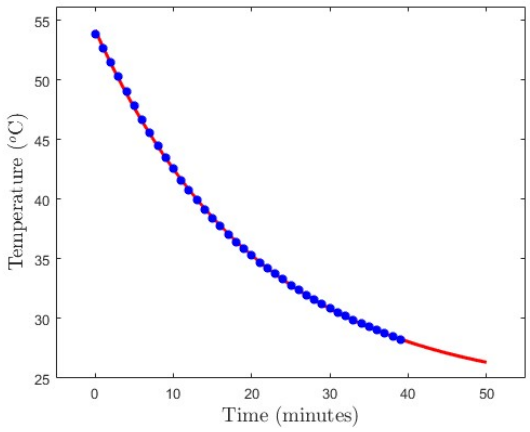

Figure 4.1: The results of the first experiment where hot water at $T_0 = 58.7°\text{C}$ was loaded into the syringe device and allowed to cool for 40 minutes. The measured data (blue dots) describes the water temperature in the syringe as a function of time and were fitted using equation 2 (red line) to determine the parameter α.

When argon gas is passed through the treatment solution additional conductive and evaporative cooling occurs. Newton's equation for cooling is therefore modified with an additional heat loss term, as given in Equation 4.4, denoted as $Q_{ev}(T)$.

$$mc_p \frac{dT}{dt} = -K_1(T - T_a) - Q_{ev}(T) \tag{4.4}$$

Figure 4.2 presents results for the cooling syringe over time in the presence of argon flow. Panel A displays the temperature obtained at each time point and Panel B displays the corresponding value of the loss parameter $Q_{ev}(T)$, calculated using Equation 5 using the fitted coefficients of K_1 and α. The loss parameter is itself a function of temperature, with the rate of heat loss much larger at high temperatures as shown in Figure 4.2.

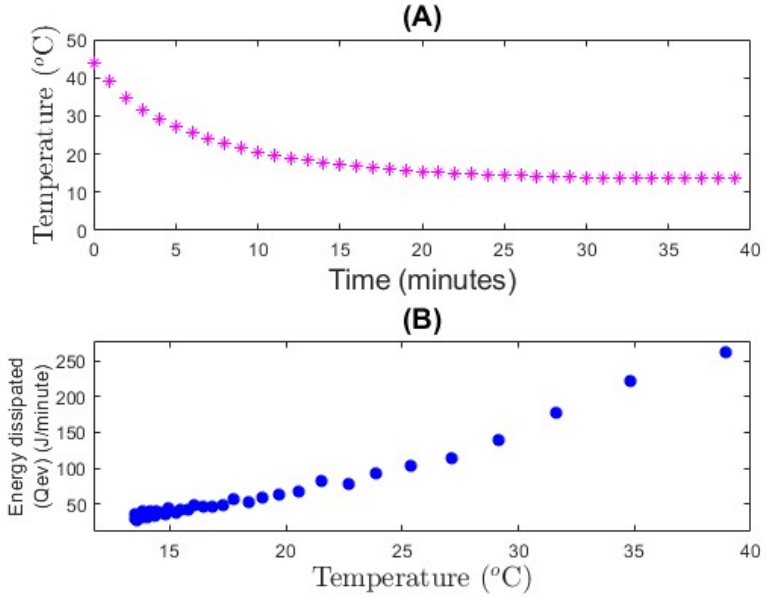

Figure 4.2: Panel A) shows the cooling curve obtained as a function of time as argon was bubbled through hot water at 2.3 L/minute in the plasma syringe device. B) is the energy dissipated (Q_{ev}) as a function of temperature, calculated using Equation 5.

Finally, in the case where the plasma pen is running, we must append the plasma heating term Q_{pl} to Equation 4.4:

$$mc_p \frac{dT}{dt} = -K_1(T - T_a) - Q_{ev}(T) + Q_{pl} \tag{4.5}$$

The results from the plasma pen calorimetry experiment are given in Figure 4.3. The observed increase in temperature of the water over time is illustrated in panel A, while the computed value of Q_{pl}, the rate of energy input from the plasma as a function of temperature, is shown in panel B. The energy input in Figure 4.3B appears somewhat dependent on temperature. The reason for the temperature dependence is that the liquid volume was assumed to be constant throughout this experiment. However, due to evaporative loss, the volume of the liquid is reduced by up to 1.5 mL during sham treatment, and up to 3.5 mL during plasma treatment. These changes in volume, as well as differences in gas temperature in the presence and absence of plasma, would explain the temperature dependence seen in Figure 4.3.

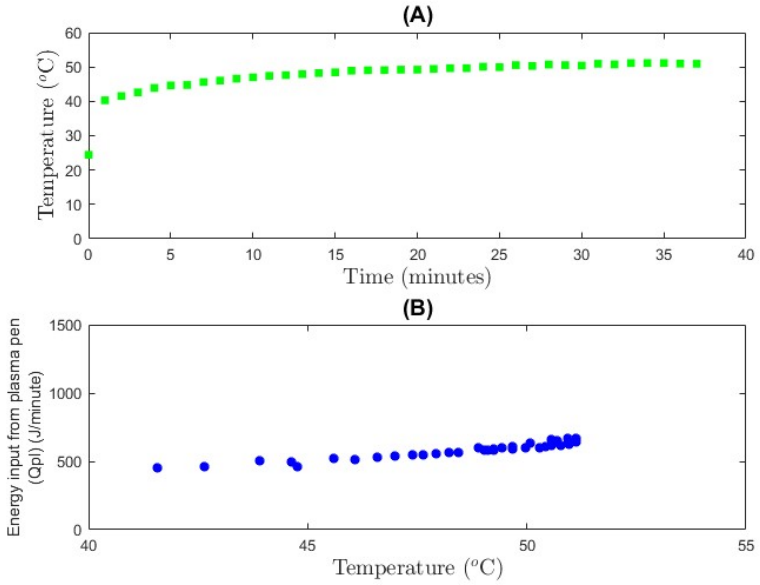

Figure 4.3: Panel A) shows the temperature of the liquid in the syringe device as a function of time during plasma treatment. Panel B) shows the energy input from the plasma pen (the power dissipated (Q_{pl})) as a function of temperature, calculated from Equation 7.

Quantity	**Symbol**	**Value**	**Unit**	**Standard error**
Inverse time constant of Newtonian cooling	α	0.0479	seconds^{-1}	0.027
Total Newtonian heat loss coefficient (including conduction, convection and radiation)	K_1	0.05	J/(s·K)	0.028
Heat delivery rate during plasma treatment	Q_{pl}	578.3	Joules/minute	32.84

Table 4.1: Mean values of constant parameters relating to the calorimetry of the plasma pen.

4.2 Electrical characterisation

The voltage applied to, and the current drawn by, the plasma is shown in Figure 2 and was measured using an oscilloscope (Agilent Technologies DSO1002A), a high voltage probe (Coline LTD, 40 kV high voltage probe HV40, serial no.1114) and a custom built current transformer. The characteristic traces were measured both when the plasma was on and off. The instantaneous power was calculated using

$$P = |VI| \cos\theta \tag{4.6}$$

where θ is the phase angle between the voltage and current AC wave forms. The average power dissipated by the plasma over a treatment was calculated and the total energy dissipated through the plasma was subsequently determined from the total treatment time (37.5 min).

Current transformers (CT), as described by R.Cross [19], are an elegant means of measuring alternating currents in high voltage systems, while simultaneously providing excellent isolation between high and low voltage circuits. A custom CT was constructed as shown in Figure 1; Approximately 50 turns of enamelled wire were wound around a toroidal ferrite core and terminated with a 2 kΩ variable resistor. An additional, single turn winding, with a 10Ω series resistance was included such that the CT could be calibrated against a known input current. Low voltage AC waveforms were applied to the calibration winding, and the variable output resistor adjusted until a linear voltage response was achieved. The

CT output was found to be proportional to the primary current for frequencies above 6 kHz, with a calibration factor of approximately (2mV per mA).

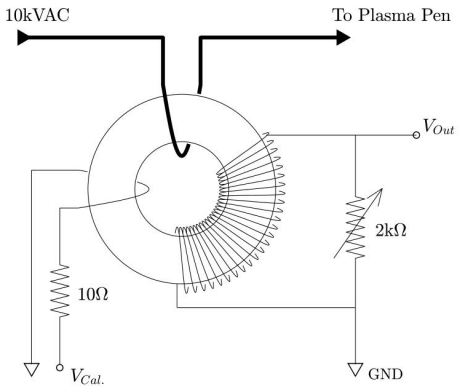

Figure 4.4: Schematic of custom current transformer used to measure the current through the plasma pen.

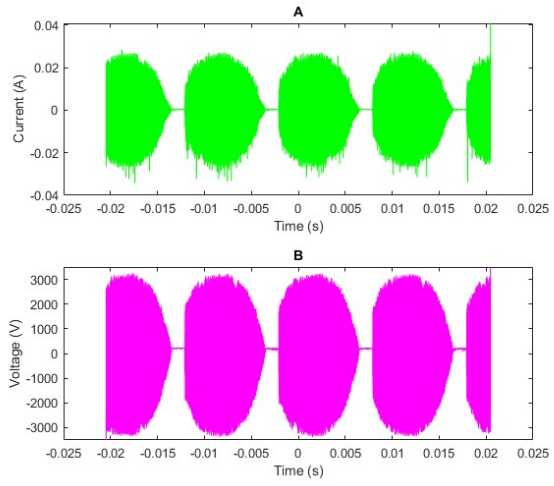

Figure 4.5: Oscilloscope trace of the (A) voltage applied to the plasma and (B) the current drawn by the plasma as measured by the current transformer, as a function of time. The waveform consists of high frequency sinusoidal oscillations with a 100 Hz envelope.

The oscilloscope traces in Figure 4.5 are consistent with [130] who also observed this modulated AC waveform from a neon light power supply.

4.3 Hydrogen peroxide assay

Among the many RONS generated in a PAL, hydrogen peroxide (H_2O_2) is one of the best understood and has the longest lifetime in liquid [37], thus was chosen as a model species for the current work. A hydrogen peroxide assay kit (Chapter 2, Section 2.1.7) was used to detect the concentration of H_2O_2 in the PAL after treatment following standard PAL generation procedure outlined in Chapter 2, Section 2.1.1 for the time periods specified in Figure 4.6.

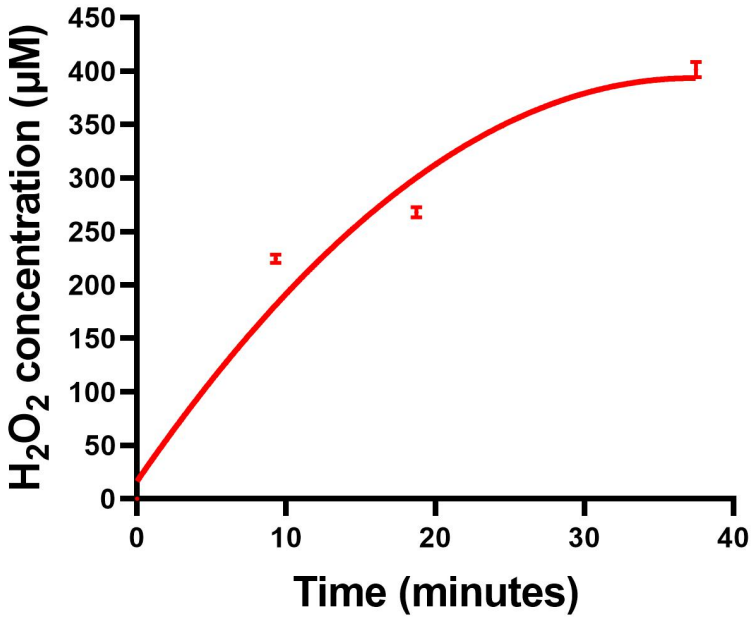

Figure 4.6: H_2O_2 concentration found in PAL made from 15 mL Hartmann's solution and plasma treated for various times. H_2O_2 concentration was analysed using Amplex Red kit. Points represent n=3 samples from individual batches of PAL. Error bars are +/- standard deviation, the red curve is the line of best fit.

Figure 4.6 shows the effect of increasing time of treatment on H_2O_2 production in 15 mL Hartmann's solution. Increased time of treatment increases H_2O_2 concentration in the PAL, however not in a linear fashion.

4.4 Energy delivered to liquid and RONS production under standard operating conditions

Table 4.2 summarises the energy deposition per unit mass to the liquid during standard operation of the plasma treatment device, measured by calorimetry and electrical monitoring. Both methods show reasonable agreement. Table 4.2 also includes the results from the quantification of H_2O_2 under standard conditions.

The unit gray (Gy) refers to the energy deposition per unit mass in joules per unit mass (usually kilogram). The heat delivery rate Q_{pl} which was established using calorimetry, can be used in the calculation of energy deposition from the plasma to the liquid during treatment using the following equation:

$$Gy = \frac{meanQ_{\mathrm{pl}} \times Time(minutes)}{mass(Kg)} = \frac{joules}{Kg} \tag{4.7}$$

	Method	**Outcome**
Energy delivered to liquid	Calorimetry	1.7 ± 0.08 MGy ($n = 3$)
Energy delivered to liquid	Electrical	1.4 ± 0.4 MGy ($n = 3$)
H_2O_2 concentration	Amplex red	510± 45 μM ($n = 11$)

Table 4.2: Characterisation of a plasma pen activation of a PAL under standard operating conditions. Uncertainties are expressed as standard error of the mean from a sample of up to 11 experiments.

The use of the electrical monitoring to assess energy deposition during plasma activation may be beneficial for experimental setups using much smaller volumes of liquid, where methods such as calorimetry

may be inconvenient. The H_2O_2 concentration is an indicator of the potential biological effects. The relationship between the biological effects of PAL and H_2O_2 will be discussed in greater detail in Chapter 6.

4.5 Discussion

The work presented above summarises the methods used to characterise our underwater plasma treatment device. The output of our device shows a time of treatment dependant increase in H_2O_2 production similar to [25]. The electrical trace is similar to that seen by [130] who also used a neon light power supply.

The construction of our device differs from other methods of generating a plasma activated liquid. Many sources in the literature generate plasma activated solutions in open topped vessels such as well plates or beakers, where the plasma pen itself is discharged several centimeters above the liquid surface ([48], [108], [116], [74]). It was noted that increasing distance between the plume and liquid surface reduced cytotoxicity [104], which was further supported by [25] who found that subsurface treatment by a plasma produced vastly larger concentrations of H_2O_2 than above surface treatment. Hence our device uses subsurface plasma treatment to maximise RONS production.

Calorimetry has not been used previously in the study of plasma activated liquids, however it has been used to examine plasma plumes. Frohlich et. al [29] used calorimetry to examine the energy flux of an atmospheric pressure plasma jet for surface modification, and both Weltmann et. al [115] and Cordaro et. al [18] used calorimetry to assess the thermal output of the kINPen and a plasma coagulation device.

Calorimetry is the industry standard method used to calibrate clinical radiation beams in Australia [85] and most international standards laboratories. During calibration, the output of the beam is correlated with the temperature increase of the absorbing material in order to calculate the amount of energy deposited. The output of the linear accelerator is not correlated to a biological outcome during calibration. It is only after many years of clinical trials and the development of models such as the Linear Quadratic dose response (more detail in Section 5.4) that the range of potential biological outcomes that could arise from a particular dose of ionising radiation is understood. Likewise with the current work, the intention of the calorimetry is not to attempt to correlate energy deposition with cytotoxicity, but to quantify the energy output of the plasma pen. The assessment of H_2O_2 concentration under the same standard conditions as those under which the calorimetry was performed was done to provide a frame of reference for potential biological outcomes after PAL treatment, not to imply a relationship between energy deposition and potential cytotoxic effects.

PAL was treated as a RONS containing drug during this study. Many studies concerned with the cytotoxic effect of plasma and PAL investigate the H_2O_2 produced by their plasma pens ([48], [74], [116], [123]). The relationship between the cytotoxic effects of PAL and H_2O_2 is explained in greater detail in Chapter 6. Using two different concepts to define dose is required since there is an activation step where the dose is delivered to the PAL by the plasma, and an administration step where a dose of PAL is delivered to cells. Calorimetry describes the 'dose *to* PAL' whereas H_2O_2 concentration can be used to describe the 'dose *of* PAL'.

The calorimetric method used in this paper is relatively simple to perform, though the treatment volumes (15mL) used in this study are fairly large and the large surface area of the syringe body further facilitates this process. Electrical monitoring may be a useful alternative method of assessing the dose to the liquid when the treatment volumes are small. At this stage, the temperature monitoring of the PAL still requires time consuming processing to convert to Gy, so as a real-time monitor of dose currently it is somewhat inconvenient. If this could be overcome using automated calculations, calorimetry could indeed be used as a real-time assessor of energy deposition.

As our calorimetry results are supported by the electrical monitoring, either method may be employed for this assessment. Further work may focus on the optimisation of real-time translation of temperature or electrical measurements into Gy.

4.6 Conclusion

In this chapter we used the heat input as well as the voltage and current traces to assess the energy deposited from the plasma to the liquid during treatment. This can be used as a quantification of plasma dose to liquid using the unit Gy used in radiation therapy. We showed that H_2O_2 concentration increased with increased time of treatment under standard conditions. H_2O_2 is a good representative species for the assessment of RONS concentration generated during plasma treatment as it is responsible for a large majority of cytotoxic effects on cancer cells exhibited by PAL. Thus the energy deposition may be used as a measure of dose to liquid, and the H_2O_2 concentration may be used to indicate potential biological effects of PAL.

Chapter 5

PAL cytotoxicity and synergy with ionising radiation

Ionizing radiation is a well-established cancer treatment, benefiting over 50% of patients diagnosed with cancer [23]. However survival rates for some cancers remain poor. Combination therapy, which boosts the efficacy of current treatments, offers an opportunity to improve outcomes for difficult to treat cancers while constraining the off-target effects.

The aim of this chapter is to compare the clonogenic plasma-activated liquid (PAL) concentration response profiles for each cell line with the respective radiation dose response profiles, to choose one PAL concentration and one radiation dose for combination therapy experiments to be assessed for synergistic interactions and determine the ability of PAL to enhance the cytotoxic effect of ionising radiation.

PAL has demonstrated time-dependent cytotoxic effects in various cell lines, including glioblastoma [107], melanoma [53] and breast cancer [49]. It has also shown selective cytotoxicity towards non-malignant cells ([66] and [121]), although not all reports agree with this conclusion [8]. However, in vivo studies support its selective cytotoxicity and have shown PAL to be effective in reducing tumor burden [53], causing no long-term negative side effects [22] and increasing life expectancy [129].

While most cytotoxicity studies have focused on PAL or direct plasma treatment alone, some studies have explored the combined effects of direct plasma treatment with radiation [80], [49], [47]. However, the assessment of synergistic/antagonistic interactions and determination of statistical significance of the synergy was not always the primary focus of these works. Hydrogen peroxide, a major component of PAL, is currently being studied as a radiosensitizing agent with promising results ([76], [5], [4]). Some evidence even suggests that PAL may be more cytotoxic than an equivalent concentration of hydrogen peroxide [48]. Thus, it was proposed that combining PAL with radiation therapy could lead to an improved therapeutic response.

Combination therapy involving the use of multiple therapeutic agents is increasingly being recognized as an effective approach. Multi-drug combinations [68] and combining immunotherapy agents [39] or radionuclides [21] with existing chemotherapeutics and external beam radiation therapy have been shown to be effective. The fractionation schedule and fraction size also influences cytotoxicity ([52] and [87]). sensitive normal tissue. Combination therapy can be effective for overcoming treatment resistance [50], however care must be taken to ensure that increased efficacy of treatment does not increase unwanted side effects. Conversely, certain combinations may inhibit the action of each other, thereby reducing overall treatment efficacy. Therefore, when studying combination therapies, it is crucial to assess whether the response to combination treatment is greater or less than the expected response to each treatment individually. Evaluating the nature and quantifying the magnitude of the response are essential for establishing dosing regimens for patients. This applies to the assessment of unwanted side effects to establish the safety of the treatment and the therapeutic window for patients, however as this work was conducted *in vitro*, here we will focus solely on efficacy of treatment.

Various methods for determining synergy exist in the literature, and opinions on the best metric to use are divided. Extensive overviews of synergy metrics are provided by [64] and [34]. Most metrics are based on either the Multiplicative Survival Principle (MSP) [9] (also known as Bliss Independence or the fractional product method [113]) or the Dose Equivalence Principle (DEP) [54], [64]. The MSP offers the advantage of determining synergy using minimal measurements and simple mathematics, although it has been criticized for overestimating interactions ([14]). Metrics based on the DEP, such as the Combination Index (CI) established by Chou and Talalay in 1984 ([15]), require multiple dose survival curves for drugs combined in specific ratios, which can become complicated when assessing multiple variations of the drug combination in question. The CI method is supported by available software for calculations. However, several flaws in the mathematics governing synergy equations have been pointed out ([34] and [119]). Despite these limitations, the CI method remains widely popular with over 7000 citations [86].

A recent development is the MuSyC metric ([119], [65]). This metric unified the DEP and MSP into a single framework, reducing bias and uncertainty in selecting a specific metric. Based on the Law of Mass Action, MuSyC allows metrics based on the MSP and DEP to be derived via the selection of various parameters. The developers of this framework also provide free access to computational software for data assessment and presentation. The MuSyC metric is designed to assess synergistic efficacy and potency across many combination doses such as might be generated during high throughput screening experiments. However the MuSyc metric has not been developed with radiation therapy in mind and does not account for the standard linear quadratic dose response widely applied in radiobiology. Hence we employed a metric based on the MSP.

Experiments were conducted to assess the effect of PAL exposure time and concentration on each cell line. The cell lines used were DU145 hormone-resistant prostate cancer and MM576 melanoma, both of which are known to be radioresistant ([120] and [38]), as well as the non-malignant prostate cell line PNT1A. In this context, the dose of PAL refers to its concentration by volume relative to a PAL generated under standard conditions described in Section 2.1.1. The data were used to inform an incubation time for the clonogenic PAL concentration response. Once the dose response profiles were established for both PAL and radiation, clonogenic combination and order of administration studies were performed. For this study we used two methods of evaluating a synergy metric based upon the MSP; one method - the Fractional Difference method - was developed for this study.

5.1 Resazurin Pilot studies of PAL cytotoxicity

The first pilot cytotoxicity study of PAL was previously described at the end of Chapter 3 (section 3.3) where a resazurin assay was used to assess the cytotoxic effect of Plasma Activated PBS for various incubation times and concentrations. After this first trial, it was decided to determine which of three solutions, PBS, 0.9% saline and Hartmann's solution, would be the least toxic to cells without plasma treatment.

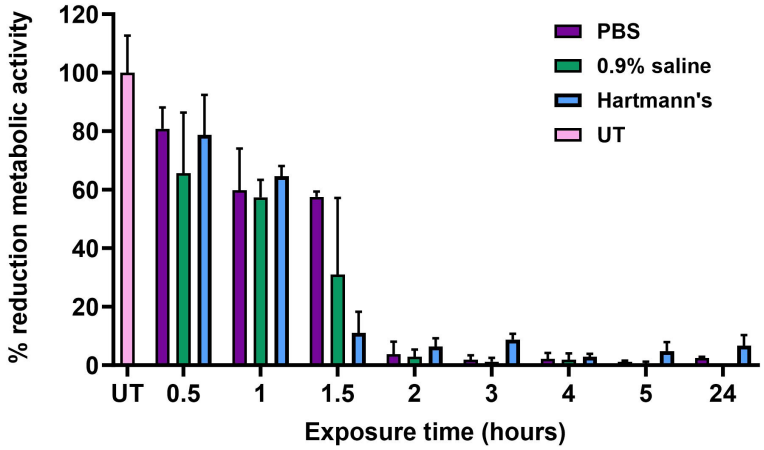

Figure 5.1: Reduction in metabolic activity of MM576 cells as a function of exposure time to 0.9% saline, PBS and Hartmann's solution indicating Hartmann's solution is the least cytotoxic solution at the time points of interest. Cells were exposed to each solution for a range of time periods and analysed using a Resazurin assay 26 hours post treatment. Error bars are +/- Std deviation, n=3.

The effect on metabolic activity of different incubation times in three types of saline solution (PBS, 0.9% saline and Hartmann's solution) was conducted using a resazurin assay on MM576 cells depicted in Figure 5.1. Hartmann's solution was found to be slightly less cytotoxic than saline or PBS to the MM576 cells for the incubation times we were considering, though it was not statistically significant. As Hartmann's solution is already approved for use in humans, further experiments were conducted using Hartmann's solution rather than PBS. After the plasma treatment device was upgraded to a 60 mL syringe from the 20 mL syringe (also described in Section 3.2.2, the volume of Hartmann's to be treated was also increased to 15 mL as greater volumes were required for future clonogenic assays. Thus to adequately upscale the treatment time, the ratio of 2.5 min/L was used, so further experiments used a 15 mL volume of Hartmann's for a treatment time of 37.5 minutes.

The pilot study depicted in Figure 3.14 in Chapter 3 was repeated on DU145 and PNT1A cells using the Hartmann's solution and the larger syringe. The PNT1A were subjected to both the time course of exposure and the dilution series, but were only analysed at 72 hours post treatment due to their slower doubling time.

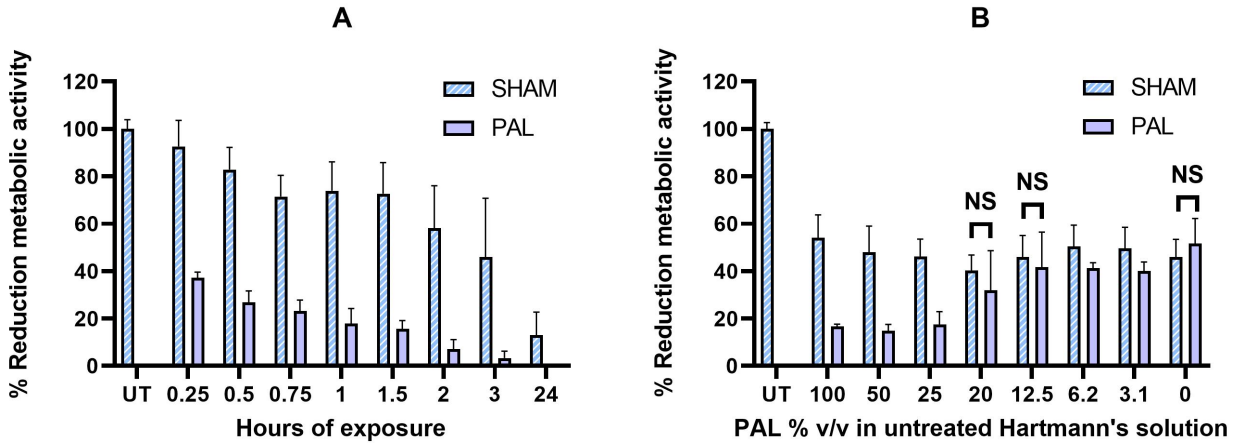

Figure 5.2: The percentage reduction in metabolic activity of PNT1A cells as a function of hours of exposure to PAL and sham treated Hartmann's solution (Sham) for 30 mins then analysed with a Resazurin assay. PNT1A cells A) time course of exposure and B) exposure to various concentrations of PAL or sham treated Hartmann's analysed 72 hours post treatment. PAL exhibits greater cytotoxicity than sham treatment in a time and concentration dependent manner. All points in panel B) were significantly different compared to the matched sham Hartmann's treatment unless otherwise stated. Error bars are +/- Std deviation, n=6.

The time course of exposure only was performed on the DU 145 cells, however the effect of the exposure was analysed at both 26 and 72 hours post treatment.

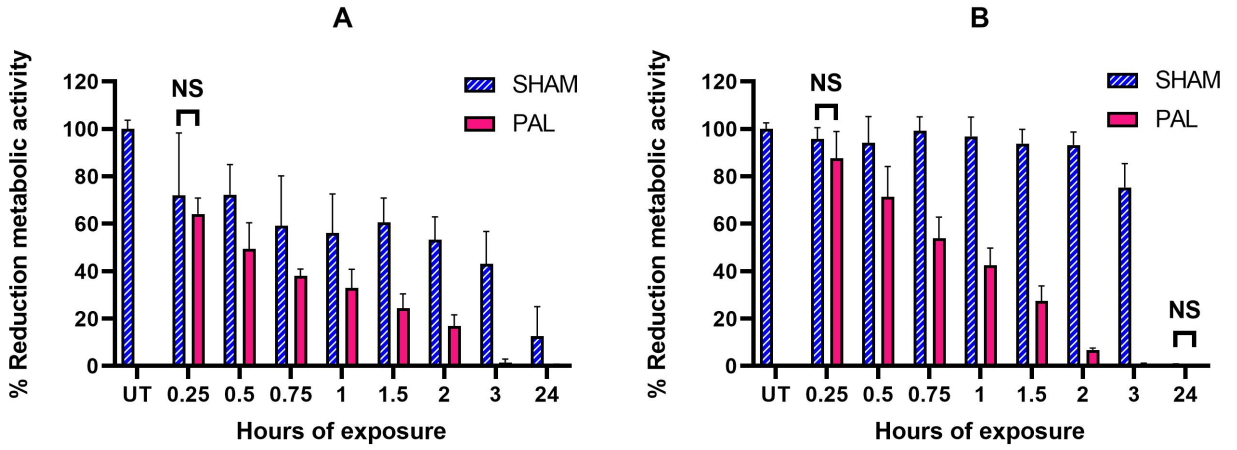

Figure 5.3: The percentage reduction in metabolic activity of DU 145 cells as a function of hours of exposure to PAL and sham treated Hartmann's solution (Sham) analysed with a Resazurin assay. Cells were analysed A) 26 hours and B) 72 hours post exposure. PAL exhibits greater cytotoxicity at all time points longer than 0.25 hours at both 26 and 72 hours post treatment All time points were significantly different compared to the matched sham Hartmann's treatment unless otherwise stated. Error bars are +/- std deviation, n=6.

Figures 5.2 and 5.3 show that for both cell lines, metabolic activity decreases with increasing time of exposure and/or concentration of PAL. Each cell line displays differing sensitivity to PAL and to sham treatment. A minimum PAL exposure time of 30 minutes resulted in a statistically significant level of

irrecoverable damage compared to sham treatment for all three cell lines. The PNT1A cells were analysed at 72 hours post exposure to ensure that the pattern of effect would be similar to those of the DU145 or MM576 shown in Section 3.3, as it was known that the incubation time for a clonogenic assay of the PNT1A cells was much longer than the DU145 or MM576 cells. The MM576 and PNT1A cells do not recover as completely as the DU145 cells, however, 30 minutes of PAL exposure was the minimum time to see a statistically significant effect for all three cell lines. Our results showing treatment dependent reduction in metabolic activity are in good agreement with the current literature [89].

5.2 Clonogenic response to radiation dose

To determine the radiation dose response DU 145, PNT1A and MM576 cells were seeded as described in Table 2.2, Chapter 2 Section 2.1.4 and allowed to adhere overnight. The cells were exposed to a 6MV photon beam, produced by a Varian Clinac^{TM} 6X linear accelerator to doses ranging from 0.1 Gy to 9 Gy at a dose rate of 6 Gy per minute, for a total n in the range 6 to 44. Complete details on the irradiation setup and conditions are given in Chapter 2, Section 2.1.5.

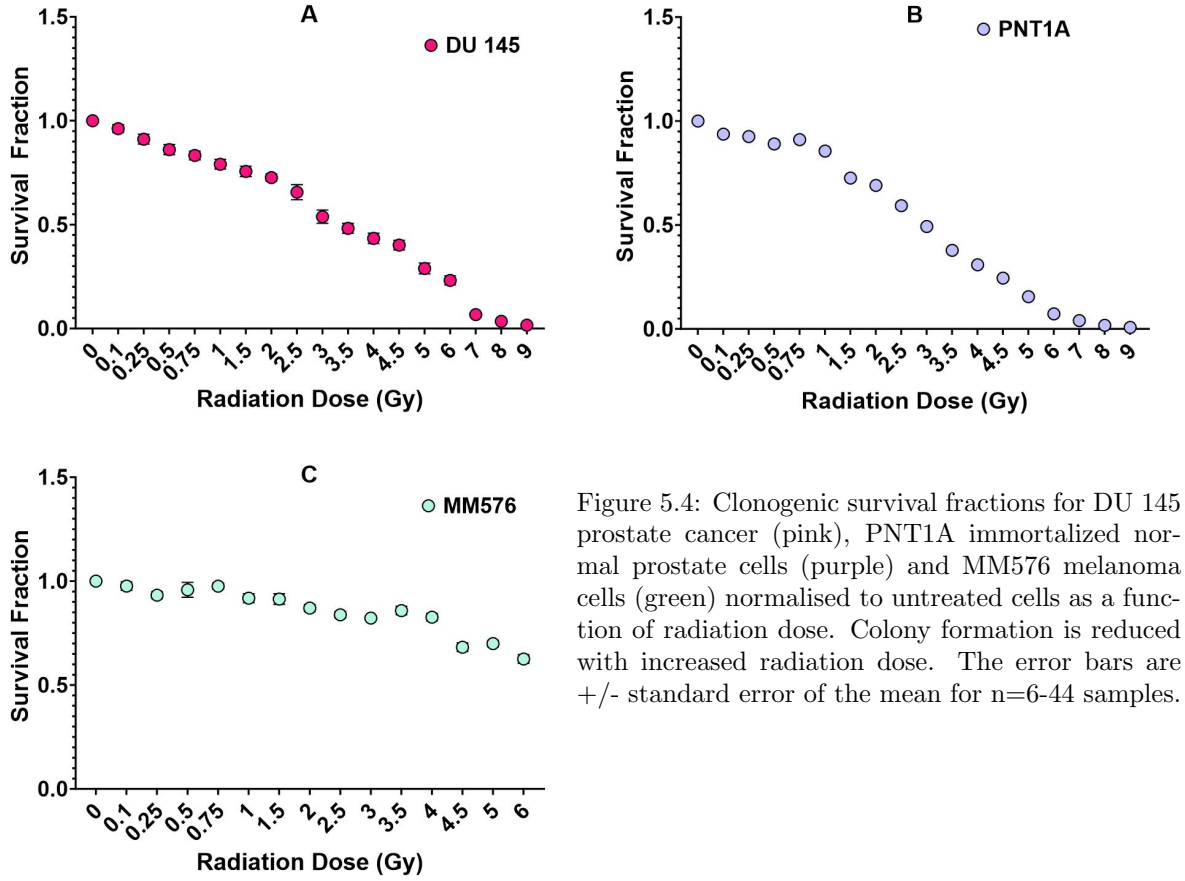

Figure 5.4: Clonogenic survival fractions for DU 145 prostate cancer (pink), PNT1A immortalized normal prostate cells (purple) and MM576 melanoma cells (green) normalised to untreated cells as a function of radiation dose. Colony formation is reduced with increased radiation dose. The error bars are +/- standard error of the mean for n=6-44 samples.

Figure 5.4 shows the clonogenic response to radiation dose. All three cell lines show decreased cell survival with increased radiation dose, though the three cell lines are differently sensitive to radiation. PNT1A cells are the most sensitive, whereas the MM576 are the most resistant. It should be noted that radiation doses only increase to 6Gy for the MM576.

5.3 Clonogenic response to PAL concentration

To determine the PAL concentration response DU 145, PNT1A and MM576 cells were seeded as described in Table 2.2, Chapter 2 Section 2.1.4 and allowed to adhere overnight. The PAL and Sham (Treatment solutions) were serially diluted with untreated Hartmann's solution to concentrations of 100%,

50%, 25%, 12.5%, 6.25%, 3.125% and 0% (untreated Hartmann's). The culture medium was removed, and cells were incubated with volumes of PAL or Sham described in Table 2.3, Chapter 2 Section 2.1.6 of the designated solution for 30 minutes before the treatment solution was removed and replaced culture medium. The duration of exposure to PAL was the same for each cell line. The cells were then allowed to grow until staining day when they were fixed and stained using 3% methylene blue in 70% ethanol or methanol. The survival fraction was calculated as the number of colonies after an intervention as a fraction of the number of colonies in the untreated or sham treated group as specified in Section 5.5.3. Each experiment was repeated three times for a total n in the range 9 to 18.

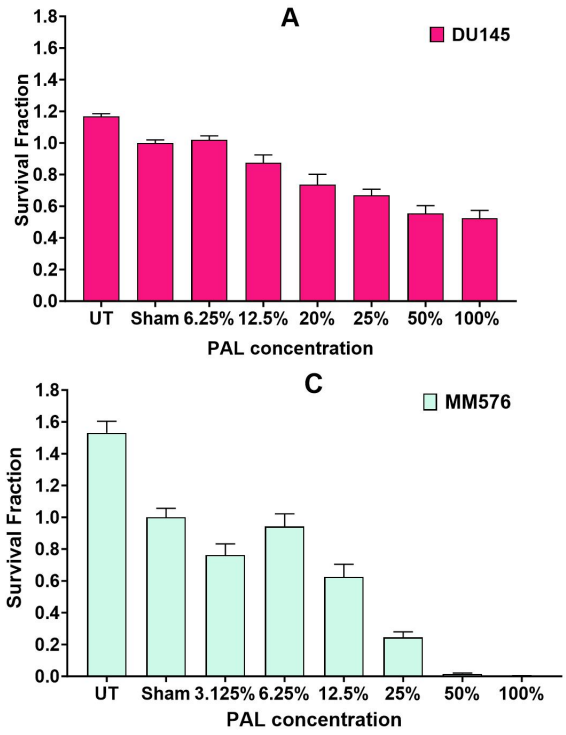

Figure 5.5: Clonogenic survival fractions for DU 145 prostate cancer (pink), PNT1A immortalized normal prostate cells (purple) and MM576 melanoma cells (green), normalised to cells exposed to sham treated Hartmann's solution (here called 'sham') as a function of PAL concentration. Colony formation is reduced with increased PAL concentration. The error bars are +/- standard error of the mean for n=6-44 samples.

Figure 5.5 shows the clonogenic response to PAL concentration. The clonogenic survival fraction of each cell line is reduced increased concentrations of PAL. The DU 145 cell line is the most resistant to PAL and the PNT1A is the most sensitive.

5.4 Dose response equation fitting

Data presented in Figures 5.4 and 5.5 was fitted to the linear quadratic equation (Figure 5.6) and the Hill equation (Figure 5.7) respectively to gain insight into PAL concentration response behaviour. The linear quadratic equation ([11]) was used to examine the cell sensitivity to a radiation dose response and the Hill equation ([32]) is common for assessing a drug's dose response effect. It should be noted that the form of the Hill equation used in this thesis is of the form required to assess cell **survival**. The form usually found in the literature such as Equations 5 and 6 in [32] is used to assess cell **death/cytotoxicity**.

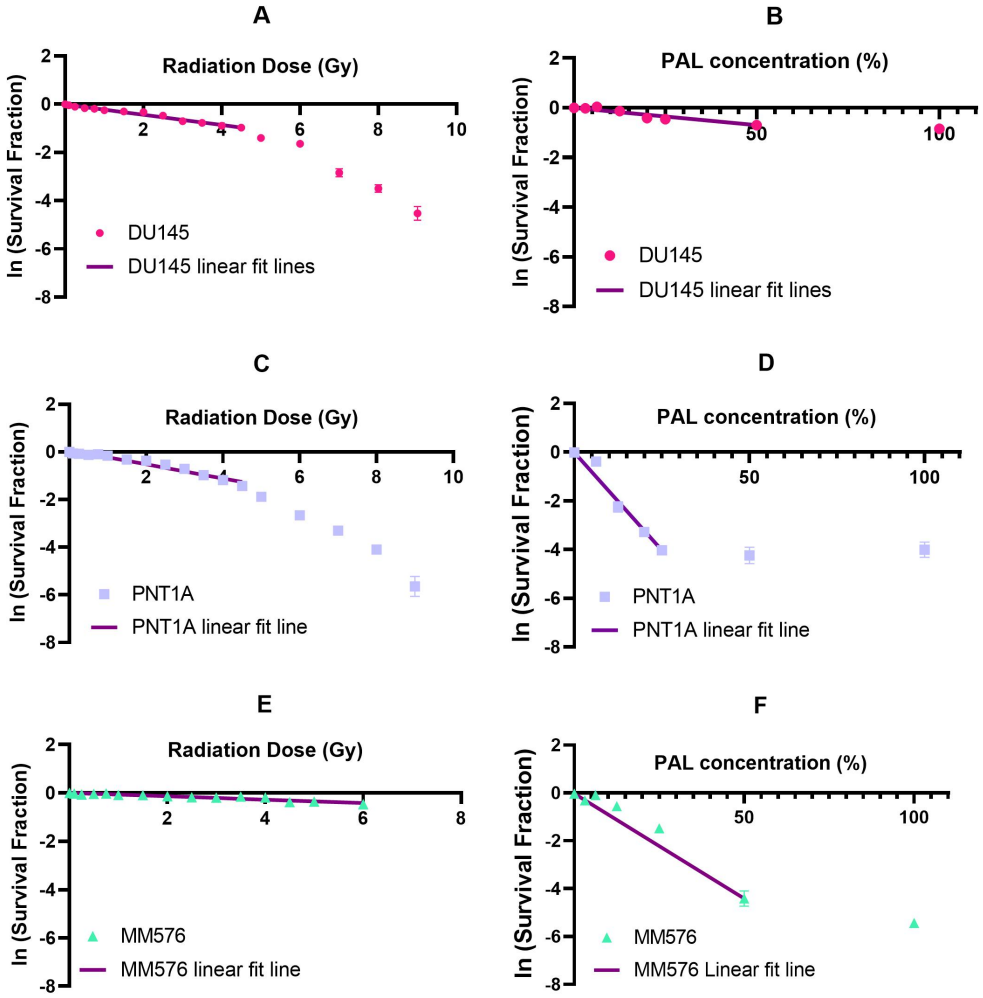

Figure 5.6: Panels A, C and E show the natural logarithm of the data from Figure 5.4 as a function of dose plotted on a linear scale, illustrating the linear portion of the dose response curve. Panels B, D and F show the natural logarithm of the data from Figure 5.5 as a function of dose plotted on a linear scale, illustrating the linear portion of the dose response curve. Error bars are +/- SEM. Each experiment was performed in duplicate or triplicate (n= 12 to 16.)

The data in Figures 5.4 and 5.5 were fitted to the linear-quadratic equation usually used to describe radiation dose responses ([11]) of the form:

$$S = e^{-\alpha D - \beta D^2} \tag{5.1}$$

Where S is the survival fraction after exposure to dose D of ionising radiation and α and β are the parameters describing the cell's radiosensitivity. The equation is plotted on a log scale which gives a typical quadratic response profile. The α term describes cell death from 'single hit' events and dominates the curve at low doses, whereas the β term describes cell death from double hit events and thus dominates the equation at higher doses. The α/β ratio is used to describe the cell's radiosensitivity - high ratios exhibit a relatively constant rate of cell killing with increasing dose, where as low ratios show an increasing sensitivity with increasing dose [61]. The two prostate cell lines exhibit typical linear quadratic behaviour, and though the log survival of the MM576 fits the equation, it exhibits only the linear part of its response in the dose range tested.

The PAL concentration response data does not exhibit typical linear quadratic behaviour. The PAL responses show a linear region followed by a plateau at high doses. As the quadratic term dominates at

high doses, the use of the linear quadratic equation is not appropriate to understand PAL concentration response effects.

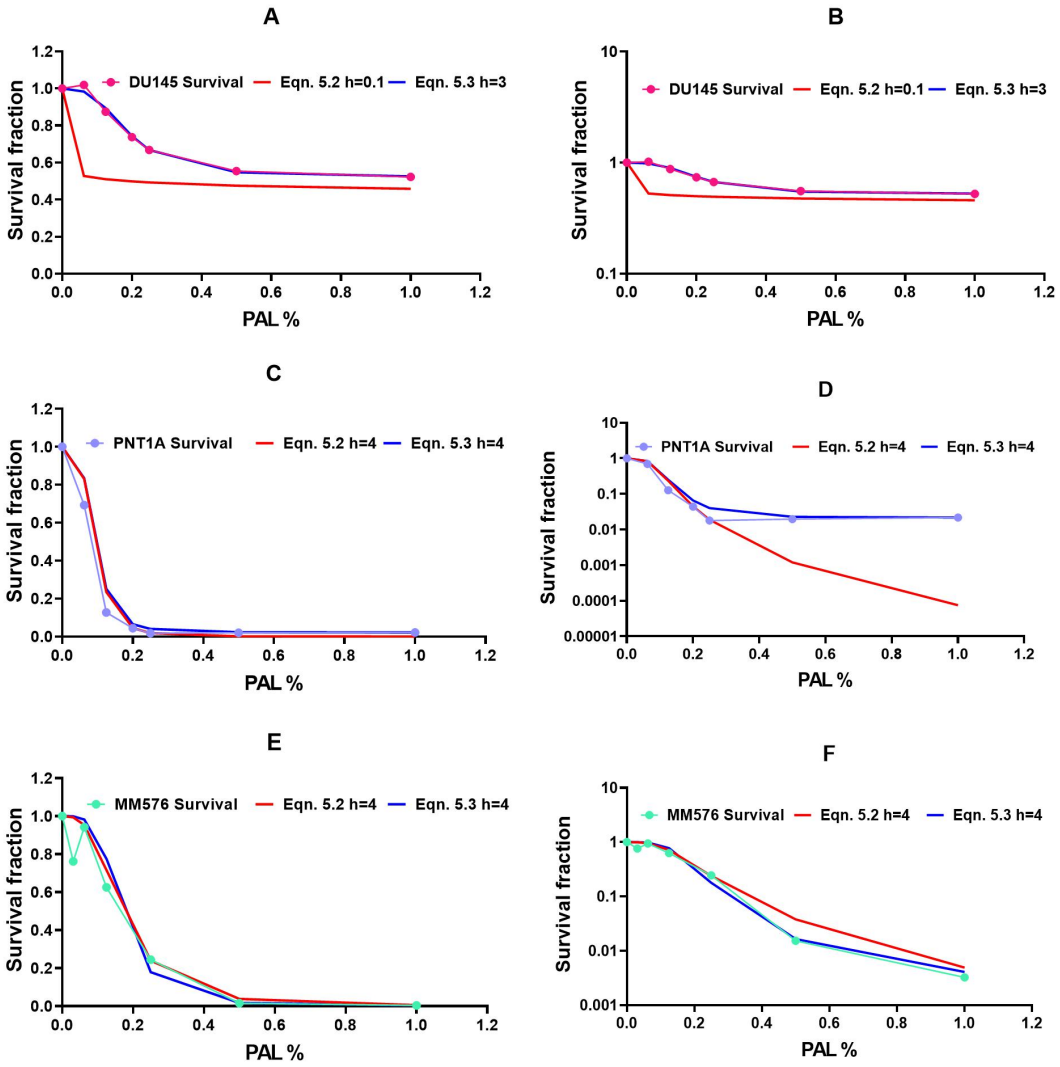

Figure 5.7: Du 145 (A and B), PNT1A (C and D) and MM576 (E and F) PAL clonogenic survival fraction as a function of PAL concentration data from Figure 5.5, fitted to the Hill equation. The red lines describe the fit using Equation 5.2 and blue lines describe the fit using Equation 5.3, represented on linear (A, C and E) and logarithmic (B, D and F) scales. The experimental data points are represented in pink for DU 145, purple for PNT1A and green for MM576 and are well fitted by Equation 5.3. The Hill coefficients (h) used are described in the legend.

The PAL concentration responses for all cell lines were then fitted to the Hill equation, frequently used for drug dose responses [32], in the form:

$$S = 1 - \frac{d^{\mathrm{h}}}{d^{\mathrm{h}} + {EC_{50}}^{\mathrm{h}}} \tag{5.2}$$

where S is the survival fraction at dose d of PAL measured as the volume percent of PAL in Hartmann's solution, h is the Hill coefficient (empirically derived) and EC_{50} is the PAL concentration required to reduce the cell survival to 50%. Equation 5.2 does not not fit the dose response for the DU 145 cells well as the total survival of the DU 145 cells does not fall below 50% of the sham treated survival (the cell

survival fraction at 100% PAL was 0.52), so a more general form of the equation is required:

$$S = S_1 + \frac{S_0 - S_1}{1 + (\frac{d}{EC_{50}})^{\mathrm{h}}} \tag{5.3}$$

where S is the total cell survival, S_1 is the cell survival at maximum PAL dose, S_0 is the cell effect at PAL dose d (PAL %), h is the Hill coefficient and EC_{50} is the PAL concentration responsible for half of the maximal effect. For the DU 145 dose response, the cell survival fraction for the half-maximal effect was 0.76. This more general equation includes the S_1 term which allows for situations where the maximal therapeutic effect does not reach a cell survival of 0%. The MM576 and PNT1A concentration responses were also fitted to this general Hill equation. The Hill coefficient describes the slope of the dose response, with a Hill coefficient of 1 resulting in a hyperbolic response, and a coefficient > 1 describing sigmoidal behaviour. As the best fit to the Hill equation 5.3 for all three cell lines is found by using a Hill coefficient of > 1, all three cell lines exhibit sigmoidal behaviour. Equation 5.3 fits the data better than Equation 5.2 as can be seen when the scale changes from linear to logarithmic. Equation 5.2 appears to fit the PNT1A and MM576 data well when using a linear scale for the survival fraction, however it breaks down when a logarithmic scale is used. Equation 5.3, the general form of the Hill equation effectively describes the PAL concentration responses for all three cell lines. When the S_1 is large, in the case of the DU 145 for which survival does not drop below 50%, this indicates resistance to PAL therapy and the need for an additional therapy.

5.5 Synergy testing: Multiplicative Survival Principle

The Multiplicative Survival Principle (MSP) (also known as Bliss Independence) was first described by Bliss in 1939 [9]. Bliss stated that if two drugs act completely independently of each other, the outcome of their combined action can be described using the equation:

$$D_{12} = D_1 + D_2 - D_1 D_2 \tag{5.4}$$

where D_1 and D_2 refer to the fractions killed (cell Death) by drugs 1 and 2 individually, $D_1 D_2$ refers to the product of the fractions killed by drugs 1 and 2 (the **predicted** outcome of combination therapy) and D_{12} is the **observed effect** - the actual clonogenic survival fraction after combination therapy. For this thesis we used the definitions from [113] for Synergy, Antagonism and Summation (no interaction):

Antagonism:

$$D_{12} < D_1 + D_2 - D_1 D_2 \tag{5.5}$$

Synergism:

$$D_{12} > D_1 + D_2 - D_1 D_2 \tag{5.6}$$

Summation (no interaction):

$$D_{12} = D_1 + D_2 - D_1 D_2 \tag{5.7}$$

Henceforth 'Summation' will be referred to as 'No interaction'. The equations 5.5-5.7 can be expressed in terms of survival and thus can be re-written into the form:

$$S_{12} = S_1 S_2 \tag{5.8}$$

where S_1 and S_2 refer to the survival fractions after treatment with drug 1 and drug 2, the **predicted** outcome of combination therapy is given by the product of the survival fractions $S_1 S_2$ and the **observed** outcome after combined therapy is given by S_{12}. Care must be taken to reverse the inequality signs for Antagonism and Synergism using this form, and can be written:

Antagonism:

$$S_{12} > S_1 S_2 \tag{5.9}$$

Synergism:

$$S_{12} < S_1 S_2 \tag{5.10}$$

No Interaction:

$$S_{12} = S_1 S_2 \tag{5.11}$$

To ensure that any interaction observed was indeed the result of the plasma treatment and not the Hartmann's solution itself, this method was applied to PAL and radiation combination treatment, as well as the sham treated Hartman's and radiation combination treatment (the no interaction condition).

Synergies within a single type of therapy exist (for example when there is a synergistic increase in cytotoxicity when two radiation treatments are given with a time delay between the two doses [87]). During the assessment of interactions between PAL and radiation, it is convenient to avoid situations where each therapy shows synergy or antagonism with itself. In order to achieve this we ensure that the portion of the dose response curve used in this calculation satisfies the following requirements.

If a therapy is administered twice, each time with dose x to give dose $2x$, the multiplicative survival principle gives the survival as the product:

$$S(x) \times S(x) = (S(x))^2 \tag{5.12}$$

which will equal $S(2x)$ when there is no interaction between individual doses. It is readily shown by substitution that this requirement is met if:

$$S(x) = e^{-ax} \tag{5.13}$$

where a is a constant. To show this:

$$(S(x))^2 = e^{-ax} \times e^{-ax} = e^{-a2x} = S(2x) \tag{5.14}$$

Hence, $(S(x))^2 = S(2x)$ as required.

Concentrations of PAL and doses of radiation were chosen to reduce the survival of each cell line to 70% after each individual treatment and would result in a predicted survival of 49%. These values were to ensure that there was sufficient survival after combination therapy to perform statistical analyses with adequate sensitivity. To avoid the effects of self synergy, the doses to be used in the combination treatments must lie within the linear region of the response curve, governed by Equation 5.13. Note that for radiation, beyond the linear region at high doses, this condition is not met because of the β term of the linear quadratic equation, leading to a synergistic response between two separate radiation treatments [11], [52], [61]. As can be seen in Figure 5.6 the concentrations of PAL and doses of radiation chosen for the combination therapy experiments (Table 5.1) fall within the linear range when expressed in the form of a linear quadratic equation and thus satisfy the requirements for no synergy using the MSP.

Cell line	**PAL concentration (%)**	**Radiation dose (Gy)**
DU 145	20	2.5
PNT1A	5	2
MM575	10	5

Table 5.1: The doses of ionising radiation and PAL concentrations used for each cell line in the synergy experiments.

Table 5.2 summarises the parameters α and R^2 used to fit the linear region of the PAL dose responses from Figure 5.5 with equation 5.13. The results of this fit are displayed in Figure 5.6.

Critics of the MSP ([14] and [30]) argue that using the MSP when the Hill coefficient is > 1 is inaccurate as it can overestimate the number of synergistic interactions, and these assessments of synergy may be inconsistent over the whole of the dose response profiles. While this is true in some cases, the MSP is regularly used when assessing the effects of combined radiation therapy ([109], [79], [101]), where radiation dose responses do not adhere to Hill type dose response curves. It should be noted here that, while MuSyC was not intended to accommodate linear quadratic dose responses used in radiobiology, the MuSyC metric has no limitations on synergy assessments when Hill coefficients are greater than 1.

Cell line	Value of α Equation 5.13	Error	Value of R^2
Radiation			
DU 145	0.218	0.006	0.991
PNT1A	0.273	0.0132	0.973
MM575	0.0697	0.004	0.9577
PAL			
DU 145	0.015	0.0014	0.949
PNT1A	6.115	0.364	0.986
MM575	12.051	1.052	0.963

Table 5.2: Summary of the α in Equation 5.13 and R^2 values for the radiation dose and PAL concentration responses, plotted as the natural logarithm of the survival fractions. These values were determined from Equation 5.13 fitted to the linear region of the responses. The error was determined from the fit.

5.5.1 Simplified synergy method

To assess the statistical deviation from the predicted outcome, a simple metric is used which will henceforth be referred to as the Simplified Method. The average survival fractions after each individual therapy are multiplied to give the predicted outcome S_1S_2, a single value. The difference between S_1S_2 and all values of S_{12} is then tested using a single sample Student's t-test, provided the distributions are approximately normal.

5.5.2 The Fractional Difference method

The Fractional Difference method is based upon the MSP and is an extension of the Simplified Method, where the extent of the synergy between the two therapies, PAL and radiation is described by:

$$m_{\mathrm{AB}} = \frac{\sum_{i,j,k=1}^{n} (S_{\mathrm{Ai}} S_{\mathrm{Bj}} - S_{\mathrm{ABk}})}{n^3} \tag{5.15}$$

which can be expanded to:

$$m_{\mathrm{AB}} = \frac{\sum_{k=1}^{n} \left[\left(\sum_{i,j=1}^{n} S_{\mathrm{Ai}} S_{\mathrm{Bj}} \right) - S_{\mathrm{ABk}} \right]}{n^3} \tag{5.16}$$

where m_{AB} is the mean of the difference between the predicted outcome of combination therapy $S_{\mathrm{Ai}}S_{\mathrm{Bj}}$ and the observed outcome of combination therapy S_{ABk} and n is the number of flasks used in the clonogenic assay for each therapy. The predicted outcome generated by the FD method assumes that the two therapies are independent. We note that the observed result is, in general, dependent on the order of the therapies. S_{AB} indicates delivery of therapy A first and S_{BA} indicates therapy B being delivered first, the outcomes of which may not be equal. By using every possible combination of survival fractions from the individual therapies to calculate the predicted outcome, the value obtained of m_{AB} takes in to consideration every measurement and gives them all an equal weighting in the calculation. Doing this provides the standard deviation of the predicted survival, which gives greater strength to statistical assessments of difference between the predicted and observed outcomes, which is not available using the Simplified Method.

The metric results in values of m_{AB} between 1 and -1, where 1 indicates synergy, 0 indicates no interaction and -1 indicates antagonism. The significance of the difference of the value of m_{AB} from zero is assessed by a t-test of the mean and standard deviations of the distributions $S_{\mathrm{Ai}}S_{\mathrm{Bj}}$ (predicted) and combination S_{ABk} (observed) which are both approximately normal. The metric product $S_{\mathrm{Ai}}S_{\mathrm{Bj}}$ and combination S_{ABk} are tested with unequal variance, the same sample size and same degrees of freedom (sample size -1) for the product $\sum_{i,j=1}^{n} S_{\mathrm{Ai}}S_{\mathrm{Bj}}$ and the sample S_{ABk}.

Table 5.5 presents the results of both of these metrics on the assessment of synergy between sham, PAL and radiation.

5.5.3 Statistical analysis

For the radiation dose response, all cell survival fractions were normalised to the survival of the untreated group (no exposure to Hartmann's solution or radiation). For the PAL concentration response, all cell survival fractions, including the untreated, were normalised to the sham treated Hartmann's group. The two separate controls were used to separate the effect of the Hartmann's solution alone from the effect of the RONS in the plasma treated sample, and to determine whether sham treated Hartmann's solution alone affects the cell survival.

To isolate the active components of the PAL and radiation treatments, the synergy data were analysed to test three hypotheses. **Synergy Hypothesis 1** was that PAL would affect the cytotoxicity of the radiation. In order to test this, all survival fractions were normalised to the untreated group. A single sample one tailed Student's t-test was performed to test whether the mean of the observed survival fraction was significantly different to the survival fraction predicted for the absence of interactions.

Synergy Hypothesis 2 was that the RONS in PAL that were responsible for the effects on radiation cytotoxicity and not the Hartmann's solution. To test this, the control for the radiation only treatment was the untreated group. In order to remove any effects of exposure to the Hartmann's solution, the sham treated Hartmann's group was used as the control for any treatments which included PAL or sham Hartmann's solution. A paired single sample t-test was carried out comparing the predicted survival with the observed survival of the combined PAL and radiation treatment. This was repeated to compare the predicted with the observed survival of the combined sham and radiation treatment. The use of the paired t-test was justified by testing the normality of the respective difference distributions. These differences were assessed for normality in Graphpad Prism version 9 using the Anderson Darling, D'Agostino and Pearson, Shapiro-Wilk and Kolmogorov-Smirnov tests and all distributions passed at least one normality test.

Synergy Hypothesis 3 was assessing the effect of the order of therapy administration. All groups were normalised to the untreated group. A one tailed Student's t-test was performed to compare the mean and standard deviations of the predicted and observed survival fractions for both orders of administration for both the PAL and radiation combination and sham and radiation combination.

5.6 Combination experiments: PAL and Radiation

The setup for the combined treatment experiments was identical to the dose response experiments. The prescribed doses of PAL and radiation were determined from the dose response curves (Figures 5.4 and 5.5) such that each individual treatment would reduce cell survival to 70%. Cells were incubated with sham treated Hartmann's solution or PAL for 30 minutes. The solution was replaced with growth medium and incubated for one hour, then immediately exposed to the prescribed dose of ionising radiation. Each experiment was repeated two to three times to achieve n in the range 12 to 16 for each sample group.

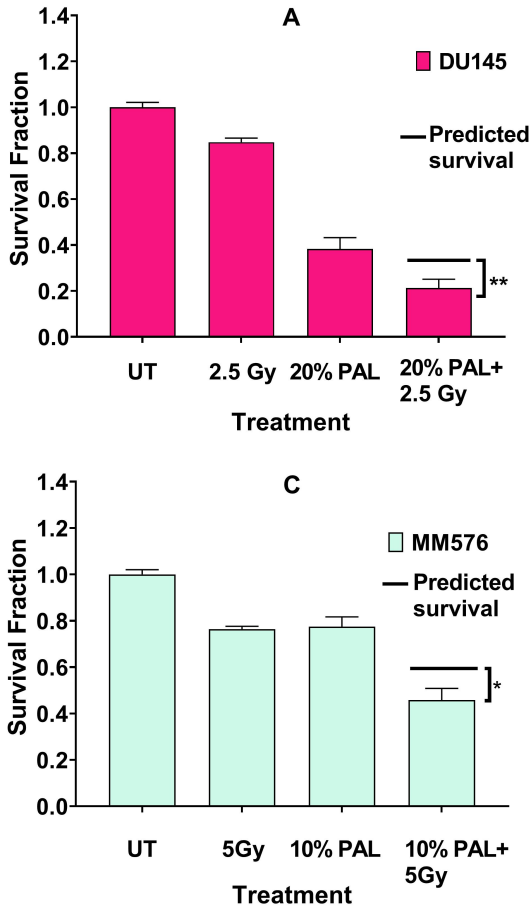

Figure 5.8: Clonogenic survival fractions comparing the observed and predicted survivals of DU 145 prostate cancer A), PNT1A immortalized normal prostate cells B) and MM576 melanoma cells C) after combination therapy using the Simplified Method and Equation 5.8, confirming **synergy hypothesis 1**. The combination treatment results were normalised to untreated cells. The 'predicted survival' was obtained by multiplying the survival fraction of the PAL alone with the survival fraction of the radiation alone for each cell line. The Simplified Method indicates that PAL and radiation exhibit synergistic enhancement of cytotoxicity for the DU 145 and MM576 cell lines and an antagonistic reduction in cytotoxicity for the PNT1A. Stars indicate significance (* $= p < 0.05$, *** $= p < 0.001$) using a one tailed Student's t-test. Error bars are +/- std deviation, n=12-16.

Figure 5.8 shows the synergy between PAL and radiation combination treatments using the clonogenic assay. The doses of radiation and concentrations of PAL given to each cell line for these experiments are summarised in Table 5.1. Both cancer cell lines showed a statistically significant decrease in survival compared to prediction, confirming our first hypothesis that pre-treatment with PAL enhances cytotoxicity in a synergistic manner. In contrast PNT1A, the immortalized normal prostate cell line, showed a statistically significant increase in survival compared to prediction, indicating an antagonistic response. This finding differentiates the immortalized normal cell response from the cancer cell response, a positive outcome for cancer treatment.

The target doses were within the linear range for each cell line and treatment according to Equation 5.13, justifying our use of the multiplicative survival principle. These results, including fitting parameters a and R^2, are displayed in Figure 5.6 and summarised in Table 5.2.

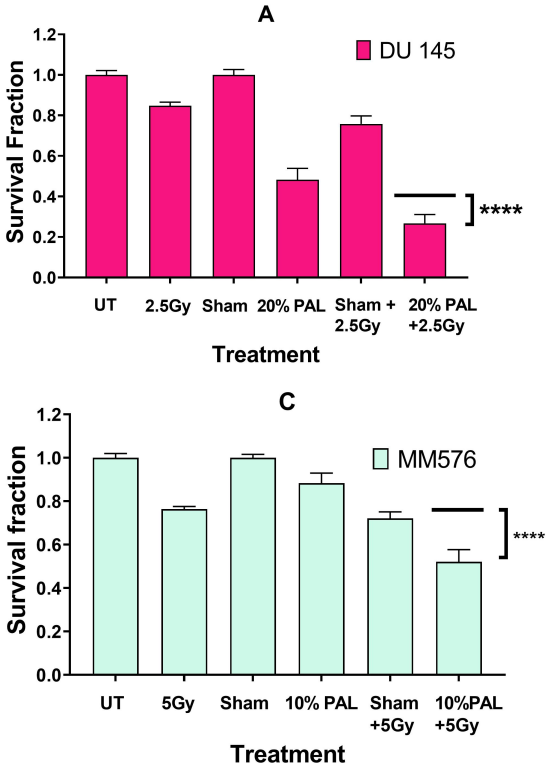

Figure 5.9: Clonogenic survival fractions comparing the observed and predicted survivals of DU 145 prostate cancer A), PNT1A immortalized normal prostate cells B) and MM576 melanoma cells C) after combination therapy using the Simplified Method and Equation 5.8, confirming **synergy hypothesis 2**. The radiation only condition was normalised to the untreated, and all other conditions were normalised to sham treated cells. The 'predicted survival' was obtained by multiplying the survival fraction of the PAL alone with the survival fraction of the radiation alone for each cell line. The Simplified Method indicates that PAL and radiation exhibit synergistic enhancement of cytotoxicity for the DU 145 and MM576 cell lines and an antagonistic reduction in cytotoxicity for the PNT1A. Stars indicate significance (* = $p < 0.05$, *** = $p < 0.001$, **** = $p < 0.0001$) calculated using a one-tailed Student's t-test. Error bars are +/- std deviation, n=12-16.

Figure 5.9 displays data re-analysed from Figure 5.8 in accordance with our second hypothesis concerning the RONS component of PAL. There are slight differences between the predicted and the observed survivals and differences in the statistical power, however the overall result does not change. The observed decrease in survival for DU 145 and MM576 cancer cell lines remains synergistic and the increase in survival of the PNT1A remains antagonistic.

Cell line	Predicted survival combined **PAL** and radiation treatment (S_1S_2)	Observed survival combined **sham** and radiation treatment (S_{12})	p-value
DU 145	0.325	0.213	0.000006 (****)
PNT1A	0.574	0.667	0.04 (*)
MM575	0.588	0.458	0.000184637 (***)

Table 5.3: Summary of the predicted survival and the observed survival calculated using the Simplified Method and Equation 5.8 for the combined PAL and radiation treatments from Figure 5.9. The Simplified Method indicates that PAL and radiation exhibit synergistic enhancement of cytotoxicity for the DU 145 and MM576 cell lines and an antagonistic reduction in cytotoxicity for the PNT1A. The p-values were evaluated using a one tailed, single sample t-test. All groups were normalised to the untreated group to address our first hypothesis.

To further interrogate this second hypothesis, the potential synergy between sham treated Hartmann's and radiation for each cell line was tested and the results are shown in Table 5.4. As there is no statistically significant difference between the predicted survival and the observed survival after combined sham and

radiation treatment for all three cell lines, we conclude that Hartmann's solution itself is not responsible for the synergy/antagonism observed with the combined PAL and radiation treatments.

Cell line	Predicted survival combined **sham** and radiation treatment (S_1S_2)	Observed survival combined **sham** and radiation treatment (S_{12})	p-value
DU 145	0.658	0.593	0.060 (ns)
PNT1A	0.591	0.623	0.196 (ns)
MM575	0.668	0.632	0.124 (ns)

Table 5.4: Summary of the predicted survival and the observed survival calculated using the Simplified Method and Equation 5.8 for the combined sham treated Hartmann's and radiation treatments from Figure 5.9. As there is no significant difference between the predicted and observed outcomes, the Simplified Method indicates no interaction between sham and radiation treatment. The p-values were determined using a one tailed, paired t-test of difference distribution. All treatment groups were normalised to the untreated group to address our first hypothesis.

5.7 Combination experiments: Order of therapy administration

The experimental setup to examine the effect of changing the order PAL and radiation treatment was identical to the initial pre-treatment experiments, and the same PAL concentration and radiation doses were used.

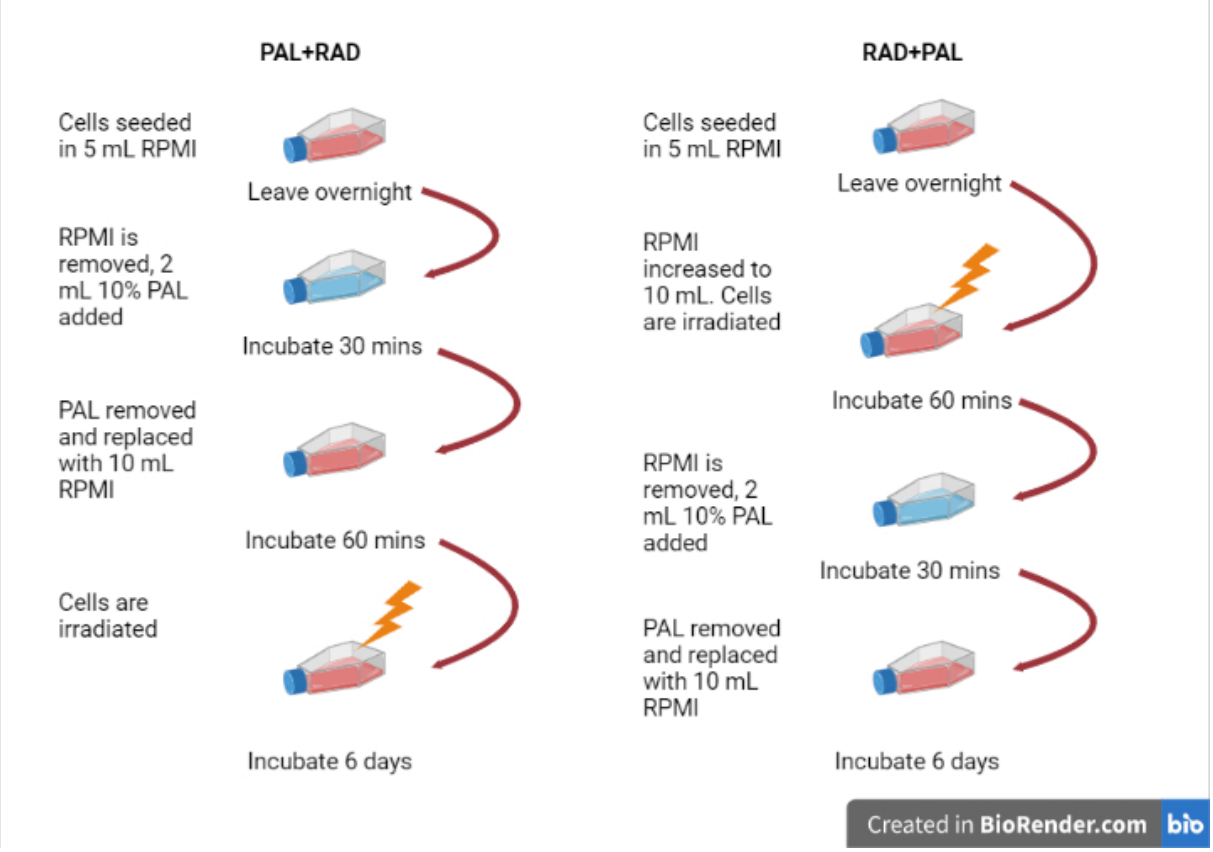

Figure 5.10: A schematic diagram of how the combination experiment was conducted and the time schedule of the treatments.

Cells were handled as schematically described above in Figure 5.10. The 5Gy only, 5Gy+sham and 5Gy+PAL groups were topped up with culture medium as described in Chapter 2 Section 2.1.6, irradiated first and allowed to incubate for one hour after irradiation. The culture medium was then removed from

all flasks and PAL or Sham treated Hartmann's was administered to all designated groups regardless of the order of administration. The PAL and Sham treatments were allowed to incubate for 30 minutes after which all groups received 10 mL of fresh culture medium. The Sham only, PAL only, 5Gy only, 5Gy+sham and 5Gy+PAL groups were then allowed to incubate until staining day. One hour after receiving fresh culture medium, the Sham+5Gy and PAL+5Gy groups were immediately irradiated, after which they were allowed to incubate until staining day.

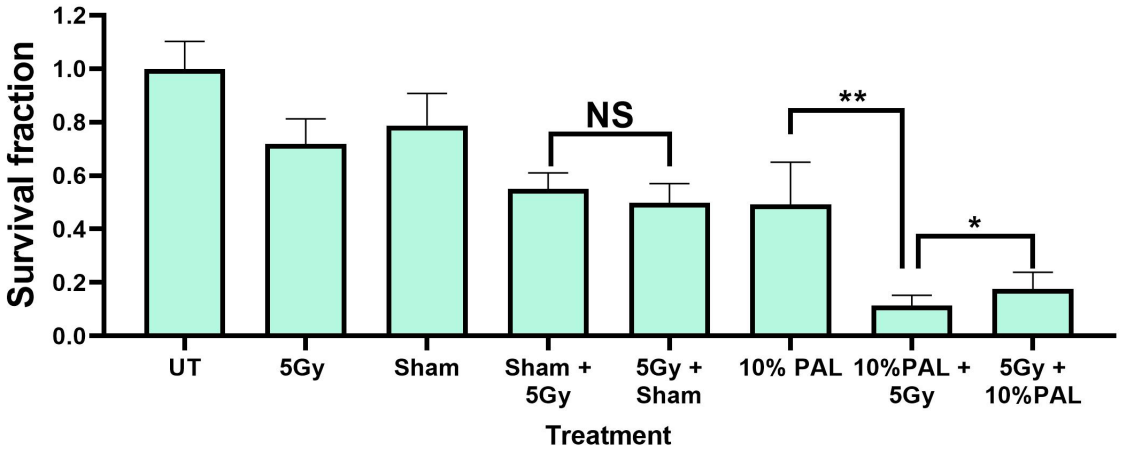

Figure 5.11: Clonogenic survival fraction of MM576 melanoma cells after exposure to PAL, ionising radiation and combinations of both treatments in accordance with **Synergy hypothesis 3**. PAL administered prior to irradiation is significantly more cytotoxic than PAL administration after irradiation, however there is no statistical difference when the order of Sham and radiation treatments are reversed. The order in which the treatments are named indicate order of administration in line with our third hypothesis. Stars indicate significance (* = $p < 0.05$, ** = $p < 0.01$) calculated using a one-tailed Student's t-test. Error bars are +/- standard deviation of n=8 samples.

PAL administered both before and after irradiation results in a statistically significant reduction in cell survival compared to individual treatment. PAL administration after irradiation is significantly less cytotoxic than pre-treatment with PAL. This could be due to a number of factors including but not limited to the PAL+5Gy cells being left in the irradiated medium during their 6 days of incubation where as for the 5Gy+PAL cells the irradiated medium was removed after one hour in order to apply the PAL. Regardless of the statistical difference, there would very little practical difference to patients when changing the order of PAL administration in these time frames, which could provide greater flexibility for administration regimens and open up greater opportunities for clinical use.

Observed survival individual therapies ($S_{\mathbf{Ai}}$ and $S_{\mathbf{Bj}}$) from Eqn. 5.15)				
S_{Ai} PAL		0.493		
S_{Bj} Radiation		0.718		
	10%PAL+5Gy	**5Gy+10%PAL**	**Sham+5Gy**	**5Gy+Sham**
Observed survival combination therapy (S_{ABk}) from Eqn. 5.15)	0.115	0.176	0.550	0.499
Observed survival stdev	0.037	0.062	0.061	0.071
Simplified Method predicted survival (S_1S_2 from Eqn. 5.8)	0.353	0.353	0.565	0.565
Simplified Method comparison of Predicted and Observed survival	$<$ .00001 (****)	0.000043 (****)	0.247959 (NS)	0.016535 (*)
FD predicted survival ($S_{\mathrm{Ai}}S_{\mathrm{Bj}}$ from Eqn. 5.15)	0.353	0.353	0.565	0.565
Standard deviation of FD predicted survival	0.116	0.116	0.108	0.108
FD comparison of Predicted and Observed survival	0.00003645 (****)	0.0009475 (***)	0.08301 (NS)	0.3649 (NS)
FD mean (m_{AB})	0.2391	0.1777	0.0154	0.0668
FD stdev of m_{AB}	0.1208	0.1295	0.1214	0.1264

Table 5.5: Summary of the predicted and observed survival after combined Sham and radiation or PAL and radiation treatment displayed in Figure 5.11 and assessment of synergy using the Simplified Method and the Fractional Difference (FD) metric. Both of the methods for assessing synergy agree that PAL administered prior to irradiation provides the greatest synergistic enhancement of cytotoxicity and that there is no interaction between Sham and radiation treatments. The p-values were determined as stated for **synergy hypothesis 3** using a one tailed Students t-test and the mean and standard deviations of the Observed survival (S_{ABk} from Eqn. 5.15) and the FD predicted survival ($S_{\mathrm{Ai}}S_{\mathrm{Bj}}$ from Eqn. 5.15) .

Analysis of synergy was performed on these experiments as described above and presented in Table 5.5. The synergistic effect between PAL and radiation is still present regardless of the order of administration and the FD method indicates that PAL application before radiation results in greater synergistic effect than PAL applied after radiation. The Fractional Difference (FD) method defined in Equation 5.15 is a convenient way of describing the **magnitude** of the synergy.

As the Fractional Difference method is based upon the MSP as is the Simplified Method, the predicted survival calculated by both metrics should be the same, which we have demonstrated above. The important new inclusion is the calculation of the standard deviation of the predicted survival. Using the standard deviation of the predicted survival in the t-test allows for more rigorous assessment of difference between predicted and observed survival which was not included previously. Using the Simplified Method, the 5Gy+Sham group presents as synergistic, which contradicts our previous conclusions in Table 5.4. Upon reassessment using the Fractional Difference method both of the sham and radiation combination groups result in a positive value of the FD mean, however the t-test indicates these results are not significantly different to 0 and therefore are not synergistic.

5.8 Effect of Ageing on PAL

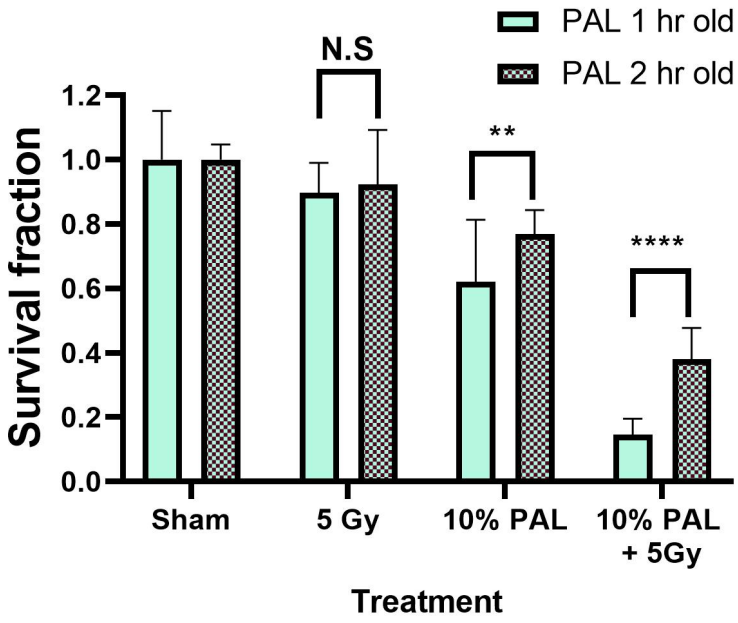

Figure 5.12: Clonogenic survival of MM576 melanoma cells after exposure to PAL of different ages after plasma treatment showing reduced synergistic effect with older PAL. The experiment was conducted as for the combination experiments, with the PAL being allowed to rest for 1 hour (standard procedure) or 2 hours post plasma treatment before application to cells. Stars indicate statistical significance (**$p< 0.01$, ****$p< 0.0001$) using a two-tailed Student's t-test. Error bars are +/- standard deviation of n=8-18 samples.

Figure 5.12 displays the radiosensitising effect of PAL of different ages. PAL was allowed to rest for either 1 hour according to standard practice, or 2 hours prior to administration to cells. All other parameters for combination experiments were the same according to steps 2-4 of Figure 5.10. The difference in the effects of aged PAL alone was not large but was statistically significant, however the difference in ability to enhance the radiation effect was both statistically significant and unexpectedly large. One other difference that could have contributed to this effect, though unlikely, is that the irradiations were performed on different linear accelerators. The flasks which received 2hr old PAL were irradiated on a Varian TrueBeam^{TM} and those which received 1 hr old PAL were irradiated on a Varian Novalis^{TM}. Due to clinical loads and machine availability this was unavoidable.

5.9 Discussion

The aim of this chapter was to establish PAL dose response profiles for three different cell lines and to assess the ability of PAL to act as a radiosensitiser. We found that PAL applied before radiation increases radiation cytotoxicity in two different cancer cell lines and results in an antagonistic decrease for the non-malignant prostate cell line. We also found a synergistic enhancement of cytotoxicity when PAL is administered after irradiation, though PAL administration prior to irradiation is significantly more cytotoxic.

Our results are consistent with other authors [49],[51] who found synergistic increase in radiation cytotoxicity with plasma treatment. The results of our experiments examining the order of therapy administration are consistent with the results of [80] who found that pre-treatment with direct plasma was more efficient at inducing apoptosis than plasma treatment after radiation. The current work independently establishes that the same phenomenon holds true for PAL and radiation: that pre-treatment with PAL is more cytotoxic than application after radiation. PAL application after radiation results in a small but significant increase in survival fraction compared to PAL pre-treatment. This difference in

survival may have been affected by unavoidable handling differences during the experiment. Extended exposure of the PAL+5Gy group to radiation induced cytokine expression ([91]) and/or ROS generation in the medium could explain why the survival of this group was lower than that of the 5Gy+PAL group, which was exposed to irradiated medium for only one hour prior to medium change for PAL treatment. However based upon the data presented here it is impossible to distinguish between handling differences and mechanistic differences.

No significant difference was found between the Sham + 5Gy and the 5Gy + Sham groups Figure 5.11. There were no interactions found between the sham and radiation groups using the Simplified Method or the Fractional Difference method with either order of administration, supporting our hypothesis that the RONS generated by the plasma are responsible for the radiosensitising effect of PAL. The data presented in this study alone cannot explain the mechanisms underlying the observed increase in cytotoxicity resulting from both methods of administration, however a short discussion on potential mechanisms follows in Chapter 6.

The Simplified MSP method is quick and effective as a first indication of interaction between two therapies, which may be further investigated using more in-depth metrics such as MuSyC or the Fractional Difference method. It is useful to have a synergy assessment method which not only allows for the assessment of the *presence* of synergy, but also the *magnitude* of the interactions. The Fractional Difference (FD) method multiplies every survival fraction after the individual therapies in every possible combination to find the average and standard deviation of the predicted outcome after combination therapy. It then takes the mean of the difference of each of these predicted values from the observed survival fractions after combination therapy. This provides a difference mean, which not only indicates 'Synergy', 'Antagonism' or 'no interaction', but also indicates strength of synergistic interaction with increasing numerical value (decreasing numerical value up to -1 indicates increasing strength of antagonistic response). This metric could prove useful for high throughput drug assessments with many combinations. As the Fractional Difference method only uses the outcome of a therapy and not the dose required to achieve this effect, it may be applicable for the assessment of interactions between many disparate therapies, including but not limited to combined radiation therapy. The synergy in general depends on the doses, therefore for a full assessment of synergistic potential more than one single combination should be investigated in future experiments. The work presented here on the Fractional Difference metric provides a useful measure of the strength of synergistic and antagonistic interactions.

5.10 Conclusion

Here we demonstrate that Plasma Activated Liquid offers an opportunity to enhance the radiation treatment of cancer, based on evidence derived for two radioresistant cell lines: melanoma and hormone resistant prostate cancer. We engaged the multiplicative survival principle to quantify interactions between PAL and radiation. In the two cancer cell lines, the cytotoxicity from radiation was synergistically increased, while in an immortalized normal prostate cell line it was antagonistically decreased. This synergistic increase in radiation cytotoxicity was also observed when the order of therapy administration was reversed, however PAL application prior to irradiation was more cytotoxic than application after radiation.

The synergistic enhancement of radiation cytotoxicity through combination with a dose of PAL observed in this study shows potential for the treatment of radioresistant cancers, ultimately improving the cancer control to enhance the patient experience.

Chapter 6

Assessing the relationship between PAL and its major components, specifically hydrogen peroxide

The final chapter of this thesis elucidates the relationship between PAL and H_2O_2 and some of the practicalities of PAL administration. It will present some theories as to the mechanisms of action of PAL and in particular PAL and radiation combination therapy.

As established in previous chapters, the RONS generated during plasma activation are responsible for the cytotoxic properties of direct plasma and PAL ([53] and [89]) and it is well documented that the plasma activation of liquids results in a large and varied cocktail of reactive species ([75], [24]). Due to this complexity and the extremely short half lives of many of these species, the two most common methods of quantifying the 'activity' of a PAL are using cytotoxicity or the concentration of H_2O_2 and/or NO_2^-. As a result of using the concentration of H_2O_2 and/or NO_2^- as a measure of activity, [99] and [35] have shown that solutions containing only H_2O_2 and NO_2^- are responsible for the vast majority of cytotoxic effect of plasma activated liquids on various cancer cell lines *in vitro*. We used both RONS concentration and cytotoxicity to investigate the cytotoxic properties of our own PAL.

The effect of storage and shelf life on the potency of a therapeutic agent are important considerations. Reports differ throughout the literature regarding the storage conditions and shelf life of a PAL. Yan *et al.* [124] report significant H_2O_2 degradation in plasma-activated medium after one day in storage at 8°C, though plasma activated PBS retained H_2O_2 concentration well up to 7 days at 8°C and at -25°C. Subramanian *et al.* [102] found that plasma treated water retained the same cytotoxic efficacy as fresh PAW (Plasma Activated Water) when stored at -20°C for two weeks. In this chapter we perform experiments to determine the most appropriate storage conditions for our PAL and use both reactive species concentration and cytotoxicity to understand how storage conditions and time affect the efficacy of our PAL. We analyse the reactive species concentrations and compare the cytotoxic capability of solutions of H_2O_2 and NO_2^- with that of PAL. The end of this chapter will discuss some possible mechanisms of PAL activity and how PAL may enhance radiation cytotoxicity.

6.1 H_2O_2 content of PAL

PAL was generated according to standard procedure for a range of time periods and H_2O_2 was analysed using the Amplex red kit (details in Chapter 2, Section 2.1.7) immediately after the plasma treatment ended. Figure 4.6 presented in Chapter 4, Section 4.3 shows a time dependent increase in H_2O_2 concentration, which is not linear. PAL generated under standard conditions for 37.5 minutes and then diluted does not have the same H_2O_2 concentration as a PAL treated for the equivalent time (e.g a PAL treated for 18.75 minutes is not the equivalent of a PAL treated for 37.5 minutes and then diluted to 50%).

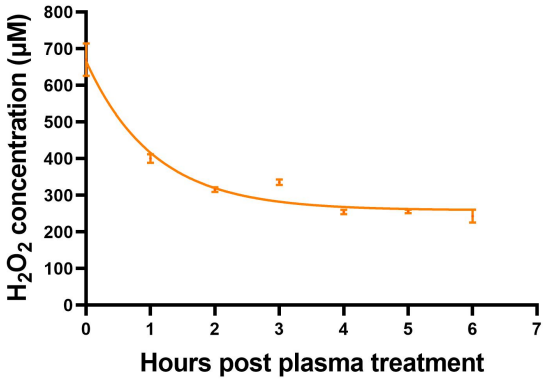

Figure 6.1: H_2O_2 concentration as a function of time post plasma treatment, showing decreasing concentration of H_2O_2 over six hours left at room temperature and analysed using the Amplex red assay. Error bars represent +/- standard deviation of n=3 samples taken at each time point.

Figure 6.1 shows the change in H_2O_2 concentration in a PAL over the first six hours from the end of plasma treatment. The PAL was generated under standard conditions and analysed using the Amplex red H_2O_2 detection kit. The PAL was left at room temperature in a sealed 15 mL falcon tube and samples were taken every hour after treatment. H_2O_2 concentration exhibits an exponential decay which reaches a plateau around 250 μM after approximately four hours.

PAL was generated using standard protocol and aliquotted for storage at different temperatures. PAL was generated fresh for comparison with stored PAL on the days of analysis. Storage for seven days at -80°C and in liquid nitrogen (LN_2) retains H_2O_2 at concentrations very similar to that of fresh PAL, however the H_2O_2 in PAL stored at -20°C had decayed beyond the limit of detection. The NO_2^- concentration in stored PAL is not changed greatly compared to fresh, even at -20°C. Therefore PAL should be stored at -80°C or in liquid nitrogen to preserve H_2O_2 concentration. Given that H_2O_2 concentration was slightly increased for stored PAL compared to fresh, a repeat of the experiment comparing the same batch of PAL was required.

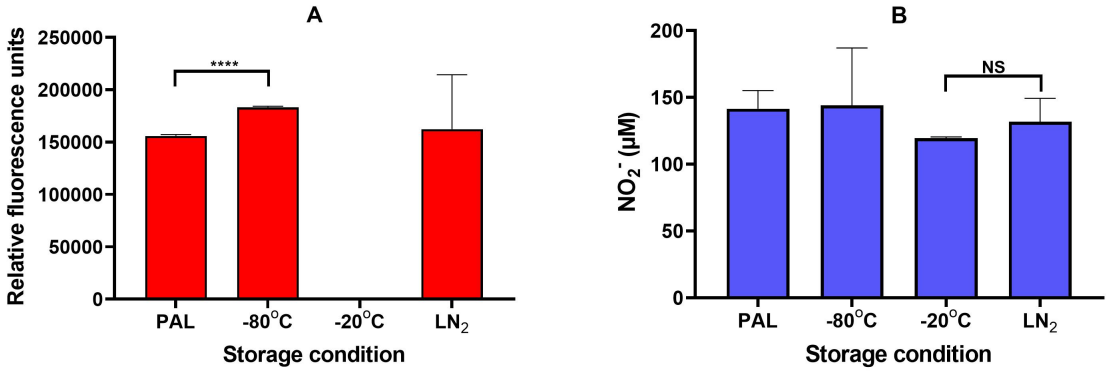

Figure 6.2: H_2O_2 concentration in relative fluorescence units (A) and NO_2^- concentration (B) of PAL stored for seven days at various temperatures below 0°C. PAL was generated fresh for comparison with stored PAL on the days of analysis. H_2O_2 stored at -20°C in panel A) decayed beyond the limit of detection though nitrite concentration is retained at the same temperature, demonstrating the need to store PAL at temperatures colder than -20°C to preserve H_2O_2 concentration. Stars indicate significance (**** = $p < 0.0001$) calculated using a one-tailed Student's t-test. Error bars represent the standard deviation for n=3 samples.

H_2O_2 concentration in stored PAL presented in Figure 6.3 confirms findings from Figure 6.2 that H_2O_2 is better preserved at lower temperatures. The PAL was analysed prior to freezing and after

8 days of storage at -80°C, so that the same batch of PAL was analysed rather than comparing two different batches. H_2O_2 degrades by approximately 30% over the 8 days, therefore cytotoxicity may still be diminished by longer storage.

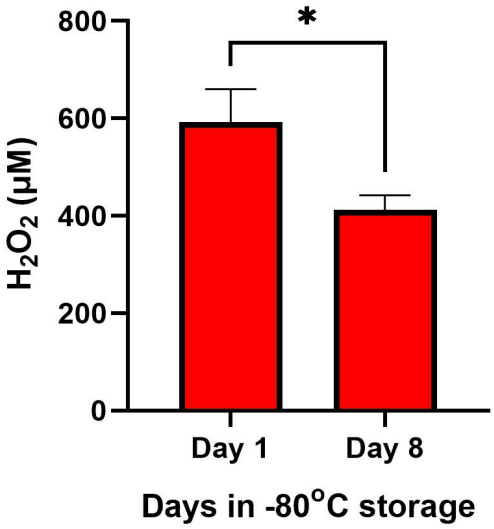

Figure 6.3: H_2O_2 concentration of the **same** batch of PAL stored for eight days at temperatures below 0°C shows small but significant decay. Stars indicate significance (* = $p < 0.05$) calculated using a one-tailed Student's t-test. Error bars represent the standard deviation for n=3 samples.

Caution must be taken when defrosting frozen samples. Though H_2O_2 content can be preserved well at low temperatures, the samples must be defrosted and analysed or used quickly, as the H_2O_2 degrades very quickly upon defrosting. A delay time of even 20 minutes between defrosting and analysis will result in greatly reduced H_2O_2 concentrations from that present at the time of freezing (data not shown).

6.2 Cell response to stored PAL

PAL was generated according to the standard procedure and was divided into aliquots for storage. PAL was stored at room temperature (RT), in a standard fridge (4°C), at -80°C and in liquid nitrogen (LN_2) for one week. DU 145 cells were seeded as described in Chapter 2, Section 2.1.3 for a Resazurin assay. On the day of the experiment, fresh PAL was generated according to standard protocol and the stored PAL was allowed to come to room temperature. Growth medium was removed and the cells were incubated for 30 minutes with the designated solutions, before the medium was replaced and the cells analysed with Resazurin 24 and 72 hours post treatment.

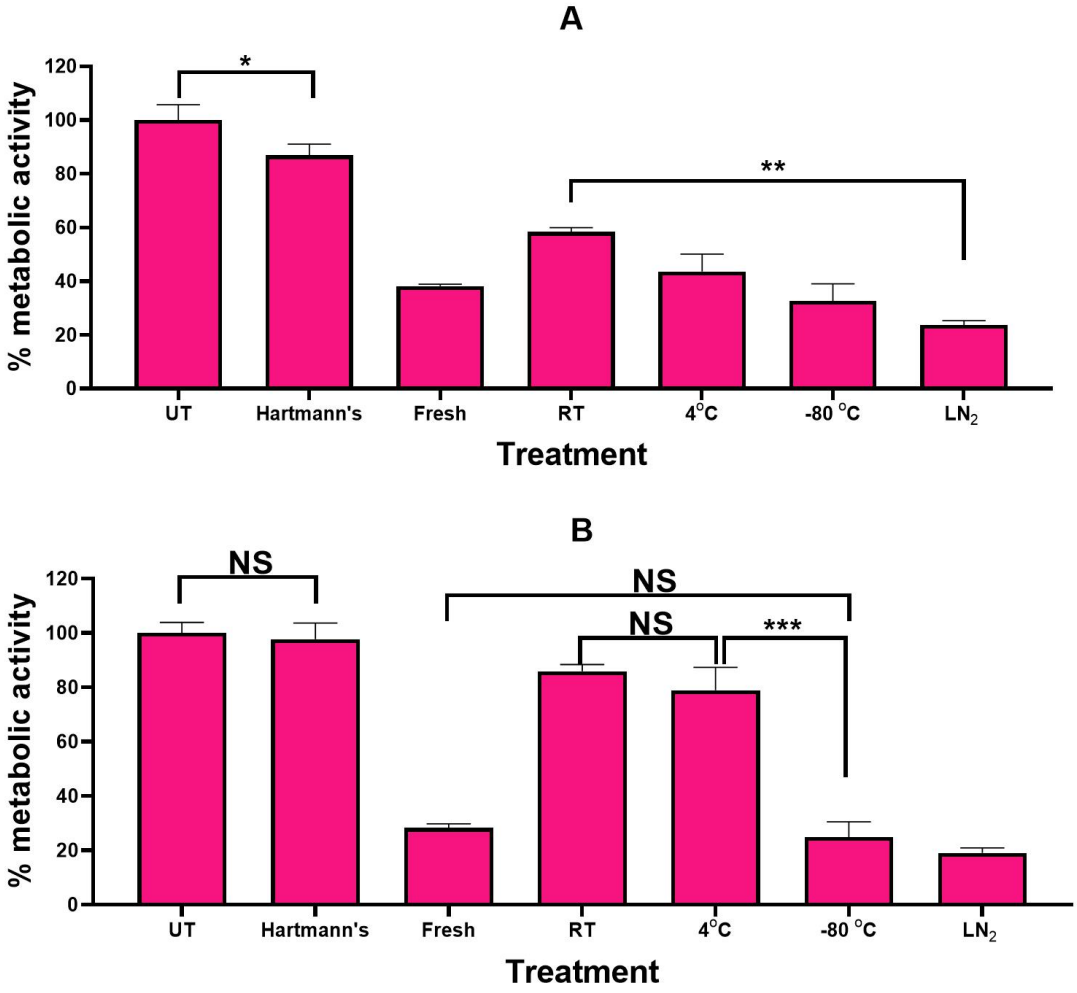

Figure 6.4: Panels (A) and (B) show the metabolic activity of DU 145 prostate cancer cells at 24 and 96 hours post exposure to fresh PAL and PAL stored under various conditions analysed with a Resazurin assay, showing that PAL stored at temperatures warmer than -80°C loses its cytotoxicity over time. Stars indicate significance (* = $p < 0.05$, ** = $p < 0.01$. ** = $p < 0.001$) calculated using a one-tailed Student's t-test. Error bars are +/- standard deviation of n=3. UT indicates Untreated, RT indicates Room Temperature.

Fresh PAL and PAL stored at -80°C and LN_2 resulted in the greatest reduction in metabolic activity at both 24 and 72 hours post treatment. PAL stored at RT and 4°C reduced metabolic viability at 24 hours after treatment, however by 72 hours the effect was no greater than incubation with untreated Hartmann's solution. Therefore, in order to retain the effectiveness of PAL, it must be stored at a minimum temperature of -80°C. These results support those presented in Figure 5.12 in Chapter 5, showing that PAL stored for longer before being applied to MM576 cells lost some of its radiosensitising ability. To retain maximum effectiveness PAL generated using our system should be used soon as possible after plasma treatment, or stored at or below -80°C if immediate administration is not possible.

There are conflicting opinions in the literature as to the 'lifetime' of a PAL, though most often 'lifetime' is defined as the concentration of reactive species such as H_2O_2 or cytotoxic capability. The data presented here confirms that PAL generated according to our protocol has a short lifetime by both standards.

6.3 Cell response to PAL and matched concentrations of key components

DU 145 hormone resistant prostate cancer and MM576 melanoma cells were seeded as described in Chapter 2, Section 2.1.3 for the Resazurin reduction assay to measure reduction in metabolic activity after exposure to PAL and after exposure to solutions of H_2O_2 and/or NO_2^- at concentrations found in PAL. PAL was generated following the standard protocol and assessed for H_2O_2 and NO_2^- concentration using the Amplex red assay and the Griess reagent nitrite detection kits, all detailed in Chapter 2, Sections 2.1.7 and 2.1.8. Solutions of H_2O_2, NO_2^- both individually and together were made in Hartmann's solution to match 100% PAL. 24 hours after seeding, the culture medium was removed and cells were incubated for 30 minutes with fresh PAL or the designated freshly made reconstituted solution. The treatment solutions were then removed and cells were incubated in culture medium until analysis. Both cell lines were analysed at 24 hours, though MM576 were analysed for the second time at 48 hours and DU 145 cells were analysed for the second time at 96 hours post treatment.

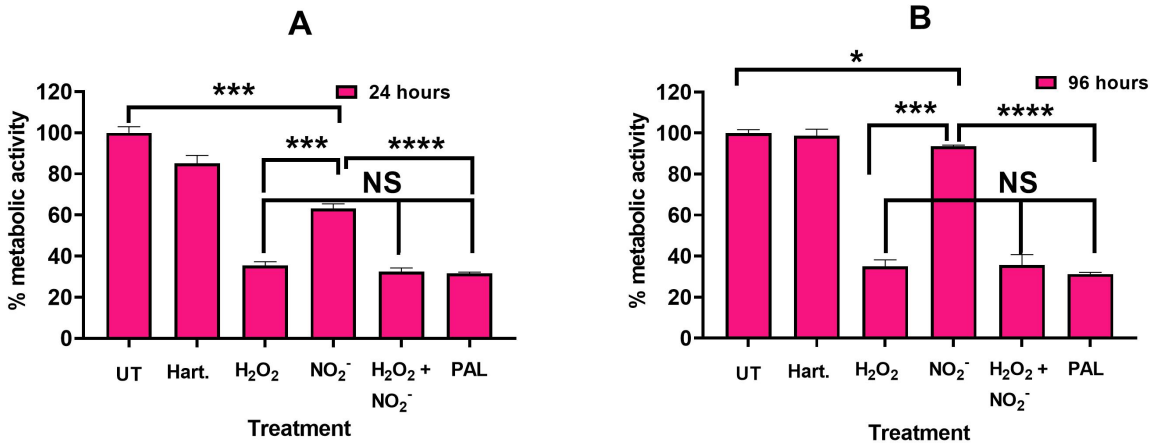

Figure 6.5: Panels (A) and (B) show the metabolic activity of DU 145 prostate cancer cells 24 and 96 hours post exposure to PAL, H_2O_2 and NO_2^- and H_2O_2, analysed using a resazurin assay. The concentrations of H_2O_2 and NO_2^- used in this experiment were 460 μM and 149 μM respectively for individual and combination solutions. No statistical difference in metabolic reduction was found between PAL, H_2O_2 and NO_2^- together and H_2O_2 alone. Stars indicate significance (* = $p < 0.05$, *** = $p < 0.001$, **** = $p < 0.0001$) calculated using a one-tailed Student's t-test. Error bars are +/- standard deviation of n=3.

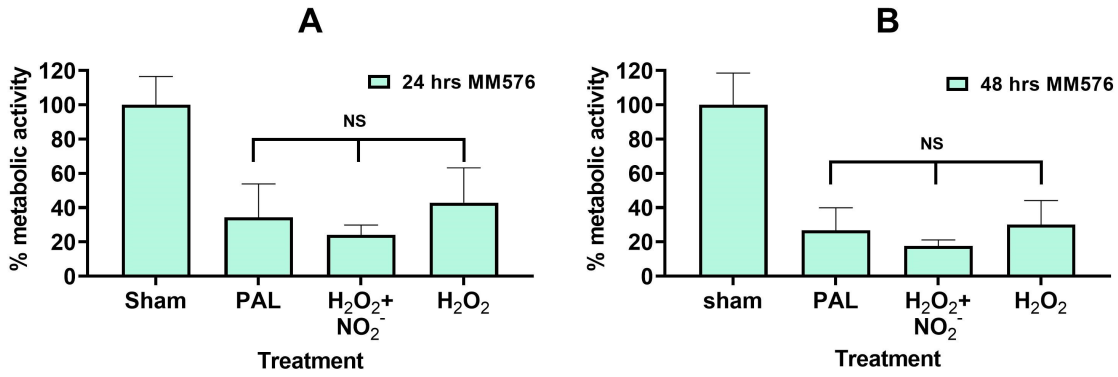

Figure 6.6: Panels (A) and (B) show the metabolic activity of MM576 melanoma cells 24 and 48 hours post exposure to PAL, H_2O_2 and NO_2^- and H_2O_2, analysed using a resazurin assay. The concentrations of H_2O_2 and NO_2^- used in this experiment were 500 μM and 150 μM respectively for individual and combination solutions. No statistical difference in metabolic reduction was found between PAL, H_2O_2 and NO_2^- together and H_2O_2 alone. Error bars are +/- standard deviation of n=3, significance was tested using a two tailed Student's t-test.

For both cell lines there was no statistical difference between PAL induced cytotoxicity and cytotoxicity induced by H_2O_2 alone or with NO_2^- at any time-point. For the MM576 cells depicted in Figure 6.6 there was a slight, but not statistically significant, reduction in metabolic activity after treatment with H_2O_2 with NO_2^- compared to PAL and H_2O_2 alone. For the DU 145 cells depicted in Figure 6.5 there were no differences.

6.4 Radiosensitisation capability of H_2O_2

The clonogenic assay, described in Chapter 2, Section 2.1.4 was used to assess the radiosensitising ability of two different concentrations of H_2O_2 representative of two different concentrations of PAL. Combination therapy experiments were conducted as described in Chapter 5, Section 5.6 and the Simplified Method and the Fractional Difference metric (FD) (both based on the Multiplicative Survival Principle (MSP)) were used to assess potential synergistic interactions.

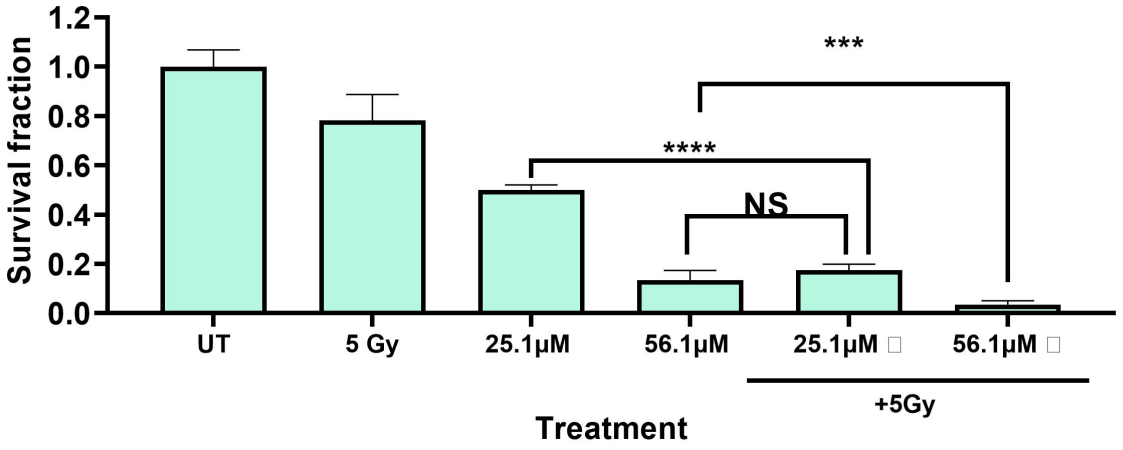

Figure 6.7: Clonogenic survival fraction of MM576 melanoma cells after exposure to various concentrations of H_2O_2 in combination with ionising radiation. Both concentrations of H_2O_2 significantly enhance radiation cytotoxicity. Stars indicate significance (*** = $p < 0.001$, **** = $p < 0.0001$) Error bars are +/- standard deviation of n=6-18 samples.

Figure 6.7 and Table **??** presents the results comparing the synergistic effect of two different concentrations of H_2O_2 and radiation combination treatment. The concentrations chosen represent the H_2O_2 content in 10% PAL and 5% PAL respectively, both of which result in statistically significant enhancement of radiation cytotoxicity. These results strongly indicate that the H_2O_2 content in the PAL is the predominant agent responsible for the synergistic enhancement of radiation. It is encouraging to see that synergy is observed using two different concentrations of H_2O_2, indicating that enhancement may be possible over greater ranges of H_2O_2 concentrations and doses of radiation used in this experiment. Our results are consistent with Fang *et al.* [26] who have also shown synergistic reduction in colony forming capacity using a similar concentration of H_2O_2 and similar doses of radiation.

6.5 Comparison of RONS generation during plasma activation and ionising radiation

The therapeutic mechanism of radiation therapy has long been though to be either via direct interaction with cellular DNA or via the generation of reactive species [36]. The quantification of reactive species generated in liquid during radiation thus becomes a point of interest. DU 145 cells were seeded overnight as described in Chapter 2, Section 2.1.3 to compare the cytotoxic potential of PAL and Radiation Conditioned Hartmann's solution. The following day PAL was generated according to standard protocol and 2 mL Hartmann's solution was irradiated to 10 Gy in a T25cm^2 flask in accordance with Section 2.1.5. The Amplex red kit was used to analyse the H_2O_2 concentration prior to incubation with cells.

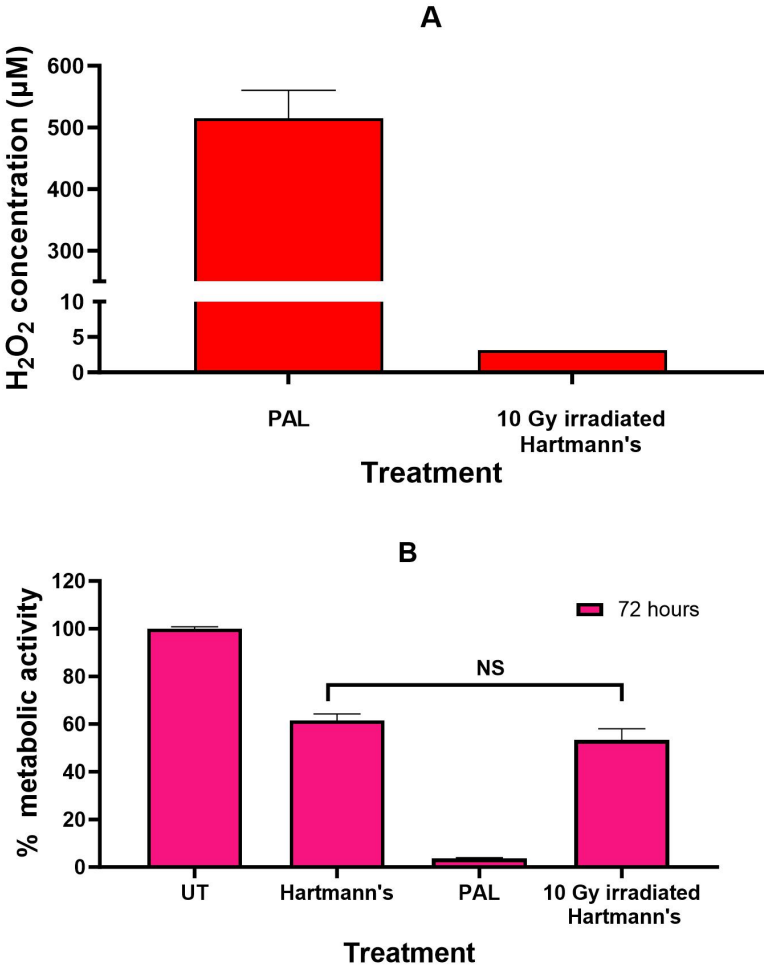

Figure 6.8: Panel (A) PAL (which was delivered 1.4 MGy calculated in Chapter 4, Section 4.4) and Hartmann's solution irradiated to 10 Gy under a clinical linear accelerator. These results show that plasma treatment results in greater concentrations of H_2O_2 in Hartmann's solution than after irradiation to 10 Gy under a clinical linear accelerator. Panel B) shows the metabolic activity of DU 145 cells 72 hours post exposure to untreated Hartmann's solution, PAL and Hartmann's irradiated to 10 Gy, analysed using a resazurin reduction assay. Data were analysed using a one-tailed Student's T-test. Error bars are +/- standard deviation of n=3 samples.

Figure 6.8 compares the H_2O_2 concentration detected after plasma treatment and after irradiation to 10 Gy. Both PAL and irradiated Hartmann's solutions were then incubated with DU 145 cells for 30 minutes and the metabolic activity of the cells assessed 72 hours post treatment. The activity of DU 145 cells incubated with fresh PAL is drastically diminished at 72 hours, whereas incubation with irradiated Hartmann's has no more effect than untreated Hartmann's. Given that PAL contains approximately 500 μM H_2O_2 and radiation is able to produce a concentration of only 3.5 μM, it is understandable that the PAL treatment is much more cytotoxic to the DU 145 than irradiated Hartmann's solution.

Method of H_2O_2 generation	**Absorbed dose**	**H_2O_2 (μM/Gy)**	**Time of treatment (minutes)**	**H_2O_2 (μM/minute)**
Plasma	1.44 MGy	$3.58\text{x}10^{-4}$	37.5	13.7± 1.20
Radiation	10 Gy	0.315	1.74	1.81± 0.003

Table 6.1: Summary of H_2O_2 concentration resulting from plasma treatment and radiation exposure as an indicator of activity of the treated liquid. Uncertainties are expressed as standard error of the mean.

Table 6.1 compares the energy requirements and the relative H_2O_2 output from irradiation and plasma treatment. Though irradiation is vastly more efficient when comparing energy deposition and H_2O_2 output, plasma generates more H_2O_2 per minute than irradiation. These results indicate, on some level, the level of crossover between the mechanisms by which PAL and radiation induce cytotoxicity. Though radiation is known to and clearly does produce some concentration of RONS in solution, the lack of cytotoxicity from the irradiated medium indicates that the majority of cytotoxicity from radiation comes from direct interaction between the cell and the beam, rather than generation of secondary reactive species in the liquid. This phenomenon is supported by Petkovic *et al.* [81] who found slightly reduced cytotoxic effects of radiation on cells pre-treated with RONS scavengers.

6.6 Mechanisms of RONS cytotoxicity

Direct plasma and PAL have been shown to kill cancer cells in a variety of ways. Cancer cells have higher intrinsic levels of RONS than normal cells due to their increased proliferation rate [84], [95]. Externally applied RONS can attack the membrane, depleting external antioxidant defences [7] and leading to increased internal RONS concentrations which the already overtaxed antioxidant stores cannot cope with, resulting in death from oxidative damage [46], [127], [111]. Other mechanisms for toxicity include DNA damage induction and activation of immunogenic cell death pathways [95]. In radiobiology, DNA double strand breaks (DSBs) are considered to result from direct interaction between the DNA and the beam, resulting in damage which is difficult to repair and, eventually, cell death [36]. There are multiple pathways for cell death following irreparable DSBs including apoptosis, necrosis and senescence [98].

There are several mechanisms through which plasma/PAL and radiation may work together as an effective combination treatment. We do not address all of them here, though we do discuss potential mechanisms which may explain why PAL administration both before and after irradiation results in such a dramatic reduction in survival fraction. Pasqual *et al.* [80] found that mitochondrial damage from plasma treatment contributed to increased cell death from combination therapy. Kariya *et al.* [44] suggest that hydrogen peroxide diminishes the antioxidant defences of the cells making them more susceptible to X-ray damage and any further RONS generation. Both radiation [59] and PAL [53] have been shown to activate p53, a regulatory protein often referred to as the Guardian of the Genome. p53 activation results in cell cycle arrest [59], phosphorylation of H2AX to initiate DNA damage response pathways and suppression of pro-survival and antioxidant gene transcription [96] resulting in excess RONS accumulation and initiation of apoptosis. Fang *et al.* [26] suggest that it is the change in the balance between pro and apoptotic signals that resulted in synergy between H_2O_2 and radiation.

Lin *et al.* [51] suggest that during G2/M phase arrest, cells are most vulnerable to radiation treatment and found that both plasma and radiation induce G2/M arrest individually and even more so after combination treatment. Lafontaine *et al.* [49] found that plasma also creates double strand DNA breaks, which could increase sensitivity to radiation when delivered in quick succession. Other methods include plasma or H_2O_2 based induction of other types of DNA damage such as single strand breaks [20] or oxidative damage [45] increasing sensitivity to DSBs. It seems reasonable that DNA damage and oxidative damage delivered in quick succession may result in similar levels of effect regardless of the order of the administration as demonstrated by these experiments.

Bauer *et al.* [7] proposes that the enhanced cytotoxicity from combining H_2O_2 and NO_2^- is due to the interactions between H_2O_2 and NO_2^- which produce intermediate singlet oxygen to inactivate membrane associated catalase, allowing RONS ingress into the cell. The RONS then inactivate intracellular antioxidants which prevents repair of lipid membrane oxidation, sensitising cells to apoptotic signaling.

The mechanisms presented above do not represent a definitive list of all possible mechanisms, rather a summary of those mechanisms which better explain how PAL and radiation combination result in similar levels of enhanced cytotoxicity regardless of the order in which they are applied. For more a more in depth review of PAL mechanisms see [84] and [95].

6.7 Discussion

The aim of this chapter was to elucidate the relationship between PAL and H_2O_2. The results in Figure 6.7 reaffirm our assessments of synergy from Chapter 5 and indicates that H_2O_2 is the main

ingredient in PAL responsible for these interactions. The results of Figures 6.5 and 6.6 show that there is no significant difference between the cytotoxic effect from PAL, H_2O_2 alone and H_2O_2 and NO_2^- together. Kurake *et al.* [48] and Ma *et al.* [58] concluded that cytotoxicity from PAL was greater than that from a solution of H_2O_2 of match concentration. However, results from [31] and [35] who have shown that concentrations of H_2O_2 and NO_2^- together which matched PAL resulted in equivalent cytotoxic effect as that provided by PAL, while H_2O_2 alone was less cytotoxic by comparison. Sklias *et al.* [99] showed that H_2O_2 and NO_2^- at a pH of 6.5 resulted in cytotoxicity that was identical to that from PAL. Bauer *et al.* [7] proposes that the enhanced cytotoxicity from combining H_2O_2 and NO_2^- is due to the interactions between H_2O_2 and NO_2^- which produce intermediate singlet oxygen to inactivate membrane associated catalase, allowing RONS ingress into the cell. The RONS then inactivate intracellular antioxidants which prevents repair of lipid membrane oxidation, sensitising cells to apoptotic signaling.

Sklias *et al.* [99] question if there is any benefit using a plasma to generate PAL when the same effect may be gained from a 'reconstituted' solution of H_2O_2 and NO_2^-. Distillation of this large and varied cocktail of reactive species down to a specified mixture of hydrogen peroxide and nitrite ions may remove much of the guesswork out of and fast track dosimetry studies, simplify stability and shelf life studies and focus efforts towards understanding mechanisms of cytotoxicity, all of which would facilitate translation into clinical use. However this may also mean that the need for a plasma activated liquid for use in cancer therapy may be super-ceded by the use of a 'reconstituted PAL'.

Initially we had hypothesised that PAL would be a better radiosensitizer than hydrogen peroxide (H_2O_2), however this could not be proven with statistical significance using our data. We showed that there was no statistical difference in cytotoxicity from H_2O_2, H_2O_2 and NO_2^- together or PAL, though this does differ from the literature cited above. H_2O_2 in the form of the KORTUC treatment has been shown to be an effective radiosensitising agent in clinical studies of cervical cancer [40] and breast cancer [78] and [97] among others. Reports show good efficacy of the KORTUC treatment platform (a mixture of H_2O_2 0.5% w/v and hyalauronic acid 0.8% w/v [77]) with manageable side effects. The recruitment of participants began in 2020 for a Phase II multi-center clinical trial of H_2O_2 sensitization in unresectable breast cancers (ClinicalTrials.gov Identifier: NCT03946202).

The authors attribute the efficacy of the KORTUC therapy to the ability of H_2O_2 to reoxygenate hypoxic tumours and efficiently deactivate catalase and other antioxidants which further sensitises the tumours to ionising radiation. Hyalauronic acid was added to KORTUC therapy for several reasons: it increases the viscosity of the H_2O_2 which slows diffusion out of the tumour, it retards the degradation of H_2O_2 to maintain increased tumour oxygenation for 24 hours after injection and when used as a therapeutic agent sodium hyalauronate has a pain controlling effect [110], [77].

Given these findings there are two paths for the future of plasma activated liquid therapies: proceed with 'reconstituted' solutions of PAL using H_2O_2 and NO_2^- together, or continue future experiments with existing H_2O_2 focused therapies. There are several advantages of the KORTUC platform: much of the preliminary investigations have already been conducted, Phase I clinical trials ([5], [4]) were successful in proving efficacy, safety and patient adherence to the trial and Phase I clinical trials have already been conducted at sites other than where the original studies were performed ([40]). Implementation of a platform with established protocols and procedures in addition to the lack of severe side effects and relatively inexpensive ingredients are great advantages towards widespread clinical use. However this pathway should not be limited just to the KORTUC therapy as other agents are emerging which can produce H_2O_2 *in situ*, such as ascorbate [12].

Alternatively if 'reconstituted' PALs (RPALs) are the chosen direction, a solution of H_2O_2 and NO_2^- provides a faster, simpler, and more reliable method of preparing PAL. The ability of PALs to be replaced by RPALs may only be applicable in certain fields; this replacement may not be feasible in other fields where *in situ* generation of $\cdot OH$ radicals is important. RPAL, prepared using stock solutions of known concentrations of H_2O_2 and NO_2^- and fine-tuned with pH adjustments, offers a more consistent and reliable solution. Consistency and reliability are crucial for the success of any treatment. Generating RPAL solutions is less time-consuming, requires fewer resources (e.g equipment, gas) and is simpler to make and scale, reducing the potential for errors and failures. Tailoring the ratios of H_2O_2 and NO_2^- in RPAL to specific tissue types would provide greater control to optimize the desired responses. Inspiration may be taken here as well from the KORTUC therapy in including a stabilising agent to preserve the activity of RPALs.

Synergy metrics such as the FD method or MuSYC can be employed to elucidate the synergistic potential of RPAL, though assessment of synergy in clinical trials is much more challenging. Ultimately the elucidation of cell mechanisms is imperative for either pathway to properly harness this radiosensitising ability of H_2O_2.

6.8 Conclusions

This chapter demonstrated that H_2O_2 concentration increases in a time dependent manner during plasma activation; the H_2O_2 concentrations decays rapidly when stored at room temperature but is retained better when stored at -80°C. We also demonstrated that solutions containing equivalent concentrations of H_2O_2 and H_2O_2 and NO_2^- together are equally cytotoxic as PAL, and that H_2O_2 is able to synergistically enhance radiation cytotoxicity. PAL is an effective radiosensitising agent and thus provides a exciting avenue of research for combination radiotherapy. The future of this work lies in the refinement of PAL generation through the use of 'reconstituted' PALs or expanding upon existing hydrogen peroxide centered therapeutics such as KORTUC or other H_2O_2 focused therapeutics.

Chapter 7

Conclusion

This PhD thesis investigated the potential of plasma activated liquids (PAL) to enhance the cytotoxicity of ionizing radiation.

Chapter 3 described the design, construction and optimisation of a custom underwater plasma treatment device. The underwater treatment maximised the reactive oxygen and nitrogen species concentration delivered to the liquid via direct contact with the plasma plume.

In Chapter 4 it was determined that two different concepts of dose were required: one to assess the dose to the liquid during plasma activation and one to predict the biological effect of the plasma activated liquid. Electrical monitoring and calorimetry were shown to be viable methods of assessing the dose - the energy deposition per unit mass in Gy - delivered to the liquid during plasma activation. We showed that H_2O_2 is generated in the liquid during plasma activation and that concentration increased in the PAL with increased plasma treatment time. The results detailed in Chapter 6 indicate that H_2O_2 is a good model species for predicting the cytotoxic potential of a PAL, supporting the idea of using H_2O_2 concentration as the 'dose of PAL'. These developments enabled the core investigation in Chapter 5, where the cytotoxic capability of PAL was assessed on three different cell lines.

The results in Chapter 5 demonstrated that PAL effectively reduces the colony-forming capacity of two radioresistant cancer cell lines (DU 145 hormone resistant prostate cancer and MM576 melanoma) and one non-malignant cell line (PNT1A). A synergy metric based upon the Multiplicative Survival Principle (MSP) and evaluated in two ways was employed to assess the combined therapies for synergistic and antagonistic therapeutic interactions. Combining PAL with ionizing radiation synergistically decreased the survival of both malignant cell lines and antagonistically increased the survival of the non-malignant cell line. An advantage of the Fractional Difference (FD) method over the Simplified Method of evaluating synergy is that the FD method provides more robust statistical assessment as well as providing a numerical value indicating the strength of the interaction. Applying PAL after radiation results in a synergistic reduction in cell survival similar to that from application of PAL prior to irradiation, however applying PAL prior to irradiation yields the most significant enhancement of cytotoxicity.

Chapter 6 revealed that H_2O_2 is able to synergistically enhance radiation cytotoxicity at concentrations similar to that found in two concentrations of PAL, according to both methods of synergy evaluation used in Chapter 5. The ability of H_2O_2 to sensitize tumors to radiation presents significant potential for treating radioresistant cancers. The KORTUC method was developed in Japan and uses a mixture of H_2O_2 and hyaluronic acid as a stabilizing agent injected into the tumour to reoxygenate hypoxic lesions, sensitising them to ionising radiation. Recent completion of Phase I clinical trials of the KORTUC therapy indicates promising efficacy and has led to the recruitment of participants for a Phase II multi-center clinical trial of H_2O_2 sensitization in unresectable breast cancers. The cost-effectiveness, availability and good general tolerance associated with KORTUC suggest potential for widespread adoption of this therapy.

Although we had initially hypothesised that PAL could be a superior radiosensitizing agent compared to H_2O_2 alone, the data obtained during this study did not support this hypothesis. The study demonstrated that a version of PAL consisting solely of H_2O_2 and NO_2^- could be produced which exhibited equivalent

cytotoxicity to PAL and may offer a more cost-effective and reliable approach for future research and clinical translation. Future directions for this work would focus on either these solutions of H_2O_2 and NO_2^- together or expanding upon other H_2O_2 focused therapies such as the KORTUC method.

The results obtained during this study have significant implications for improving patient outcomes and expanding the therapeutic options available for the management of radioresistant cancers. Further research in this area has the potential to leverage the benefits of synergy between H_2O_2 based therapies and ionising radiation, ultimately leading to improved therapeutic outcomes and enhanced quality of life for cancer patients.

Bibliography

[1] E. Abdel-Fattah. Atmospheric pressure helium plasma jet and its applications to methylene blue degradation. *Journal of Electrostatics*, 101:103360, 2019.

[2] J. C. Alamilla-Presuel, A. M. Burgos-Molina, A. González-Vidal, F. Sendra-Portero, and M. J. Ruiz-Gómez. Factors and molecular mechanisms of radiation resistance in cancer cells. *International Journal of Radiation Biology*, 98(8):1301–1315, 2022.

[3] T. Ando, M. Suzuki-Karasaki, M. Suzuki-Karasaki, J. Ichikawa, T. Ochiai, Y. Yoshida, H. Haro, and Y. Suzuki-Karasaki. Combined anticancer effect of plasma-activated infusion and salinomycin by targeting autophagy and mitochondrial morphology. *Frontiers in Oncology*, 11:593127, 2021.

[4] N. Aoyama, Y. Ogawa, M. Yasuoka, K. Ohgi, H. Iwasa, K. Miyatake, R. Yoshimatsu, T. Yamanishi, N. Hamada, T. Tamura, et al. Therapeutic results of a novel enzyme-targeting radiosensitization treatment, kochi oxydol-radiation therapy for unresectable carcinomas ii, in patients with stage i primary breast cancer. *Oncology letters*, 13(6):4741–4747, 2017.

[5] N. Aoyama, Y. Ogawa, M. Yasuoka, M. Takahashi, H. Iwasa, K. Miyatake, T. Yamanishi, N. Hamada, T. Tamura, A. Nishioka, et al. Therapeutic response to a novel enzyme-targeting radiosensitization treatment (kochi oxydol-radiation therapy for unresectable carcinomas) in patients with recurrent breast cancer. *Oncology letters*, 12(1):29–34, 2016.

[6] N. Barekzi and M. Laroussi. Dose-dependent killing of leukemia cells by low-temperature plasma. *Journal of Physics D: Applied Physics*, 45(42):422002, 2012.

[7] G. Bauer. The synergistic effect between hydrogen peroxide and nitrite, two long-lived molecular species from cold atmospheric plasma, triggers tumor cells to induce their own cell death. *Redox biology*, 26:101291, 2019.

[8] E. Biscop, A. Lin, W. Van Boxem, J. Van Loenhout, J. De Backer, C. Deben, S. Dewilde, E. Smits, and A. Bogaerts. The influence of cell type and culture medium on determining cancer selectivity of cold atmospheric plasma treatment. *Cancers*, 11(9):1287, 2019.

[9] C. I. Bliss. The toxicity of poisons applied jointly 1. *Annals of applied biology*, 26(3):585–615, 1939.

[10] N. Brix, D. Samaga, C. Belka, H. Zitzelsberger, and K. Lauber. Analysis of clonogenic growth in vitro. *Nature protocols*, pages 1–29, 2021.

[11] D. Catcheside, D. Lea, and J. Thoday. The production of chromosome structural changes intradescantia microspores in relation to dosage, intensity and temperature. *Journal of genetics*, 47(2):137, 1946.

[12] Q. Chen, M. G. Espey, M. C. Krishna, J. B. Mitchell, C. P. Corpe, G. R. Buettner, E. Shacter, and M. Levine. Pharmacologic ascorbic acid concentrations selectively kill cancer cells: action as a pro-drug to deliver hydrogen peroxide to tissues. *Proceedings of the National Academy of Sciences*, 102(38):13604–13609, 2005.

[13] Z. Chen, H. Simonyan, X. Cheng, E. Gjika, L. Lin, J. Canady, J. H. Sherman, C. Young, and M. Keidar. A novel micro cold atmospheric plasma device for glioblastoma both in vitro and in vivo. *Cancers*, 9(6):61, 2017.

[14] T.-C. Chou and P. Talalay. Analysis of combined drug effects: a new look at a very old problem. *Trends in pharmacological sciences*, 4:450–454, 1983.

[15] T.-C. Chou and P. Talalay. Quantitative analysis of dose-effect relationships: the combined effects of multiple drugs or enzyme inhibitors. *Advances in enzyme regulation*, 22:27–55, 1984.

[16] E. Claridge Mackonis, L. Hammond, A. I. Esteves, and N. Suchowerska. Radiation dosimetry in cell biology: comparison of calculated and measured absorbed dose for a range of culture vessels and clinical beam qualities. *International Journal of Radiation Biology*, 94(2):150–156, 2018.

[17] E. Claridge Mackonis, N. Suchowerska, P. Naseri, and D. R. McKenzie. Optimisation of exposure conditions for in vitro radiobiology experiments. *Australasian physical & engineering sciences in medicine*, 35(2):151–157, 2012.

[18] L. Cordaro, G. De Masi, A. Fassina, C. Gareri, A. Pimazzoni, D. Desideri, C. Indolfi, and E. Martines. The role of thermal effects in plasma medical applications: biological and calorimetric analysis. *Applied Sciences*, 9(24):5560, 2019.

[19] R. C. Cross. Current transformers. *American Journal of Physics*, 54(12):1110–1113, 1986.

[20] W. A. J. Dahm-Daphi, C. Sass. Comparison of biological effects of dna damage induced by ionizing radiation and hydrogen peroxide in cho cells. *International journal of radiation biology*, 76(1):67–75, 2000.

[21] T. S. Damiana and S. U. Dalm. Combination therapy, a promising approach to enhance the efficacy of radionuclide and targeted radionuclide therapy of prostate and breast cancer. *Pharmaceutics*, 13(5):674, 2021.

[22] X. Dehui, C. Qingjie, X. Yujing, W. Bingchuan, T. Miao, L. Qiaosong, L. Zhijie, L. Dingxin, C. Hailan, and G. K. Michael. Systemic study on the safety of immuno-deficient nude mice treated by atmospheric plasma-activated water. *Plasma Science and Technology*, 20(4):044003, 2018.

[23] G. Delaney, S. Jacob, C. Featherstone, and M. Barton. The role of radiotherapy in cancer treatment: estimating optimal utilization from a review of evidence-based clinical guidelines. *Cancer: Interdisciplinary International Journal of the American Cancer Society*, 104(6):1129–1137, 2005.

[24] J. Duan, X. Lu, and G. He. On the penetration depth of reactive oxygen and nitrogen species generated by a plasma jet through real biological tissue. *Physics of Plasmas*, 24(7):073506, 2017.

[25] M. El Shaer, M. Eldaly, G. Heikal, Y. Sharaf, H. Diab, M. Mobasher, and A. Rousseau. Antibiotics degradation and bacteria inactivation in water by cold atmospheric plasma discharges above and below water surface. *Plasma Chemistry and Plasma Processing*, 40(4):971–983, 2020.

[26] Y. Fang, B. J. Moore, Q. Bai, K. M. Cook, E. J. Herrick, and M. B. Nicholl. Hydrogen peroxide enhances radiation-induced apoptosis and inhibition of melanoma cell proliferation. *Anticancer research*, 33(5):1799–1807, 2013.

[27] N. A. Franken, H. M. Rodermond, J. Stap, J. Haveman, and C. Van Bree. Clonogenic assay of cells in vitro. *Nature protocols*, 1(5):2315–2319, 2006.

[28] G. Fridman, A. Shereshevsky, M. M. Jost, A. D. Brooks, A. Fridman, A. Gutsol, V. Vasilets, and G. Friedman. Floating electrode dielectric barrier discharge plasma in air promoting apoptotic behavior in melanoma skin cancer cell lines. *Plasma Chemistry and Plasma Processing*, 27(2):163–176, 2007.

[29] M. Fröhlich, S. Bornholdt, C. Regula, J. Ihde, and H. Kersten. Determination of the energy flux of a commercial atmospheric-pressure plasma jet for different process gases and distances between nozzle outlet and substrate surface. *Contributions to Plasma Physics*, 54(2):155–161, 2014.

[30] P. K. Gessner. A straightforward method for the study of drug interactions: an isobolographic analysis primer. *Journal of the American College of Toxicology*, 7(7):987–1012, 1988.

[31] P.-M. Girard, A. Arbabian, M. Fleury, G. Bauville, V. Puech, M. Dutreix, and J. S. Sousa. Synergistic effect of h 2 o 2 and no 2 in cell death induced by cold atmospheric he plasma. *Scientific reports*, 6:29098, 2016.

[32] S. Goutelle, M. Maurin, F. Rougier, X. Barbaut, L. Bourguignon, M. Ducher, and P. Maire. The hill equation: a review of its capabilities in pharmacological modelling. *Fundamental & clinical pharmacology*, 22(6):633–648, 2008.

[33] D. B. Graves. The emerging role of reactive oxygen and nitrogen species in redox biology and some implications for plasma applications to medicine and biology. *Journal of Physics D: Applied Physics*, 45(26):263001, 2012.

[34] W. R. Greco. The search for synergy: a critical review from a response surface perspective. *Pharmacol Rev*, 47:331–385, 1995.

[35] E. Griseti, N. Merbahi, and M. Golzio. Anti-cancer potential of two plasma-activated liquids: Implication of long-lived reactive oxygen and nitrogen species. *Cancers*, 12(3):721, 2020.

[36] E. J. Hall, A. J. Giaccia, et al. *Radiobiology for the Radiologist*, volume 6. Philadelphia, 2006.

[37] J. C. Harley, N. Suchowerska, and D. R. McKenzie. Cancer treatment with gas plasma and with gas plasma–activated liquid: Positives, potentials and problems of clinical translation. *Biophysical Reviews*, pages 1–18, 2020.

[38] A. R. Harwood and B. J. Cummings. Radiotherapy for malignant melanoma: a re-appraisal. *Cancer treatment reviews*, 8(4):271–282, 1981.

[39] J. W. Hodge, A. Ardiani, B. Farsaci, A. R. Kwilas, and S. R. Gameiro. The tipping point for combination therapy: cancer vaccines with radiation, chemotherapy, or targeted small molecule inhibitors. In *Seminars in oncology*, volume 39, pages 323–339. Elsevier, 2012.

[40] R. Hu, A. I. Saito, T. Mitsuhashi, T. Inoue, T. Ota, T. Ujihira, K. Yoshida, and K. Sasai. Radiosensitization using hydrogen peroxide in patients with cervical cancer. *Molecular and Clinical Oncology*, 15(1):1–7, 2021.

[41] F. Huang, L. Chen, H. Wang, and Z. Yan. Analysis of the degradation mechanism of methylene blue by atmospheric pressure dielectric barrier discharge plasma. *Chemical Engineering Journal*, 162(1):250–256, 2010.

[42] H. M. Joh, S. J. Kim, T. Chung, and S. Leem. Comparison of the characteristics of atmospheric pressure plasma jets using different working gases and applications to plasma-cancer cell interactions. *AIP Advances*, 3(9):092128, 2013.

[43] M. Joiner and A. v. d. Kogel. *Basic clinical radiobiology*. Hodder Arnold, London, 4th ed. edition, 2009.

[44] S. Kariya, K. Sawada, T. Kobayashi, T. Karashima, T. Shuin, A. Nishioka, and Y. Ogawa. Combination treatment of hydrogen peroxide and x-rays induces apoptosis in human prostate cancer pc-3 cells. *International Journal of Radiation Oncology* Biology* Physics*, 75(2):449–454, 2009.

[45] T. Katsube, M. Mori, H. Tsuji, T. Shiomi, B. Wang, Q. Liu, M. Nenoi, and M. Onoda. Most hydrogen peroxide-induced histone h2ax phosphorylation is mediated by atr and is not dependent on dna double-strand breaks. *The journal of biochemistry*, 156(2):85–95, 2014.

[46] N. K. Kaushik, N. Kaushik, D. Park, and E. H. Choi. Altered antioxidant system stimulates dielectric barrier discharge plasma-induced cell death for solid tumor cell treatment. *PloS one*, 9(7):e103349, 2014.

[47] A. J. Kenari, S. N. Siadati, Z. Abedian, F. Sohbatzadeh, M. Amiri, K. E. Gorji, H. Babapour, E. Zabihi, S. M. Ghoreishi, R. Mehraeen, et al. Therapeutic effect of cold atmospheric plasma and its combination with radiation as a novel approach on inhibiting cervical cancer cell growth (hela cells). *Bioorganic Chemistry*, 111:104892, 2021.

[48] N. Kurake, H. Tanaka, K. Ishikawa, T. Kondo, M. Sekine, K. Nakamura, H. Kajiyama, F. Kikkawa, M. Mizuno, and M. Hori. Cell survival of glioblastoma grown in medium containing hydrogen peroxide and/or nitrite, or in plasma-activated medium. *Archives of biochemistry and biophysics*, 605:102–108, 2016.

[49] J. Lafontaine, J.-S. Boisvert, A. Glory, S. Coulombe, and P. Wong. Synergy between non-thermal plasma with radiation therapy and olaparib in a panel of breast cancer cell lines. *Cancers*, 12(2):348, 2020.

[50] M. Leary, S. Heerboth, K. Lapinska, and S. Sarkar. Sensitization of drug resistant cancer cells: a matter of combination therapy. *Cancers*, 10(12):483, 2018.

[51] L. Lin, L. Wang, Y. Liu, C. Xu, Y. Tu, and J. Zhou. Non-thermal plasma inhibits tumor growth and proliferation and enhances the sensitivity to radiation in vitro and in vivo. *Oncology reports*, 40(6):3405–3415, 2018.

[52] P.-S. Lin and A. Wu. Not all 2 gray radiation prescriptions are equivalent: cytotoxic effect depends on delivery sequences of partial fractionated doses. *International Journal of Radiation Oncology* Biology* Physics*, 63(2):536–544, 2005.

[53] J.-R. Liu, Y.-M. Wu, G.-M. Xu, L.-G. Gao, Y. Ma, X.-M. Shi, and G.-J. Zhang. Low-temperature plasma induced melanoma apoptosis by triggering a p53/pigs/caspase-dependent pathway in vivo and in vitro. *Journal of Physics D: Applied Physics*, 52(31):315204, 2019.

[54] S. t. Loewe and H. Muischnek. Über kombinationswirkungen: Mitteilung: Hilfsmittel der fragestellung. *Naunyn-Schmiedebergs Archiv für experimentelle Pathologie und Pharmakologie*, 114:313–326, 1926.

[55] X. Lu, G. Naidis, M. Laroussi, S. Reuter, D. Graves, and K. Ostrikov. Reactive species in non-equilibrium atmospheric-pressure plasmas: Generation, transport, and biological effects. *Physics Reports*, 630:1–84, 2016.

[56] X. Lu, Q. Xiong, Z. Xiong, J. Hu, F. Zhou, W. Gong, Y. Xian, C. Zou, Z. Tang, Z. Jiang, et al. Propagation of an atmospheric pressure plasma plume. *Journal of Applied Physics*, 105(4):043304, 2009.

[57] A. L. Lucas, M. Malvezzi, G. Carioli, E. Negri, C. La Vecchia, P. Boffetta, and C. Bosetti. Global trends in pancreatic cancer mortality from 1980 through 2013 and predictions for 2017. *Clinical Gastroenterology and Hepatology*, 14(10):1452–1462, 2016.

[58] J. Ma, H. Zhang, C. Cheng, J. Shen, L. Bao, and W. Han. Contribution of hydrogen peroxide to non-thermal atmospheric pressure plasma induced a549 lung cancer cell damage. *Plasma Processes and Polymers*, 14(7):1600162, 2017.

[59] P. Maier, L. Hartmann, F. Wenz, and C. Herskind. Cellular pathways in response to ionizing radiation and their targetability for tumor radiosensitization. *International journal of molecular sciences*, 17(1):102, 2016.

[60] T. Matsui, E. Nuryadi, S. Komatsu, Y. Hirota, A. Shibata, T. Oike, and T. Nakano. Robustness of clonogenic assays as a biomarker for cancer cell radiosensitivity. *International journal of molecular sciences*, 20(17):4148, 2019.

[61] S. J. McMahon. The linear quadratic model: usage, interpretation and challenges. *Physics in Medicine & Biology*, 64(1):01TR01, 2018.

[62] P. Metcalfe. *The physics of radiotherapy x-rays and electrons*. Medical Physics Pub., Madison, Wis, 2007.

[63] H.-R. Metelmann, C. Seebauer, V. Miller, A. Fridman, G. Bauer, D. B. Graves, J.-M. Pouvesle, R. Rutkowski, M. Schuster, S. Bekeschus, et al. Clinical experience with cold plasma in the treatment of locally advanced head and neck cancer. *Clinical Plasma Medicine*, 9:6–13, 2018.

[64] C. T. Meyer, D. J. Wooten, C. F. Lopez, and V. Quaranta. Charting the fragmented landscape of drug synergy. *Trends in pharmacological sciences*, 41(4):266–280, 2020.

[65] C. T. Meyer, D. J. Wooten, B. B. Paudel, J. Bauer, K. N. Hardeman, D. Westover, C. M. Lovly, L. A. Harris, D. R. Tyson, and V. Quaranta. Quantifying drug combination synergy along potency and efficacy axes. *Cell systems*, 8(2):97–108, 2019.

[66] S. Mohades, N. Barekzi, H. Razavi, V. Maruthamuthu, and M. Laroussi. Temporal evaluation of the anti-tumor efficiency of plasma-activated media. *Plasma Processes and Polymers*, 13(12):1206–1211, 2016.

[67] S. Mohades, M. Laroussi, and V. Maruthamuthu. Moderate plasma activated media suppresses proliferation and migration of mdck epithelial cells. *Journal of Physics D: Applied Physics*, 50(18):185205, 2017.

[68] R. B. Mokhtari, T. S. Homayouni, N. Baluch, E. Morgatskaya, S. Kumar, B. Das, and H. Yeger. Combination therapy in combating cancer. *Oncotarget*, 8(23):38022, 2017.

[69] C. Moncharmont, A. Levy, M. Gilormini, G. Bertrand, C. Chargari, G. Alphonse, D. Ardail, C. Rodriguez-Lafrasse, and N. Magné. Targeting a cornerstone of radiation resistance: cancer stem cell. *Cancer letters*, 322(2):139–147, 2012.

[70] R. Moniruzzaman, M. U. Rehman, Q.-L. Zhao, P. Jawaid, K. Takeda, K. Ishikawa, M. Hori, K. Tomihara, K. Noguchi, T. Kondo, et al. Cold atmospheric helium plasma causes synergistic enhancement in cell death with hyperthermia and an additive enhancement with radiation. *Scientific reports*, 7(1):1–12, 2017.

[71] K. Morita, Y. Nishimura, S. Nakamura, Y. Arai, C. Numako, K. Sato, M. Nakayama, H. Akasaka, R. Sasaki, C. Ogino, et al. Titanium oxide nano-radiosensitizers for hydrogen peroxide delivery into cancer cells. *Colloids and Surfaces B: Biointerfaces*, 198:111451, 2021.

[72] K. Nakamura, N. Yoshikawa, Y. Mizuno, M. Ito, H. Tanaka, M. Mizuno, S. Toyokuni, M. Hori, F. Kikkawa, and H. Kajiyama. Preclinical verification of the efficacy and safety of aqueous plasma for ovarian cancer therapy. *Cancers*, 13(5):1141, 2021.

[73] G. R. Nakayama. Assessment of the alamar blue assay for cellular growth and viability in vitro. *J Immunol Methods*, 204:205–208, 1997.

[74] N. H. Nguyen, H. J. Park, S. Y. Hwang, J.-S. Lee, and S. S. Yang. Anticancer efficacy of long-term stored plasma-activated medium. *Applied Sciences*, 9(4):801, 2019.

[75] L. Nie, Y. Yang, J. Duan, F. Sun, X. Lu, and G. He. Effect of tissue thickness and liquid composition on the penetration of long-lifetime reactive oxygen and nitrogen species (rons) generated by a plasma jet. *Journal of Physics D: Applied Physics*, 51(34):345204, 2018.

[76] S. Nimalasena, L. Gothard, S. Anbalagan, S. Allen, V. Sinnett, K. Mohammed, G. Kothari, A. Musallam, C. Lucy, S. Yu, et al. Intratumoral hydrogen peroxide with radiation therapy in locally advanced breast cancer: Results from a phase 1 clinical trial. *International Journal of Radiation Oncology* Biology* Physics*, 108(4):1019–1029, 2020.

[77] Y. Ogawa. Paradigm shift in radiation biology/radiation oncology—exploitation of the "h2o2 effect" for radiotherapy using low-let (linear energy transfer) radiation such as x-rays and high-energy electrons. *Cancers*, 8(3):28, 2016.

[78] Y. Ogawa, K. Kubota, H. Ue, Y. Kataoka, M. Tadokoro, K. Miyatake, K. Tsuzuki, T. Yamanishi, S. Itoh, J. Hitomi, et al. Phase i study of a new radiosensitizer containing hydrogen peroxide and sodium hyaluronate for topical tumor injection: A new enzyme-targeting radiosensitization treatment, kochi oxydol-radiation therapy for unresectable carcinomas, type ii (kortuc ii). *International journal of oncology*, 34(3):609–618, 2009.

[79] T. J. Ow, C. D. Fulcher, C. Thomas, P. Ó. Broin, A. López, D. E. Reyna, R. V. Smith, C. Sarta, M. B. Prystowsky, N. F. Schlecht, et al. Optimal targeting of bcl-family proteins in head and neck squamous cell carcinoma requires inhibition of both bcl-xl and mcl-1. *Oncotarget*, 10(4):494, 2019.

[80] G. Pasqual-Melo, S. K. Sagwal, E. Freund, R. K. Gandhirajan, B. Frey, T. von Woedtke, U. Gaipl, and S. Bekeschus. Combination of gas plasma and radiotherapy has immunostimulatory potential and additive toxicity in murine melanoma cells in vitro. *International journal of molecular sciences*, 21(4):1379, 2020.

[81] V. D. Petković, O. D. Keta, M. Z. Vidosavljević, S. Incerti, A. M. Ristić Fira, and I. M. Petrović. Biological outcomes of γ-radiation induced dna damages in breast and lung cancer cells pretreated with free radical scavengers. *International Journal of Radiation Biology*, 95(3):274–285, 2019.

[82] J.-M. Plewa, M. Yousfi, C. Frongia, O. Eichwald, B. Ducommun, N. Merbahi, and V. Lobjois. Low-temperature plasma-induced antiproliferative effects on multi-cellular tumor spheroids. *New Journal of Physics*, 16(4):043027, 2014.

[83] M. Potter, N. Suchowerska, S. Rizvi, and D. McKenzie. Hidden stressors in the clonogenic assay used in radiobiology experiments. *Australasian physical & engineering sciences in medicine*, 34(3):345–350, 2011.

[84] A. Privat-Maldonado, C. Bengtson, J. Razzokov, E. Smits, and A. Bogaerts. Modifying the tumour microenvironment: Challenges and future perspectives for anticancer plasma treatments. *Cancers*, 11(12):1920, 2019.

[85] G. Ramanathan, P. Harty, T. Wright, J. Lye, D. Butler, D. Webb, and R. Huntley. The australian primary standard for absorbed dose to water (graphite calorimeter). Technical report, Australian Radiation Protection and Nuclear Safety Agency (ARPANSA), 2014.

[86] K. R. Roell, D. M. Reif, and A. A. Motsinger-Reif. An introduction to terminology and methodology of chemical synergy—perspectives from across disciplines. *Frontiers in pharmacology*, 8:158, 2017.

[87] L. J. Rogers, J. C. Harley, D. R. McKenzie, and N. Suchowerska. Radiation responses of cancer and normal cells to split dose fractions with uniform and grid fields: increasing the therapeutic ratio. *International Journal of Radiation Biology*, 98(9):1424–1431, 2022.

[88] J. G. Rothwell, D. Alam, D. A. Carter, B. Soltani, R. McConchie, R. Zhou, P. J. Cullen, and A. Mai-Prochnow. The antimicrobial efficacy of plasma-activated water against listeria and e. coli is modulated by reactor design and water composition. *Journal of Applied Microbiology*, 132(4):2490–2500, 2022.

[89] Y. Sato, S. Yamada, S. Takeda, N. Hattori, K. Nakamura, H. Tanaka, M. Mizuno, M. Hori, and Y. Kodera. Effect of plasma-activated lactated ringer's solution on pancreatic cancer cells in vitro and in vivo. *Annals of surgical oncology*, 25(1):299–307, 2018.

[90] A. Y. Satoh, J. E. Trosko, and S. J. Masten. Methylene blue dye test for rapid qualitative detection of hydroxyl radicals formed in a fenton's reaction aqueous solution. *Environmental science & technology*, 41(8):2881–2887, 2007.

[91] D. Schaue, E. L. Kachikwu, and W. H. McBride. Cytokines in radiobiological responses: a review. *Radiation research*, 178(6):505–523, 2012.

[92] M. Schuster, R. Rutkowski, A. Hauschild, R. K. Shojaei, T. von Woedtke, A. Rana, G. Bauer, P. Metelmann, and C. Seebauer. Side effects in cold plasma treatment of advanced oral cancer—clinical data and biological interpretation. *Clinical Plasma Medicine*, 10:9–15, 2018.

[93] M. Schuster, C. Seebauer, R. Rutkowski, A. Hauschild, F. Podmelle, C. Metelmann, B. Metelmann, T. von Woedtke, S. Hasse, K.-D. Weltmann, et al. Visible tumor surface response to physical plasma and apoptotic cell kill in head and neck cancer. *Journal of Cranio-Maxillofacial Surgery*, 44(9):1445–1452, 2016.

[94] F. Scientific. Bd plastipak™ plastic concentric luer-lock syringe. *https://www.fishersci.se/shop/products/plastipak-plastic-concentric-luer-lock-syringe/10569215*, Accessed: 16.10.2023.

[95] M. L. Semmler, S. Bekeschus, M. Schäfer, T. Bernhardt, T. Fischer, K. Witzke, C. Seebauer, H. Rebl, E. Grambow, B. Vollmar, et al. Molecular mechanisms of the efficacy of cold atmospheric pressure plasma (cap) in cancer treatment. *Cancers*, 12(2):269, 2020.

[96] Y. Shi, F. Nikulenkov, J. Zawacka-Pankau, H. Li, R. Gabdoulline, J. Xu, S. Eriksson, E. Hedström, N. Issaeva, A. Kel, et al. Ros-dependent activation of jnk converts p53 into an efficient inhibitor of oncogenes leading to robust apoptosis. *Cell Death & Differentiation*, 21(4):612–623, 2014.

[97] T. Shimbo, M. Nakata, H. Yoshioka, C. Sato, A. Hori, K. Kimura, M. Iwamoto, K. Yoshida, Y. Uesugi, H. Akiyama, et al. New enzyme-targeting radiosensitizer (kortuc ii) treatment for locally advanced or recurrent breast cancer. *Molecular and Clinical Oncology*, 15(5):1–7, 2021.

[98] J. Sia, R. Szmyd, E. Hau, and H. E. Gee. Molecular mechanisms of radiation-induced cancer cell death: a primer. *Frontiers in cell and developmental biology*, 8:41, 2020.

[99] K. Sklias, J. Santos Sousa, and P.-M. Girard. Role of short-and long-lived reactive species on the selectivity and anti-cancer action of plasma treatment in vitro. *Cancers*, 13(4):615, 2021.

[100] B. Smolková, M. Lunova, A. Lynnyk, M. Uzhytchak, O. Churpita, M. Jirsa, S. Kubinova, O. Lunov, and A. Dejneka. Non-thermal plasma, as a new physicochemical source, to induce redox imbalance and subsequent cell death in liver cancer cell lines. *Cell. Physiol. Biochem*, 52:119–140, 2019.

[101] C. Streffer and W.-U. Müller. Radiation risk from combined exposures to ionizing radiations and chemicals. In *Advances in radiation biology*, volume 11, pages 173–210. Elsevier, 1984.

[102] P. G. Subramanian, A. Jain, A. M. Shivapuji, N. R. Sundaresan, S. Dasappa, and L. Rao. Plasma-activated water from a dielectric barrier discharge plasma source for the selective treatment of cancer cells. *Plasma Processes and Polymers*, 17(8):1900260, 2020.

[103] T. Takaoka, Y. Shibamoto, M. Matsuo, C. Sugie, T. Murai, Y. Ogawa, A. Miyakawa, Y. Manabe, T. Kondo, K. Nakajima, et al. Biological effects of hydrogen peroxide administered intratumorally with or without irradiation in murine tumors. *Cancer Science*, 108(9):1787–1792, 2017.

[104] S. Takeda, S. Yamada, N. Hattori, K. Nakamura, H. Tanaka, H. Kajiyama, M. Kanda, D. Kobayashi, C. Tanaka, T. Fujii, et al. Intraperitoneal administration of plasma-activated medium: proposal of a novel treatment option for peritoneal metastasis from gastric cancer. *Annals of surgical oncology*, 24(5):1188–1194, 2017.

[105] H. Tanaka, M. Mizuno, K. Ishikawa, K. Nakamura, H. Kajiyama, H. Kano, F. Kikkawa, and M. Hori. Plasma-activated medium selectively kills glioblastoma brain tumor cells by down-regulating a survival signaling molecule, akt kinase. *Plasma Medicine*, 1(3-4), 2011.

[106] H. Tanaka, M. Mizuno, K. Ishikawa, K. Takeda, H. Hashizume, K. Nakamura, F. Utsumi, H. Kajiyama, Y. Okazaki, S. Toyokuni, et al. Glioblastoma cell lines display different sensitivities to plasma-activated medium. *IEEE Transactions on Radiation and Plasma Medical Sciences*, 2(2):99–102, 2017.

[107] H. Tanaka, M. Mizuno, Y. Katsumata, K. Ishikawa, H. Kondo, H. Hashizume, Y. Okazaki, S. Toyokuni, K. Nakamura, N. Yoshikawa, et al. Oxidative stress-dependent and-independent death of glioblastoma cells induced by non-thermal plasma-exposed solutions. *Scientific reports*, 9(1):1–12, 2019.

[108] H. Tanaka, K. Nakamura, M. Mizuno, K. Ishikawa, K. Takeda, H. Kajiyama, F. Utsumi, F. Kikkawa, and M. Hori. Non-thermal atmospheric pressure plasma activates lactate in ringer's solution for anti-tumor effects. *Scientific reports*, 6:36282, 2016.

[109] C. Tarapacki and R. Karshafian. Enhancing laser therapy using pegylated gold nanoparticles combined with ultrasound and microbubbles. *Ultrasonics*, 57:36–43, 2015.

[110] S. Tokuhiro, Y. Ogawa, K. Tsuzuki, R. Akima, H. Ue, S. Kariya, and A. Nishioka. Development of a novel enzyme-targeting radiosensitizer (kortuc) containing hydrogen peroxide for intratumoral injection for patients with low linear energy transfer-radioresistant neoplasms. *Oncology Letters*, 1(6):1025–1028, 2010.

[111] K. Tomita, Y. Takashi, Y. Ouchi, Y. Kuwahara, K. Igarashi, T. Nagasawa, H. Nabika, A. Kurimasa, M. Fukumoto, Y. Nishitani, et al. Lipid peroxidation increases hydrogen peroxide permeability leading to cell death in cancer cell lines that lack mtdna. *Cancer science*, 110(9):2856–2866, 2019.

[112] H. Tresp, M. U. Hammer, J. Winter, K. Weltmann, and S. Reuter. Quantitative detection of plasma-generated radicals in liquids by electron paramagnetic resonance spectroscopy. *Journal of Physics D: Applied Physics*, 46(43):435401, 2013.

[113] J. L. Webb. *Enzyme and metabolic inhibitors.* Academic Press, New York, 1963.

[114] M. Weller, M. Van Den Bent, K. Hopkins, J. C. Tonn, R. Stupp, A. Falini, E. Cohen-Jonathan-Moyal, D. Frappaz, R. Henriksson, C. Balana, et al. Eano guideline for the diagnosis and treatment of anaplastic gliomas and glioblastoma. *The lancet oncology*, 15(9):e395–e403, 2014.

[115] K.-D. Weltmann, E. Kindel, R. Brandenburg, C. Meyer, R. Bussiahn, C. Wilke, and T. Von Woedtke. Atmospheric pressure plasma jet for medical therapy: plasma parameters and risk estimation. *Contributions to plasma physics*, 49(9):631–640, 2009.

[116] K. Wende, P. Williams, J. Dalluge, W. Van Gaens, H. Aboubakr, J. Bischof, T. Von Woedtke, S. M. Goyal, K.-D. Weltmann, A. Bogaerts, et al. Identification of the biologically active liquid chemistry induced by a nonthermal atmospheric pressure plasma jet. *Biointerphases*, 10(2):029518, 2015.

[117] WHO. International agency for research on cancer. survival, incidence, and mortality over time. *https://gco.iarc.fr/survival/survmark*, Accessed: 02.07.2023.

[118] WHO. Cancer. *https://www.who.int/news-room/fact-sheets/detail/cancer*, Accessed: 12.12.2022.

[119] D. J. Wooten, C. T. Meyer, A. L. Lubbock, V. Quaranta, and C. F. Lopez. Musyc is a consensus framework that unifies multi-drug synergy metrics for combinatorial drug discovery. *Nature Communications*, 12(1):4607, 2021.

[120] C.-T. Wu, W.-C. Chen, and M.-F. Chen. The response of prostate cancer to androgen deprivation and irradiation due to immune modulation. *Cancers*, 11(1):20, 2019.

[121] L. Xiang, X. Xu, S. Zhang, D. Cai, and X. Dai. Cold atmospheric plasma conveys selectivity on triple negative breast cancer cells both in vitro and in vivo. *Free Radical Biology and Medicine*, 124:205–213, 2018.

[122] X. Xu, X. Dai, L. Xiang, D. Cai, S. Xiao, and K. Ostrikov. Quantitative assessment of cold atmospheric plasma anti-cancer efficacy in triple-negative breast cancers. *Plasma Processes and Polymers*, 15(8):1800052, 2018.

[123] D. K. Yadav, M. Adhikari, S. Kumar, B. Ghimire, I. Han, M.-H. Kim, and E.-H. Choi. Cold atmospheric plasma generated reactive species aided inhibitory effects on human melanoma cells: An in vitro and in silico study. *Scientific reports*, 10(1):3396, 2020.

[124] D. Yan, N. Nourmohammadi, K. Bian, F. Murad, J. H. Sherman, and M. Keidar. Stabilizing the cold plasma-stimulated medium by regulating medium's composition. *Scientific reports*, 6(1):1–11, 2016.

[125] Y. Yue, X. Pei, and X. Lu. Oh density optimization in atmospheric-pressure plasma jet by using multiple ring electrodes. *Journal of Applied Physics*, 119(3):033301, 2016.

[126] Y. Yue, X. Pei, and X. Lu. Comparison on the absolute concentrations of hydroxyl and atomic oxygen generated by five different nonequilibrium atmospheric-pressure plasma jets. *IEEE Transactions on Radiation and Plasma Medical Sciences*, 1(6):541–549, 2017.

[127] S. Zhao, Z. Xiong, X. Mao, D. Meng, Q. Lei, Y. Li, P. Deng, M. Chen, M. Tu, X. Lu, et al. Atmospheric pressure room temperature plasma jets facilitate oxidative and nitrative stress and lead to endoplasmic reticulum stress dependent apoptosis in hepg2 cells. *PloS one*, 8(8):e73665, 2013.

[128] R. Zhou, R. Zhou, P. Wang, Y. Xian, A. Mai-Prochnow, X. Lu, P. Cullen, K. K. Ostrikov, and K. Bazaka. Plasma-activated water: Generation, origin of reactive species and biological applications. *Journal of Physics D: Applied Physics*, 53(30):303001, 2020.

[129] X. Zhou, D. Cai, S. Xiao, M. Ning, R. Zhou, S. Zhang, X. Chen, K. Ostrikov, and X. Dai. Invivopen: A novel plasma source for in vivo cancer treatment. *Journal of Cancer*, 11(8):2273, 2020.

[130] R. M. Zin, C. F. Soon, N. M. Yusof, E. R. Rizon, M. Morsin, K. S. Tee, M. K. Ahmad, and N. Nayan. Dimmer and neon transformer as a power controllable generator for atmospheric pressure plasma jet. *Int J Pow Elec & Dri Syst ISSN*, 2088(8694):8694, 2019.

Appendix A

Appendix

The below link is a link to a public GitHub repository containing the raw data from the work presented here. I have endeavoured to present it in a way which makes the most sense to someone other than myself, but if there are any queries regarding the data please don't hesitate to get in contact. https://github.com/Juliette-Harley/plasma-activated-liquid